DOPPLER-SHIFTS IN THE SPECTRUM OF THE ZODIACAL LIGHT

by

Ian Robert East

BSc

Astronomy Group

Blackett Laboratory

Imperial College of Science and Technology

London SW7

A thesis submitted for the degree of

Doctor of Philosohy of the University of London

and for the

Diploma of Membership of the Imperial College

April 1983

ABSTRACT

In order to investigate the kinematics of interplanetary dust a scanning Fabry-Perot interferometer has been assembled and used to measure Doppler-shifts in the Zodiacal Light.

The etalon was servo-controlled for both parallelism and gap, control and data-logging being performed by microprocessor.

This instrument has been used on five observing trips each of ~3 weeks duration, creating by far the largest data set of it's type.

The method employed was to record scans of the MgI5183.6A Fraunhofer absorption line at points covering the whole ecliptic plane.

Data reduction was performed using cross-correlation between scans and a gaussian of width and position equal to that of the solar line.

A theoretical framework for interpretation of Doppler-shift measurements has been developed and used to test various models of particle properties and distribution in both size and space. Some deductions about the particle's orbits and optical properties have been possible. No evidence for the hyperbolic velocities reported by Fried, 1978, has been found.

The existence of a small recessional velocity of the Gegenschein, (reported by Hicks et al, 1974), is supported by the data presented here.

CONTENTS

1. INTRODUCTION. 14

1.1 PREAMBLE. 14

1.2 THE ZODIACAL LIGHT. 14

1.3 MODERN OBSERVATIONAL APPROACHES. 16

1.3.1 Colour. 16

1.3.2 Brightness and Polarisation. 18

1.3.3 Thermal Emission. 21

1.3.4 In-situ Measurements. 22

1.3.4.1 Discussion. 22

1.3.4.2 Discovery of Beta-meteoroids. 24

1.3.4.3 Size Distribution at 1 A.U.. 24

1.3.4.4 Kinematic Studies From Space. 25

1.3.5 Particle collections. 27

1.3.5.1 Brownlee Particles. 27

1.3.5.2 Oceanic Sediments and Polar Ices. 28

1.3.6 Spectrometric Measurements. 30

1.3.6.1 Information Content. 30

1.3.6.2 Past Work. 31

1.3.6.3 The work of J.W.Fried. 32

1.3.6.4 Behaviour of Dust in the Solar Neighbourhood. 33

1.4 SUMMARY OF PRESENT CONCLUSIONS AND IDEAS CONCERNING THE ZODIACAL DUST CLOUD. 35

1.4.1 Characterisation of the Dust Cloud. 35

1.4.2 Conclusions. 36

1.5 THEORETICAL CONSIDERATIONS. 36

1.5.1 Possible Sources of Dust. 36

1.5.1.1 Asteroidal Collisions. 36

1.5.1.2 Comets. 37

1.5.1.3 Possible Sources for Beta-meteoroids. 38

1.5.2 Dynamics of a Dust Particle. 39

1.5.2.1 Radiation Pressure. 39

1.5.2.2 Poynting Robertson Effect. 39

1.5.2.3 E-M Forces. 40

1.5.2.4 Radzievskii/Yarkovsky Effect. 41

1.5.2.5 Tidal effects. 42

1.5.3 Particle Lifetimes. 42

1.6 CONCLUSIONS. 43

2. AN INTERFEROMETER TO MEASURE DOPPLER-SHIFTS IN THE ZODIACAL LIGHT. 45

2.1 INTRODUCTION. 46

2.2 INSTRUMENTAL REQUIREMENTS AND CONSTRAINTS. 46

2.2.1 Information Required. 46

2.2.2 Choice of Spectral Line/Resolution. 47

2.2.3 Required Accuracy/Efficiency. 50

2.2.4 Control Requirements. 54

2.3 INSTRUMENT DESIGN. 55

2.3.1 Why a Fabry-Perot. 55

2.3.2 Plate Seperation/Resolution. 56

2.3.3 Finesse. 58

2.3.4 Input Optics. 61

2.3.5 The Instrumental Function. 62

2.3.6 Detector System. 65

2.3.7 Blocking of Outer Orders. 66

2.3.8 The Compensation Channel. 67

2.3.9 Environmental Effects. 68

2.3.9.1 The Interferance Filter. 68

2.3.9.2 The Fabry-Perot. 68

2.3.10 Pulse Counting. 70

2.3.11 Overall System Configuration. 70

2.3.12 Software Design. 70

2.3.12.1 Top-Down Task Analysis. 70

2.3.12.2 Structure. 71

2.3.12.3 Limitations of Present System. 72

2.4 EXPERIMENTAL METHOD. 72

2.4.1 Modes for F.P Control. 72

2.4.1.1 Scan Mode. 72

2.4.1.2 Chop Mode. 74

2.4.1.3 Dynamic Chop Mode. 76

2.4.2 Calibration. 77

2.4.2.1 Absolute Calibration. 77

2.4.2.2 Scale Calibration. 78

2.4.2.3 Dark Count. 78

2.4.2.4 Pre-Filter Position. 79

2.5 ERROR SOURCES. 80

2.5.1 "Shot" Noise. 80

2.5.2 Calibration Errors. 80

2.5.3 Sky Background. 81

2.5.4 Systematic Error due to Reduction Method. 82

2.5.5 Pre-Filter Drift. 82

2.6 OBSERVING TRIPS. 83

2.6.1 Site & Facilities. 83

2.6.2 Trips in 1981. 84

2.6.3 Trips in 1982. 85

3. DATA REDUCTION. 87

3.1 INTRODUCTION. 88

3.2 COMPOSITION AND SCOPE OF DATA. 88

3.3 RAW DATA PROCESSING. 89

3.3.1 First Steps. 89

3.3.2 Corrections. 90

3.3.2.1 Dark Count. 90

3.3.2.2 Extinction/Twilight. 91

3.3.2.3 Pre-Filter Drift. 91

3.4 REQUIREMENTS OF A REDUCTION METHOD. 91

3.4.1 Assumptions. 91

3.4.2 Output. 92

3.5 DOPPLER-SHIFT DERIVATION. 92

3.5.1 Centre of Gravity Technique. 92

3.5.2 Cross-Correlation Technique. 94

3.5.2.1 Description. 94

3.5.2.2 Choice of Referance Function. 95

3.5.2.3 Error Resulting From Photometric Noise. 96

3.5.3 Derivation of a Doppler-Shift From a Chop Ratio. 99

3.5.4 Combination of Results. 99

3.6 LINE PROFILE INFORMATION. 100

3.7 COMPUTING. 102

4.INTERPRETATION OF RESULTS. 103

4.1 MODELLING THE ZODIACAL DUST CLOUD. 104

4.1.1 Preamble. 104

4.1.2 Parameterisation of Particle Distribution in Space. 106

4.1.3 Parameterisation of Particle Size Distribution. 108

4.1.4 Parameterisation of Particle Properties. 109

4.2 THE PREDICTION OF DOPPLER-SHIFTS FROM VARIOUS MODELS. 115

4.2.1 Circular Keplerian Orbits Confined to the Ecliptic Plane. 115

4.2.1.1 Derivation of the Expression for Doppler-Shift vs. Elongation. 115

4.2.1.2 Dependance on Scattering Function. 117

4.2.1.3 Dependance on Radial Distribution. 118

4.2.2 The Mean Particle Velocity Reduction Factor χ. 119

4.2.2.1 Definition of χ. 119

4.2.2.2 Components of χ. 122

4.2.3 Models with Non-Zero Orbital Eccentricity and Inclination. 123

4.2.4 Models Including the Effect of Radiation Pressure. 124

4.2.4.1 Empirical Results. 124

4.2.4.2 Restrictions on Usable Particle Models. 127

4.2.4.3 Homogeneous Spherical Particles. 128

4.3 OTHER INFORMATION EXTRACTED FROM THE DATA. 129

4.3.1 Line Profiles. 129

4.3.2 Seasonal Variations. 130

4.3.3 The Recession of the Gegenschein. 130

4.3.4 The Form of $\chi(\varepsilon)$. 131

4.4 CONCLUSIONS. 131

4.4.1 The Results of Fried (1978). 131

4.4.2 Orbits. 132

4.4.3 Size Distribution. 132

4.4.4 Particle Properties. 132

5. FUTURE PROSECTS. 134

5.1 ACHIEVEMENTS TO DATE. 135

5.2 THE REQUIREMENT FOR FURTHER GROUND-BASED OBSERVATIONS. 136

5.3 THE CASE FOR MAKING RADIAL VELOCITY MEASUREMENTS FROM SPACE. 137

5.4 LABORATORY SUPPORT. 138

ACKNOWLEDGEMENTS. 139

APPENDICES. 140

A3.1 FUNCTIONAL DEPENDANCE OF $So(\lambda')$ ON $So'(\lambda')$. 141

A4.1 DERIVATION OF RADIAL DISTRIBUTION OF NUMBER DENSITY FROM THE ORBITAL DISTRIBUTION. 144

A4.2 THE RADIATION PRESSURE FACTOR. 148

A4.3 DERIVATION OF THE COMPONENT OF χ DUE TO ORBITAL ECCENTRICITY AND INCLINATION. 152

A4.4 THE CONTRIBUTION OF RADIATION PRESSURE TO χ. 155

FIGURE LIST. 157

REFERENCES. 166

FIGURES. 174

CHAPTER ONE

INTRODUCTION

1.1 PREAMBLE.

There are many diverse theoretical and experimental areas making up the field of interplanetary particle studies. To put into context the work described in this thesis it is considered necessary to offer a brief, but up to date, review encompassing those areas which are relevant.

1.2 THE ZODIACAL LIGHT.(FIG.1.1)

The earliest recorded observations of this phenomenon are those of Cassini (1730). His conclusion, that the ZL is sunlight reflected by dust left in the trail of comets, still stands today.

It remained until the 1950's before an interplanetary source could be proved. Earlier workers, (this century), attributed it to terrestrial phenomena (Hulbert, 1930: Schmid, 1935: Vegard, 1938), a few still do, (Gillett, 1967). The smooth curve of brightness with elongation, continuous with the F-corona vs. evidence against this data, (requiring photometric techniques to acquire). Final confirmation of an interplanetary source came with in-situ observations.

Early measurements of polarisation (Huruhata, 1951: Elasser, 1958: Blackwell and Ingham, 1961), seemed to indicate that a substantial component of the ZL scattering was from electrons. Earlier, (smaller), values had allowed Whipple and Gossner, (1949), to conclude that metallic dust particles could be responsible (Lyot, 1929). (In 1934 Grotrian had detected Fraunhofer lines in the spectrum indicating the presence of dust). By comparing Fraunhofer line depths, both in the solar and ZL spectra, photometrically, Beggs et al., (1964), concluded that the number density of electrons in interplanetary space was only 16 +/-20 per cc. Later, in-situ results, (Pioneers) give approx. 5 per cc. In either case the contribution of electron scattering to the ZL must then be insignificant for elongations greater than 20 degrees.

Further confirmation arrived on the detection of an I.R. excess in the inner F-corona, (Blackwell, 1952).

Although there have been many interpletary spacecraft collecting data on interplanetary dust, the ZL remains far the most important tool. This is because it contains information on the properties of the dust cloud as a whole. Observations are not limited by a small sample of dust or of the space in which it resides.

Recent reviews are available, (with varying areas and degrees of coverage), by Blackwell et al., (1967), Leinert, (1976), Mcdonnell(ed.), (1978) and Giese, (1980).

It is interesting to note that interplanetary dust now appears to be of importance in the synthesis of large molecules in space, (Greenberg, 1980).

1.3 MODERN OBSERVATIONAL APPROACHES.

1.3.1 Colour.

The amplitude of light scattered by small particles is independant of wavelength provided $\lambda << a$ where "a" is the radius of the smallest particle present. In this case Lambertian scattering applies.

Diffraction is unimportant for elongations greater than about 25 degrees.

For $\lambda \sim a$ Mie theory is appropriate and implies a degree of wavelength dependance.

Where $\lambda >> a$ the scattering will be strongly wavelength dependant, (Rayleigh regime). Hence the point at which the ZL ceases to be of solar colour, in either direction, will be an important indicator of size and chemical composition.

The magnitude of i.r. excess as a function will give similar information when sufficient data is available.

The definition of a colour ratio relative to the sun is usually given as;

$$C(\lambda_1,\lambda_2) = \frac{Izl(\lambda_1)/Isun(\lambda_1)}{Izl(\lambda_2)/Isun(\lambda_2)}$$

with colour index being given by;

$$CIzl-CIsun = -2.5\log C(\lambda_1,\lambda_2)$$

Most results for the ZL colour prior to 1960 suffer from contamination by airglow. Those afterwards use interference filters to exclude the brightest airglow lines.

The consensus view from this seems fairly conclusively that, for elongations of 30 degrees out to the Gegenschein, no difference between solar colour and ZL colour exists. (Robley, 1962 finds a slight reddening; Wolstencroft and Brandt a slightly bluer colour for the ZL; Dumont and Sanchez-Martinez find no difference; Peterson, 1967 found no differencewith an upper limit of +/-0.02 in B-V!).

However, evidence has been brought forward for a U-V excess from satellite observations, (Lillie, 1972; Pitz et al., 1976). One group's results differ, however, (Kurt & Syunyev, 1967).

A u.v. excess in the background starlight has been found in observations from the D2B-AURA satellite, (Maucherat et al. , 1976).

A slight red excess away from the sun, but at low

elongations, has been reported by various workers, (Sandford et al., 1973; Mercer et al., 1973; Leinert, 1974).

A coronal reddening has been demonstrated by Blackwell, (1952). (See section 1.3.3).

Presently work is under way to make predictions of broad band colour (i.r and u.v. fluxes) from models using Mie theory, (Roser&Staude, 1978, 1979, 1980).

Severe doubts have been expressed about the applicability of Mie theory by Giese, (1978). These are founded on the inability of models involving homogeneous spheres to explain the observed volume scattering and polarisation functions.

Inspite of these difficulties, a knowledge of the ZL colour would be of great value in distinguishing between the various particle and size distribution models, (Giese, 1980; Greenberg, 1980).

1.3.2 Brightness and Polarisation vs. Elongation.

Being for some years the major observational evidence for the properties of the dust, brightness and polarisation measurements give a test of radial distribution and scattering function. However, until such measurements were possible from a range of solar distances, it was not possible to uniquely derive either.

This has now been achieved using the Helios 1,2 and Pioneer 8,9,10,11 spacecraft, (Leinert et al., 1980; Hanner et al., 1976).

From the ground the brightness is seen to decrease rapidly away from the sun out to about 45 degrees followed by a shallow minimum, centred at about 135 degrees. An increase of about 20% occurs at the anti-solar point, which is commonly known as the Gegenschein.

Polarisation is generally positive with a maximum between 60 and 80 degrees elongation, (~0.2). Reports of a slightly negative value for the Gegenschein appear to be confirmed now, (Weinberg, 1964; Wolstencroft & Rose, 1967; Frey et al., 1974).

FIG.1.2 shows the viewing geometry of the ZL from an observer at solar distance "r".

Integrating along the line of sight (L.O.S.), the brightness will be given by;

$$I(\varepsilon, r) = \frac{Fo.Ro.\int\sigma(\theta).n(r).d\Delta}{r^2} \text{ erg.cm.A.ster.s.}$$

(e.g. Leinert, 1975),

where; Fo = Total solar irradiance as seen from 1A.U.

Ro = 1 A.U.

r = Solar distance.

Δ = Distance from Earth along L.O.S.

n(r) = No. density of partcles at solar distance "r".

$\sigma(\theta)$ = Proportion of incident radiation scaterred along direction θ . (Volume scattering function).

The integral may be simplified using;

$$r = \frac{R_o . \sin \varepsilon}{\sin \theta} \qquad d\Delta = \frac{R_o . \sin\varepsilon \, d\theta}{\sin^2\theta}$$

(Ingham, (1961), to give;

$$I(\varepsilon) = R_o . F_o . n_o . \operatorname{cosec}^{1+\nu}\varepsilon \int_{\varepsilon}^{\pi} \sin^{\nu}\theta . \sigma(\theta) . d\theta$$

where n(r) has been assumed to obey a power law such that;

$$n(r) = no . r^{-\nu}$$

The general form for the brightness integral for observations at a solar distance R is;

$$I(\varepsilon,R) = R_o . F_o . n_o . \left(\frac{R_o}{R . \cos \varepsilon} \right)^{1+\nu} \int_{\varepsilon}^{\pi} \sigma(\theta) . \sin^{\nu}\theta \, . d\theta$$

The method for inverting this integral is due to Dumont (1972, 1973).

Results, so far have been obtained indicate a value for ;

$$\nu = 1.3 \pm 0.1 \quad (0.1 < r < 1.0 \text{ A.U.})$$

$$\nu = 1.0 \quad (1.1 < r < 3.3 \text{ A.U.})$$

(Leinert et al., 1978; Hanner et al., 1976)

Volume scattering functions have been derived by Dumont and Sanchez (1975), Dumont, (1976), Leinert et al., (1976), Leinert, (1978), and Levasseur-Regourd and Dumont, (1978).

1.3.3 I.R. Measurements.

The importance of a measure of the thermal radiation emitted by the ZL has already been stated in section 1.3.1. It is, however, a very difficult measurement to perform far from the sun, because of the expected low flux level.

There have been few attempts to date, (Soifer et al., 1971; Briotta et al., 1976), and these have been regarded as affected by earthlight, (Roser & Staude, 1978).

An attempt to make measurements at 5 microns using a balloon platform is being made by Pitz, (1980).

The most important contribution of I.R. measurements so far, if confirmed, is the detection of peaks in emission within a few solar radii of the sun, (Peterson, 1967; McQueen,

1968; Lena et al., 1974). This will be fully discussed in section 1.3.6.4.

The detection of I.R. excess in the solar corona at eclipse (Blackwell, 1952), together with brightness and polarisation data both in and out of the corona, led Blackwell et al., (1967), to propose a model of the Zodiacal cloud in which the albedo varies as a function of solar distance "r". This cannot yet be ruled out as a possibility. (See Hanner, 1980).

1.3.4 In-situ Measurements.

1.3.4.1 Discussion.

A summary of the types of instrument employed to date and the information recovered follows;

Inst. Type	Information content	Flown on:
Microphone	Momentum	V2,Pioneers 8,9 L.E.A.M.,GIOTTO
Impact Plasma	ElementalComposition Mass,Velocity	OGO-1,L.E.A.M. Helios,GIOTTO
Penetration i) Cap. dielectric ii) Optical iii)Gas pressure	Momentum/Shape	Pegasus,MTS, Pioneers 10,11
Electrostatic Charge Sensing	Charge,Vel.	Helios
Optical Refln.	Albedo	Pioneer 10,11
ZL Photometer	Brightness	ISPM,Skylab

The results from in-situ measurements suffer from two main disadvantages. Firstly, the samples studied are usually very small, (typically a few hundred particles on an entire flight for particle sensors). Particle sensors also suffer from difficult calibration, relying very heavily on laboratory simulations, (Fechtig, Grun, Kissel, 1978).

Secondly, they are restricted to the small part of the Zodiacal cloud lying on the flight path.

Neither of these objections is true of photometers designed to acquire brightness, polarisation and colour data from remote parts of the solar system, albeit expensively. It is these data which has yielded a reliable radial distribution function, (in the inner solar system at least).

Other major results are;

1.3.4.2 The Discovery of Beta-Meteoroids:

A flux of low-mass particles with hyperbolic velocities coming from the solar direction; discovered using Pioneers 8,9 and confirmed with Helios 1,2 data. (Berg & Grun, 1973; McDonnell, 1975; Grun et al., 1973).

1.3.4.3 Mass Distribution at 1 A.U..

From micro-crater statistics of lunar regoliths recovered during the Apollo programme. Because the conversion to sizes depends on choice of a value for particle density, it

is not surprising to find more than one published.

One, (LeSergeant and Lamy,1978), is bimodal, adopting different densities for sub-micron and larger particles. In this way, the authors provide consistency with the masses observed for Beta-meteoroids.

The other interpretation, (Giese & Grun, 1976), is one of one mode only. It also requires only one value for density. The authors present two models, the Minimum and the Maximum consistent with the data.

The underlying difference between the models of Giese & Grun and that of LeSergeant & Lamy is the relative numbers of sub-micron particles.

If these particles can be identified with Beta-meteoroids they must exhibit large Doppler-shifts. Since under the L/L model they will also contribute a substantial part of the ZL, radial velocity meaurements will be able to distinguish the better model.

1.3.4.4 Kinematic Sudies from Space.

There have been four spaceborne instruments designed to measure velocity and/or momentum of impacting particles. These are detailedon the following page:

Mission	Active Period	Orbit	Sensor Orientation
Pioneer 8	1968-1972	Heliocentric	Scanning in Ecliptic
Pioneer 9	1969-1972	Heliocentric	Scanning in Ecliptic
Heos II	1972-1974	Geocentric	Ecliptic North/South Earth Apex/Antapex
Helios 1	1974 on	Eccentric/ Heliocentric	Scanning in Ecliptic+ Ecliptic Hemisphere South

As already mentioned the two Pioneer spacecraft were responsible for the discovery of Beta-meteoroids.

The most important by far,for dynamical studies is Helios 1 due to it's coverage of the whole inner ecliptic plane, twin sensors and long duration of flight.

This mission has confirmed the existence of Beta-meteoroids and may have established a third class intermediate in size between these and sporadic meteors. Some conclusions have been possible about their orbits;

$\bar{i} \sim 20$ degrees

$\bar{e} \sim 0.4$

Although velocities are only measured to within a factor two, these data are in conflict with those of Fried, (1978), achieved by ground-based radial velocity measuremenrs in the ZL.

1.3.5 Particle Collections.

1.3.5.1 Brownlee Particles.

The important point to note about atmospheric collection of particles is that the probability of survival of entry into the Earth's atmosphere is size, shape, composition and velocity dependent. Small, high surface area, low velocity particles are favoured.

The theory of small particle atmospheric entry is now well developed, (Opik, 1937; Whipple, 1950, 1951; Kornblum, 1969).

Particles reaching the Earth's surface may arrive either as debris from a larger body or directly,as they were in interplanetary space. It is unlikely, though, that meteoroid debris would survive since it cannot survive deceleration at the lower altitude (80 km) at which the larger bodies decelerate.

These surviving bodies are collected either by a settling plate or by impaction. The latter consists of a high speed air jet directed at the collection plate. Depending on the air speed and plate size, a size threshold is established

below which particles flow with the air and are thus not collected.

Separation of extra-terrestrial matter from contamination sources,such as pieces of aluminium from rocket exhaust, is achieved by matching elemental abundances with those of meteorites or by detecting by-products of the solar wind such as Helium or Wustite. The size range is typically from 3 microns to 40 microns.

The majority are aggregates of carbonaceous spheres of ~0.1 micron known as chondrules.

Brownlee, (1978), suggests that most are chondritic, opaque, of low reflectance and have densities between 1 and 3 g/cc.

Whilst having similar characteristics to primitive meteorites on the fine scale, they differ in porosity. Thus a diferent origin is suggested.

A recent paper by Brownlee et al. , (1983), presents evidence that components of these particles (enstatite whiskers) are primordial and thus probably of cometary origin. If so there is the prospect of learning something of the formation of solid matter in space and, perhaps, of comets themselves.

1.3.5.2 Oceanic Sediments and Arctic Ices.

This form of collection presumes interplanetary particle properties to enable separation. Four conditions have

been used, for instance, to identify which of many black magnetic spherules have a terrestrial origin, (Millard & Finkelman, 1970);

i) Fe,Ni,Co content with ratios comparable with those of meteorites,
ii) Wustite content,
iii) Fe,Ni metal content,
iv) Lack of elements of low cosmic abundance.

Black magnetic spherules,found in this way, are abundant and are thought to be ablation debris from iron rich meteorites, (Blanchard, 1972). They have diameters between 30 and 200 microns and can be found,not only in deep sea sediments, but also in arctic ice, (Hodge et al., 1964), sea floor mangenese nodules, beach sands, ancient salt deposits and even roof tops, (Finkelman,1972; Marvin & Einaudi, 1967; Mutch, 1966; Shima & Kimoto, 1966).

Another possible origin is in asteroidal collisions as "sparks", (Parkin et al., 1968).

Whatever their origin, it is interesting to note that temporary enhancements have been demonstrated from oceanic sediment data, (Parkin et al., 1968).

1.3.6 Spectrometric Measurements.

1.3.6.1 Information Content.

Although it is possible to derive orbital parameters of dust particles by in-situ instruments, Doppler-shift measurements in the ZL remain the only method capable of acquiring such information on the dust complex as a whole.

Which parameters are recoverable depends on what assumptions are made. To summarise;

Size distribution:

The relative number of small particles will affect the L.O.S. Doppler-shift observed through the size dependent effect of radiation pressure.

Distribution of orbits:

Any non-zero orbital inclination or eccentricity will reduce the mean component oforbital velocity seen along the L.O.S. from it's Keplerian, (circular), value.

Density and composition:

The composition decides the refractive index, which in turn decides the radiation pressure efficiency coefficient Qrp. Together with density, Qrp will decide the radiation pressure as a function of size. The mean value of this, (over the size distribution), in part determines the magnitude of shift observed.

Doppler-shifts for elongations in the range 25 to 180 degrees are only slightly sensitive to, (reasonable), choice of scattering function.

In addition, measurements made with good coverage and sustained for a period of years, could identify any inhomogeneities or seasonal fluctuations.

1.3.6.2 Past Work.

Early radial velocity measurements using F-P's, (Clarke et al., 1967; Reay & Ring, 1968), suffered from a strong emission core in the Hβ4861Å line chosen. Hence later attempts used a different line (MgI5184Å), (James & Smeethe, 1970). These early measurements were sufficient to conclude that the majority of dust, at least, is in prograde orbit.

Later efforts, (Hicks et al. , 1974), confirmed all previous data at low elongations but found a maximum at about 110 degrees in the evening light and corresponding minimum in

the morning light. This was similar to model predictions made by Reay, (1969). However, the data were not of sufficient precision to enable firm conclusions for the parameters used. It did demonstrate that circular, Keplerian orbits were at least a good approximation for the region of ecliptic plane covered.

An interesting point arising from their data was an apparent seasonal fluctuation manifested by a +12km/s shift for the Gegenschein in the Sept. '71 data, not present in April the same year. The cause of this remains unknown although Jovian perterbation was suggested by Bandermann & Wolstencroft, (1969) and interstellar dust by the authors.

1.3.6.3 The Work of J. W. Fried, (1978).

During 1976 and 1977 J. W. Fried of the Max. Planck Institute, Heidelberg, conducted Doppler-shift measurements in the ZL using a Griffin mask grating interferometer from a site in Namibia. He reported the results depicted in FIG.1.4.

Even from a cursory glance they are at variance with those of his predecessors, (e.g. the results of Hicks et al., FIG.1.5).

The effectively zero values for elongations 70 to 180 degrees admit of no explanation. As he admits, the hyperbolic shifts he depicts for the inner solar system cannot be explained, even by Beta-meteoroids.

It is particularly important to note that the scatter

of his data points is inconsistent with the standard error he quotes.

The method he used to arrive at Doppler-shifts from scanning the line, (simply taking the minimum), is poor since it uses only a small portion of the information gathered in the scan and is sensitive to drift, especially given the long integration time per point, (2-5 mins.).

Finally, the method used to determine standard error is only vaguely hinted at in his paper.

Despite these points, Fried's results may still stand. Further work was obviously essential in order to check them and was a major factor in giving rise to the efforts resulting in this thesis.

1.3.6.4 he Behaviour of Dust in the Solar Neighbourhood.

There are two dominant mechanisms expected to operate within a few solar radii of the sun;collisions and sputtering. (One other, suggested by Paddack & Rhee, (1976), is that of rotational bursting as a result of spin-up due to either "windmilling" or "paddle wheeling" by solar radiation).

As particles spiral in toward the sun, there must come a time when they are destroyed by one of these effects, (Zook & Berg, 1975;Beard, 1979). Spherical dust free zones may therefore be created, the radius of a particular zone depending primarily on composition. Peterson, (1963), predicted on this basis that peaks in thermal emission might be seen

corresponding to the inner edges of these zones.

There is considerable controversy over whether or not such peaks exist or are even detectable, (see Selby, 1983), for summary).

Calbert & Beard, (1972), have suggested an alternative explanation of electron streamers even should such peaks eventually be confirmed.

Apart from i.r. results, a search was made using in-situ brightness data, (Leinert, 1978), with a negative result. On the other hand, radial velocity data taken at eclipse confirms the existance of one zone (at 4.0 solar radii), (Beavers, Cook et al., 1980).

This feature is predicted by Beard, (1979) as a result of "death by sputtering" for silicate particles, (FIG.1.6).

Another reason for studying this region in this way is to discover the origin of Beta-meteoroids.

Zook & Berg, (1975), beleive them to be small collisional fragments blown away by radiation pressure. Dohnanyi, (1976), suggests that this is an adequate source of supply.

The much higher flux deduced by LeSergeant & Lamy, (1978), from an assumption of metallic densities and lunar microcrater statistics, would require a different origin. They suggest a cometary source .

Clearly more work of the latter type needs to be done, both to understand the sink mechanisms for solar system dust, and for what may be learned of it's composition.

1.4 SUMMARY OF PRESENT CONCLUSIONS AND IDEAS CONCERNING THE ZODIACAL DUST CLOUD.

1.4.1 Characterisation of the Dust Cloud.

The Zodiacal cloud may be characterised by the following paramaters/functions;

Particle Properties: Size distribution.
Shape/Morphology.
Composition.

Cloud Properties: Orbital element distribution.
Temporal fluctuations.
Homogeneity

The number density as a function of position in space follows directly from the orbital distribution. It may be determined, given certain reasonable assumptions from the Haug integral, (Haug, 1958). (See appendix 4.1).

1.4.2 Conclusions.

The size distribution could be taken as fairly well determined from lunar microcrater data, given a reliable estimate of density. Further information on the colour of the ZL would be of value.

The shape, morphology and composition data rests heavily on Brownlee collections. Indirect evidence comes from laboratory microwave analogue measurements still in progress. Results so far for the latter are encouraging, (Giese, 1978;Greenberg, 1980).

Radial distributions of number density are now reliable for the inner solar system at least. Information on orbital eccentricities is so far sparse; in-situ measurements of a few hundred particles only.

The only evidence apart from this for the distribution of inclinations is the thickness of the ZL cone. This suggests a mean i of around 20 degrees.

The questions of temporal fluctuation and homogeneity would appear open at the moment.

1.5 THEORETICAL CONSIDERATIONS.

1.5.1 Possible Sources of Dust.

1.5.1.1 Asteroidal Collisions.

As has already been explained, the black magnetic spherules found in the terrestrial environment have been explained as the "sparks" from asteroidal collisions. The majority , however, of Brownlee particles are of too low a density to be of asteroidal origin.

Another objection is the absence of any detectable ZL in the asteroid belt itself. It is difficult to explain how asteroidal debris could find it's way into the inner solar system without leaving, at least, observable quantities of dust in the asteroid belt, (Dohnanyi, 1976).

1.5.1.2 Comets.

Comets are traditionally viewed as the major dust sources in the solar system. They can be seen to be prodigous dust generators by their striking dust tails which reflect the solar spectrum.

Of the two types of comet, old and new, new comets are seen to eject the greater quantity of dust, significant tails being seen out to up to 10 A. U.

There are two objections to new comets being

responsible for the greater part of the Zodiacal cloud.

Firstly, they are only 1/10 to 1/100 as numerous as old comets.

Secondly, the dust they eject is much more easily expelled by radiation pressure since the parent body is in an orbit of greater eccentricity.

Short period (old) comets are more numerous and in bound orbits, although they produce much less dust.

From optical scattering data, the dust produced by comets appears to be a few tenths of a micron in size. However, i.r. emission from anti-tails suggests sizes of tens of microns, (Ney, 1974).

Whipple, (1967) beleives that mass loss from comets is sufficient to sustain the Zodiacal cloud. Kresak, (1980), on the other hand, maintains that it is not.

Alternatives to explain the source include the idea that the dust cloud is not in equilibrium, (Delsemme, 1976), and unobservable devolatised comet remnants which are still disintegrating, (Kresak, 1976, 1978).

1.5.1.3 Possible Sources for Beta-meteoroids.

Two posible origins for Beta-meteoroids have already been discussed in section 1.3.6.4, (collisional debris and fresh cometary material).

Two others are the formation of dust in the solar atmosphere, (Hemenway, 1976), and capture of interstellar

dust.

Mullen, (1977), objected to the former on theoretical grounds, whilst the latter bears the problem of interstellar dust overcoming radiation and solar wind pressures, (the latter dominates for very small, ~0. 1 micron, particles with which we are concerned).

It has been suggested that interstellar dust grains could penetrate the solar system as a result of E-M effects, (Morfill & Grun, 1979).

Hence one may conclude that, to date, there is no proven, satisfactory explanation of this phenomenon.

1.5.2 Forces Acting on a Dust Particle.

1.5.2.1 Radiation Pressure.

Radiation pressure will cause the ejection of all particles below a certain size density product. This value depends on the velocity of orbit injection from the source.

The effect of radiation pressure is independent of solar distance and serves to reduce the orbital velocity expected for a given particle in a given orbit.

For a full treatment of it's effects see ch. 4.

1.5.2.2 The Poynting Robertson Effect.

In the rest frame of the particle the mean energy scattered in the form of sunlight is the same for the apex and

apex directions. In the solar rest frame this is not the case .

A relativistic wavelength shift occurs which although small is sufficient to have two effects;

i) the semi-major axis decreases

ii) because the magnitude of the effect depends on radial distance, the

eccentricity of the orbit is reduced.

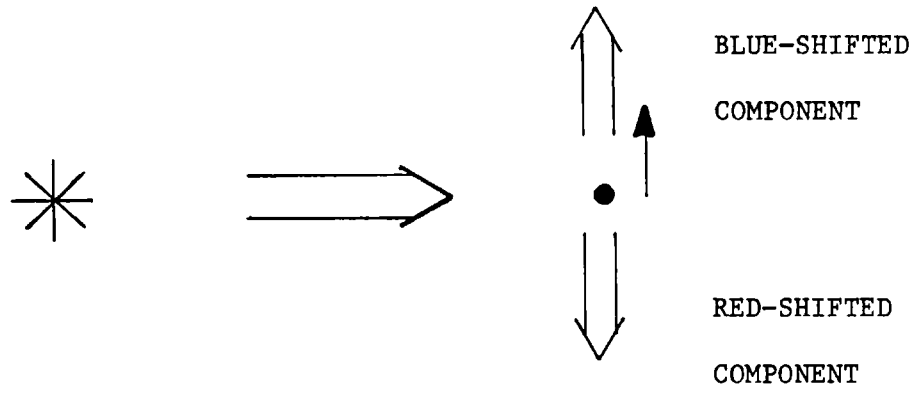

The time taken for a particle of radius "z" microns, density "s" g/cc and semi-major axis "a" A. U. to reach the sun is given by;

$$Tpr = 7.\ s.\ z.\ a^{2} \quad \text{million yrs.}$$

(Wyatt & Whipple, 1950).

It is the existance of this force that leads to the widespread belief that most of the Zodiacal cloud is in more or less circular orbit and is being constantly replenished.

The quantity of material required per unit time for equilibrium is thus dependent on the value of the dust's size and density.

1.5.2.3 E-M Forces.

Dust in the solar system is expected to hold a charge. The mechanism generating the charge being the photo-electric effect.

Against this, recombination should be taking place. Both of these are proprtional to $1/r^2$, implying a constant net charge on the particle.

The solar magnetic field is divided into sectors of unequal size and opposite polarity. Stochastic scattering may be expected of orbital inclination. The resulting upper limit being calculable, (Morfill & Grun, 1979).

A computed maximum value for a size of 100 microns is approx. 24 degrees, which may be compared with the observed MEAN value of 20 degrees.

The conclusion is that the observed range of elongations must be a property of the particle source. This is a bit high for short period comets, (mean i of about 15 degrees).

1.5.2.4 The Radzievskii/Yarkovsky Effect.

An orbiting body with a spin axis aligned with the

orbital axis will present a cooler face viewed from it's apex than it's antapex. Hence it radiates more energy along the latter. As a result it's semi-major axis and eccentricity will increase.

The reverse occurs if the spin axis is inverted.

The time taken for a measureable effect to take place on a particle of size < 1 mm is much greater than Tpr however, (Dohnanyi, 1978).

1.5.2.5 Tidal Effects.

Jupiter is the only body in the solar system capable of producing significant tidal effects in dust grain orbits.

Until more is known about the eccentricity distribution the importance of tidal effects will not be known.

1.5.3 Particle Lifetimes.

There are four mechanisms operating to limt the life of a dust particle;

i) Collisions

ii) P. R. Effect

iii) Sputtering

iv) Radiation Pressure

All these combine, of course, but one or other effect will usually dominate depending on size, (Dohnanyi, 1978);

z>>10 mns.	---Collisions dominate.
1 mn.<z<10 mns.	---P.R. effects " .
1 mn.>>z	---Sputtering dominates if particle is dense, otherwuse radiation pressure dominates.

1.6 CONCLUSIONS.

There are still many unknowns concerning the Zodiacal cloud. It would seem that the most lacking is knowledge of;

i) the nature, number and source of Beta-meteoroids,
ii) the behaviour of the dust cloud near the sun,
iii) the nature of the particles' orbits,
iv) the albedo, density and composition of the dust.

The importance of checking Fried's results, together

with the lack of kinematic data in general provided the impetus for the work which led to this thesis.

In addition, as was pointed out in section 1.3.6.1, Doppler-shift data contains information on the optical properties and density of the dust.

It must also be added that, given the opportunity to observe low elongations and the solar neighbourhood, information on i and ii (above) could also be gained in this way. It is perhaps the only reliable method with which to do so.

CHAPTER TWO

AN INTERFEROMETER TO MEASURE DOPPLER-SHIFTS IN THE ZODIACAL LIGHT.

2.1 INTRODUCTION.

In this chapter the design and performance of an interferometer to measure Doppler-shifts in the ZL are discussed together with it's subsequent use.

The recovery of line profiles is also treated.

Sources of error are summarised and assessed.

2.2 INSTRUMENTAL REQUIREMENTS AND CONSTRAINTS.

2.2.1 Information Required.

It is desired to build a data base of Doppler-shifts vs. elongation of the highest precision possible. A target figure for this precision would be of help. It was decided that the errors quoted by Fried, (1978), should be, at least , matched, (+/- 3 km/s).

Comprehensive coverage of the ecliptic plane will be required for meaningful interpretation of results.

Greater coverage will be needed at low elongations since the observed shift is expected to change more quickly there and is more affected by choice of model.

Assuming information on the line profile aswell as position is desired, the free spectral range (f.s.r.) of the

instrument must obey;

$$\Delta\lambda_{ios} > 4.\ (\ \delta\lambda_{\frac{1}{2}} + \delta\lambda'_{M})$$

where;

$\Delta\lambda_{ios}$=Free spectral range.

$\delta\lambda_{\frac{1}{2}}$ =Max. half-width of spectral line used.

$\delta\lambda'_{M}$ =Max. D/S expected.

For the maximum D/S, the velocity of an object in parabolic orbit about the sun at 1 A.U. could be used, added to the Earth's orbital velocity to give a "worst case" for (bound orbits);

$$\delta\lambda'_{M} = (42+30)/60\ \mathring{A}$$

$$= 1.2\ \mathring{A}$$

(60 km/s=1 $\mathring{A}$).

The maximum half-width of the line depends on the spread of Doppler-shifts along the L.O.S. and on the natural width of the line chosen.

2.2.2 Choice of Spectral Line/Resolution.

The line chosen must be free from in-filling by any emission source. These sources are;

i) airglow

ii) stellar background

iii) meteoric combustion (Ring et al. , (1964).

It must also be free from asymmetry as may be caused, for instance, by blending, and be as deep as possible to give greatest sensitivity to shift.

Finally, the question must be asked, what is the ideal line width ?

This turns out to depend solely on the size of the shift yet to be measured.

Consider a waveform of infinitessimal bandwidth in the time domain, (i.e. a straight forward sine wave). For how long must it be observed before a second waveform of a frequency differing by can be distinguished ?

If t=0 when the two were in equal phase, and the criterion for differentiating the two is a π phase difference then a time t must elapse such that;

$$\sin(2.\pi.\nu_1.t) = \sin(2.\pi.\nu_2.t + \pi)$$

i.e $$t = 1/2.\delta\nu$$

A filter of gaussian profile of F.W.H.M. $\Delta\nu$ has a gaussian shape in the time domain also, it's F.W.H.M. being $\simeq 1/2.\Delta\nu$.

The sampling theorem dictates that to fully describe a waveform it must be sampled at least twice per cycle of it's highest frequency component. Hence;

$$1/2.\Delta\nu \geq 1/\delta\nu$$

which implies;

$$\Delta\nu < \delta\nu/2$$

(FIG. 2. 1)

To maximise signal;

$$\Delta\nu \sim \delta\nu/2$$

The frequency of the line is restricted to values lying in the visible range since it is here that Fabry-Perot and detector technology peak and, of greater import, the solar, and hence the ZL, luminosity is greatest.

A Fraunhofer absorption line meeting our requirements is the MgI5183. 6Å line used by James & Smeethe, (1968), Reay & Ring, (1967) and Hicks et al., (1974).

Taking this line and 1.0 Å for the highest shift expected a value for the required resolution is arrived at;

$$R=5000/0.5 = 10,000$$

The ideal width of the line may be found using the matched filter theorem in reverse. The width of the filter is

approximately 0. 5 Å (from the above). Hence the width of the chosen line is a little large at 1. 5 Å. It's symmetry, cleaness and the fact that it has been proven to be relatively contamination free, however, make it still to be the best candidate, (see FIG. 2. 2).

2.2.3 Required Accuracy/Efficiency.

The best data so far published are that of Hicks et al. (1974) with a standard error close to +/- 10 km/s.

In order to match the quoted error of Fried (1978) an improvement of at least a factor 3 is thus required.

A simplistic arguement to relate D/S error to photometric accuracy is as follows.

If λ' is the difference between wavelength λ and the natural line centre then;

$$\text{Doppler-shift} = \Delta\lambda = \int_{\lambda_2}^{\lambda_1} \lambda' . I(\lambda') . d\lambda' \Big/ \int_{\lambda_2}^{\lambda_1} I(\lambda') . d\lambda'$$

where $I(\lambda')$ is the intensity for λ'.

On dividing up wavelength into N "bins" each of width $\delta\lambda$;

$$\Delta\lambda = \sum_{n=1}^{N} Y_n . \lambda' . \delta\lambda \Big/ \sum_{n=1}^{N} Y_n . \delta\lambda$$

if Y_n is now considered to be the number of photons arriving in bin n (centred on λ').

If the fractional error in Y_n is $+/-e_n$ and the mean of e_n is e then the error in $\Delta\lambda$ is given by;

$$e_{\Delta\lambda} = +/- 2.e.N^{\frac{1}{2}}.(\lambda_2-\lambda_1)$$

However, the fractional error depends on line depth after all background radiation is accounted for.

If "e_1" refers to the photometric (standard) error 1/2 way down the line then the fractional error in Y at this point is e_1. ((2/depth)-1) for these purposes. Now;

$$\text{Depth}=1/1+bg$$

where;

bg=total background brightness as a fraction of the ZL. Hence;

$$e_{\Delta\lambda} \simeq 4.e_1.(1 + 2.bg).N^{\frac{1}{2}}\ \overset{\circ}{A}$$

(Given that $(\lambda_2-\lambda_1) \simeq 2\overset{\circ}{A}$)

Since $1/e_1$=s/n ratio (photometric);

$$e_{\Delta\lambda} \simeq 4.(1 + bg).N^{\frac{1}{2}}/ (s/n)$$

Inverting this the s/n required to obtain a D/S error $e_{\Delta\lambda}$ is given by;

$$s/n \simeq 4.(1 + bg).N^{\frac{1}{2}} / e_{\Delta\lambda}$$

The ZL is a very faint source such that the dark count of even the best available detector is significant. For an integration time per point t, dark count D and observed source count S per second;

$$s/n = \frac{S.t^{\frac{1}{2}}}{(S + 2.D)^{\frac{1}{2}}}$$

Hence;

$$t = (s/n)^2.\frac{(S + 2.D)}{S^2} \quad \text{sec}$$

If eff is the instrumental efficiency and Z the source brightness seen by the collecting surface in photons per second then;

$$t = (s/n)^2.\frac{(eff.Z + 2.D)}{eff^2.Z^2} \quad \text{sec}$$

(Note: If $Z \gg D$ then $t \alpha 1/eff$ but if $Z \ll D$ then $t \alpha 1/eff$. Efficiency is more important for a faint source !!)

Hence, the total integration time for N points, T , is given by;

$$T = N.t = \frac{16.(1 + 2.bg)^2.(eff.Z + 2.D)}{eff^2.Z^2.e_{\Delta\lambda}^2} \quad \text{sec}$$

The important points raised by this equation are;

i) the importance of site quality since, if the background is a significant proportion of the ZL in intensity then $T \alpha bg^2$.

ii) the importance of a low dark count, since otherwise $T. \alpha\ 1/eff^2$. Since eff is inevitably going to be only ~0. 1, (mainly limited by detector quantum effiiency) , a factor of ~10 difference in T may lie between the two cases; D>>Z and D<<Z.

iii) $T\ 1/e_{\Delta\lambda}^2$. For twice the precision four times the integration time is required.

2.2.4 Control requirements.

To take full advantage of micro-processors the software should allow for the maximum possible versatility of control and data management. re-programming on-site, for instance, should be avoided at all costs.

The best approach is therefore a system of program

modules, preferably written in machine-code, for speed of operation and memory efficiency, under the control of a program in a high level language. The high level language allows ease of editing. BASIC has the advantage of been executable in "command mode". This, together with it's cheapness and availability made it the obvious choice.

Ideally the system should reduce the data on-line. This enables a better insight into the quality of the data being gathered, problems to be more readily identified and decisions to be better taken at the time concerning, for instance, source coverage. For instance, a low elongation, (near horizon), run may be contaminated by fluctuations in the background. This is often hard to identify in raw data but could be made clear at the processing stage. The decision could be taken to better spend integration time looking elsewhere.

However, a good high level language is required for this with plenty of memory available. Unfortunately, at the time, funding would not permit on-line reduction.

2.3 INSTRUMENT DESIGN.

2.3.1 Why a Fabry-Perot ?

The resolving power arrived at in section 2.1.2 can easily be met by a Michelson, Fabry-Perot or a suitable grating interferometer. The basis for the choice must be luminosity-resolution product for a source as faint as the ZL.

Jacquinot, (1954), pointed out the superiority of the F-P over the grating in this respect.

The Griffin technique improves the R-L product of the grating. The difficulty of making a Griffin mask of suitable accuracy and the relative complexity of the Michelson make the F-P the best option.

Another point in the F-P's favour being the availability of a proven, simple to use servo/control system for the F-P, (QI CS100), developed within the I.C. Astronomy Group, (Hicks, 1974).

However, if the main object of these investigations were to recover line profiles rather than positions it is relevant to poimt out that the Michelson would have one advantage over the F-P. Convolutions of hypothetical spectral line shapes with the instrumental profiles of both types of interferometer reveal that the Michelson loses less of the original shape than the F-P.

2.3.2 Plate Separation/Resolution.

The form of the instrumental function (response to a δ-function) for a F-P etalon is the Airy function;

$$A(\lambda) = \frac{\tau}{(1+4.N_R^2/\pi^2)} \cdot \frac{1}{\sin^2(2.\pi.n.t.\cos\theta/\lambda)}$$

where;

τ = $(1-k/1-r)$

k = absorptance of each mirror.

r = reflectance of each mirror.

N_R = reflective finesse.

t = plate separation.

n = refractive index.

θ = angle of incidence.

λ = wavelength of radiation.

The effective finesse is defined;

N_e = width of peak/inter order spacing.

The required etalon is characterised by the following parameters which all result from it's plate separation, refractive index of separating medium and the wavelength at which it is to be used ;

i) Free spectral range = Inter order spacing $\Delta\lambda_{ios}$.

ii) Resolution R.

To derive a value for the required plate separation the following relationships are used ;

$$t = n.\lambda/2 \qquad (1)$$

Inter-order spacing;

$$\Delta\lambda_{ios} = \lambda/n \qquad (2)$$

Resolution and Effective Finesse are related by;

$$R = n.N_e \qquad (3)$$

From (1), (3);

$$t = R.\ \lambda/2.N_e \qquad (4)$$

i.e an equation giving the required plate separation for any combination of wavelength, resolution and free spectral range.

As stated bfore, we require;

$$\left.\begin{array}{l} R \sim 10^{4} \\ \Delta\lambda_{ios} > 12\ \text{Å} \\ \lambda \sim 5000\text{A} \end{array}\right\} \quad N > 24$$

Assuming an effective finesse of 30 we need;

$$t \sim 83\ \mu m$$

A measured value for the etalon used was;

$$t = 98.3\ \mu m$$

2.3.3 Finesse.

When working at a particular wavelength "λ" the etalon plate separation "t" defines the order "n". Hence the inter order spacing is defined.

From the definition of finesse it is apparent that it is a measure of the half width of the instrument pass band. It is most important to point out that to improve the finesse does

not affect the energy passed, even though the pass band becomes narrower. Because of this the highest possible finesse is desirable.

There are three separate parameters defining the finesse ;

i) the reflectance "r" of the plates.

ii) the accepted solid angle through the F-P.

iii)the scale and distribution of plate defects.

We can define three separate finesses ; reflective (N_R) , aperture (N_A), and defect (N_D).

The reflective finesse is simply a function of the plate reflectance;

$$N = \pi . r^{\frac{1}{2}}/(1-r)$$

The defect finesse may be most simply be expressed as;

$$N_D \sim m/2$$

where the defects are of scale λ/m. These defects more often seem to be plate bowing or kinks rather than roughness.

The aperture finesse may be defined;

$$N_A = 2.\ \pi/n.\Omega$$

where;

Ω = solid angle of acceptance through F-P.

Hence;

$$N = 2/n.\Delta\theta^2$$

where;

$\Delta\theta$ = range of angles passed through F-P.

Jacquinot, (1954), has shown that to include all the rays from the central spot of the ring pattern and no more ;

$$\Delta\theta^2 \sim 2/R \qquad (5)$$

This has the effect of making $N_A \sim N_R$ which is the most efficient case, (Chabbal, 1953;Jacquinot, 1960).

If the distributions of passed as a result plate reflectivity, range of angles passed and defects can be considered gaussian ;

$$N_e \sim (N_A^2 + N_R^2 + N_D^2)^{\frac{1}{2}}/3$$

The peak transmittance occurs when ;

$$N_R \sim N_A \sim N_D$$

From (5), for R~10,000 we have;

$$\Delta\theta = 14 \text{ mr} \quad (\text{mr=milliradians})$$

2.3.4 Input Optics.

Theoretical studies (Reay, 1969; Bandermann & Wolstencroft, 1969) and previous data (e, g, Hicks et al. , 1974) suggest an upper limit to usable field of view (F.O.V.) to be around 1.5 degrees, (26 mr).

This, together with the largest available size of etalon that will give a defect finesse no larger than the reflective finesse, defines the throughput T;

$$T = A.\Omega$$

where;

Ω = solid angle seen by F-P.

A=area of F-P surface.

Since all apertures are circular it is easier to define a quantity D such that;

$$D = d.\theta$$

where;

θ = divergance of wavefront.

d = diameter of beam.

This is a conserved quantity as a result of throughput being conserved.

Since only 14mr divergence at the F-P is required, the diameter of the input optics should be ~ a factor 2 larger.

The F-P used had a diameter of 80mm. Of this only 76mm was used because of defects around the rim.

A 6inch coelostat was used giving a sky F.O.V. of 28mr (1.6 degrees). FIG.2.3 shows the arrangement of the input optics as used.

The lower limit for the F no. of the coelostat lens is given by ensuring the spherical aberration is small compared to the entrance aperture diameter, (e.g. Longhurst, p.349). F5 was chosen on this basis.

To avoid vignetting a coelostat lens of slightly larger diameter than that of the mirrors was used, together with field lens L2.

2.3.5 The Instrumental Function.

The detected signal, $D(\lambda)$, may be defined;

$$D(\lambda) = \tau_A . \tau_D . S(\lambda) . F(\lambda) * A(\lambda)$$

where;

τ_o = optical efficiency of lenses and mirrors used assuming no vignetting.

τ_D = detector efficiency in the region of λ.

$A(\lambda)$ = Airy function appropriate to etalon used.

$F(\lambda)$ = pre-filter profile.

$S(\lambda)$ = source function, (ZL + bg)

(Note: * denotes convolution).

It is desired to recover $S(\lambda)$ from data which consists of $D(\lambda)$ together with photometric noise and dark count.

The effect of noise may only be minimised by gathering a lot of data.

To remove the effect of $F(\lambda)$ one possibility is deconvolution. (i.e Fourier transform $D(\lambda)$ and divide by the Fourier transform of $F(\lambda)$, then inverse transform the result). This technique suffers from the disadvantage that any noise at high spatial frequency can produce spurious oscillations in the resulting profile.

The method finally used was to simply divide the data by an experimentally derived $(F(\lambda) * A(\lambda))$.

This function must be determined at frequent intervals during observation to null the effects of

interference filter drift.

Whether or not this offers a good approximation depends on the form of both $A(\lambda)$ and $F(\lambda)$. For instance, if $A(\lambda)$ were a δ-function ;

$$A(\lambda) * F(\lambda) = W(\lambda) = F(\lambda) \quad (6)$$

If $F(\lambda)$ is flat over a range much wider than $A(\lambda)$ this situation is approximated.

The pre-filter must not be more than one F-P order wide to avoid inter order contamination. It must therefore be as flat as possible over this range.

A grating large enough to reflect the whole beam would suffer from low luminosity. The best candidate is a multi-cavity interference filter. The flattest profile will result if it is large enough to be placed in the collimated beam with the F-P.

If placed here, any component of the F.O.V. "sees", effectively, the whole filter. This is not the case with the filter in the diverging beam, (which is acceptable when the F.O.V. is small).

A tungsten filament at ~2000 deg.C. can be considered of flat enough spectrum for a "white light" source when measuring $W(\lambda)$, (0.05% per A).

2.3.6 Detector System.

The detector optics is shown in FIG. 2.4.

The most sensitive detector available in the mid-visible is the RCA31403A-02 PMT working at -60 to -70 deg.C.. This tube uses a Gallium-Arsenide photocathode. Some of these, when tested , reveal quantum efficiencies exceeding ~0.2 and dark counts of only a few per second. The tube used was one of these.

The central spot, seen at infinity through the F-P must be brought to focus on the photocathode. Collimator lens L4 and field lens L5 achieve this.

The sensitivity of the PMT is a function of both E.H.T. and pulse height threshold. These were optimised against s/n ratio. s/n was determined using;

$$s/n = S+D1-D2/(S+D1+D2)^{\frac{1}{2}}$$

where;

S+D1 = observed source brightness+dark count.

D2 = dark count (shutter closed).

A beta-light offered sufficient stability for a source.

FIG. 2.5 shows s/n vs. E.H.T for the tube used. FIG.2.6 shows the pulse height distribution, (i.e cumulative).

2.3.7 Blocking of Outer Orders.

The blocking efficiency for the interference filter used is 10^{-5} . This is the only blocking for F-P orders which lie within the domains of both the transmission of glass and detector sensitivity.

Because the bandwidth of the F-P is to be so small, this matter deserves serious attention if in-filling of the line is to be avoided.

Transmission domain for crown glass: 3,000-30,000 Å

Detector sensitivity domain: 1,000-10,000 Å

Using $n.\lambda = 2.t$ it is clear that there are 420 orders blocked only by the interference filter.

Hence, the total energy transmitted and detected from outer orders will be 0.0042/0.33 of that from the principle one. (The transmittance of the filter=0.33 within the bandwidth).

This amounts to 1.2%.

This can be considered negligible compared to the orders within the unblocked region.

For purposes of calculation, a linear blocking function may be assumed from +/- 100 Å to +/- 10 Å from the filter centre of value from 0.00001 to 0.01.

From the 11 orders in this range a total of 16. 5% may be expected. The assumption of linearity may mean that this is an exaggeration.

The contribution of the one remaining outer order lying within +/-10 Å will vary as the F-P scans but could be as much as 2%. The choice of width for the filter must therefore take account of this possibility, and be less than an order wide (14Å for the plate separation used).

Stray light entering the system at any point between the detector and the coelostat will have a similar effect. To inhibit this the entire optical train from the coelostat lens on was sealed, and velvet-on-velvet seats were used for the two hatches, (see FIG.2.7).

2.3.8 The Compensation Channel.

There are several reasons why sky brightness may change during the course of a scan, (passing clouds, patches of dust, extinction at low altitudes). For this reason a compensation channel was included in the design.

A beam splitter was used to reflect about 1-2% of the light along a path perpendicular to the main optic axis. Just before the focal plane the beam passes through a single cavity, 300Å interference filter.

Allowing for the attenuation due to the F-P and the interference filter, the relative sensitivities of the two PMTs

used(RCA 31403A-02 and EMI 6256) and the respective bandwidths, the comp. ch. signal should be about 500X that of the signal ch. .

To avoid possible saturation of the photon counting system an iris diaphragm was situated just in front of the 300A filter, (see FIG.2.3).

2.3.9 Environmental Effects.

2.3.9.1 The interference Filter.

One of the advantages of pulse counting over d.c. techniques for detecting radiation is that it is, for practical purposes, immune to environmental effects.

There are however, still two devices which are not immune.

Because of it's solid construction the interference filter is not susceptible to changes in pressure. The one purchased for this project was also hermetically sealed to protect against humidity variation.

It has a temperature coefficient of ~0.2Å per deg.C., moving to the blue as temperature increases.

2.3.9.2 The Fabry-Perot.

In the case for the F-P, temperature, pressure and humidity all have their effects with humidity dominating.

For air;

$$\Delta\mu = 3.10^{-7} p$$

where;

n=refractive index of air

Since for air ~1;

$\lambda \tilde{.} \Delta\mu = \Delta\lambda \quad (\lambda = 2.t\mu/n)$

Hence;

$$\Delta\lambda = 3.10^{-7}.\Delta p$$

This works out to be ~0.17 Å for 100 mb change.

To deduce the temperature effect ;

$$\frac{dP}{P} = \frac{dT}{T} = \frac{d\mu}{(\mu-1)} = \frac{dt}{t.\ 3.10^{-4}} \quad \text{for air.}$$

This follows from the pressure dependance of refractive index;

$$(\mu-1) = K.P$$

$n.\lambda = 2.\ \mu\ .\ t$ and the fact that $(\mu-1)$ for air is ~ 3.10^{-4}. So for very small changes in temperature ;

$$\frac{\Delta t}{t} = \frac{3.10^{-4}.\Delta T}{293} \qquad (\text{at } 20 \text{ deg.C})$$

$$\sim 10^{-6}\,\Delta T$$

Since $\frac{\Delta\lambda}{\lambda} = \frac{\Delta t}{t}$;

$$\frac{\Delta\lambda}{\lambda} = T.10^{-6}$$

Because of the relatively high value of the refractive index for water any change in moisture content between the plates has a profound effect on the optical path. To ensure the etalon is not sensitive to atmospheric humidity changes it was flushed continuously with a dry gas. Nitrogen was used on account of it's cheapness and availability.

2.3.10 Pulse Counting.

Because of the low count rate expected, (~10-20 Hz), it was possible to use the microcomputer itself as the counter. This technique is limited to count rates below about 50 kHz because the computer requires a pulse duration of not less than 1s. The dead time is approximately twice the pulse width so a non-linearity will begin to become apparent above this value.

All that is required external to the computer is a pulse conditioning circuit. This converts the pulse from the photocathode, (300 V/100 ns for the RCA tube), into a TTL one of adjustable width.

2.3.11 Overall System Configuration.

The electronics is shown in FIG.2.8 and the optical overview in FIG.2.9.

2.3.12 Software Design.

2.3.12.1 Top Down Task Analysis.

One long program written to include all the needs would have very little chance of being understood by anybody, including the author at a later date. It makes for something difficult to write and close to impossible to debug. The correct approach is to write the program as a series of independantly testable modules. Identifying these is the programmer's most difficult task.

Top Down Task Analysis is the process of repeatedly sub-dividing the overall task until arriving at tasks which may be translated into program modules. Such a treatment for the problem of running the experiment described here is shown in FIG.2.10.

2.3.12.2 Structuring.

The requirement of maximum versatility of control dictates that everything that may need alteration while the experiment is in progress be written in a high level language.

All the routines controlling the mode of operation and data storage were written in BASIC . A seperate module for calculation of equatorial co-ordinates from geocentric solar elongation and inclination was also written in BASIC to make use of it's in-built trigonometric functions.

The flow-chart the BASIC program and a listing are depicted in FIG.2.11 and 2.12 respectively.

2.3.12.3 Limitations of Present System.

Because of the limited memory available on the machine used and the slowness of an interpreted language, it was not possble to do on-line reduction. The advantages of doing this have been set out in section 2.2.4.

It would now be possible to buy a system capable of doing this, complete with monitor interface, for the same cost as the one used.

2.4 EXPERIMENTAL METHOD.

2.4.1 Modes of F-P Control.

2.4.1.1 Scan Mode.

The optimum no. of points is the number which will give maximum information per unit integration time.

No more information is available above a limit, set by the resolution, which will be that of changes occurring no

smaller than twice the instrumental pass-band, (sampling thearem). If it is not wished to degrade this then the profile must be sampled at intervals of half the instrumental pass-band.

As discussed earlier reslution is directly proportional to finesse. The sampling interval must be appropriate to the effective finesse. It must also be held constant for ease and consistency of data reduction.

Using (4) and a finesse of 35 (as measured before shipment);

$$\delta\lambda = \frac{\lambda^2}{2.N_e.t} = 0.42\text{Å}$$

For reasons not wholly understood , however, the finesse never reached this value in Tenerife. A value for the sampling interval of 0.26A was used corresponding to exactly 10 steps on the digital input of the CS100 F-P. controller. This was appropriate to finesse of 28, ($\delta\lambda$=0.524Å, R=9885).

25 points of this separation were taken per scan, giving a total scan range of ~6.5Å or just under half an order. This was sufficiently wide to cover the whole line, for any Doppler-shift, over and above that corresponding to the maximum possible radial velocity for parabolic orbits (72Km/s-1.2Å Doppler shift). (See section 2.2.1.)

The integration time alotted each point was 10s giving a total scan time of 4'10s. Any longer would invite accidental fluctuations, such as passage of a cloud through the field of view not to be noticed. Any shorter and the quantity of data generated would get progressively less easy to deal with.

Every individual scan was dumped to audio tape. Scans were grouped and summed by microcomputer and then dumped to digital tape. The size of the group depended on the length of time for which the point could be observed, but was never greater than 10. The data could then be easily inspected using the print out (every scan). Any problems (glitches, malfunction etc.) could thus be identified and if necessary the data on audio tape could be used as back up.

2.4.1.2 Chop Mode.

The method of chopping between the points of inflection of a spectral line can be the most efficient method to gain the lines position to within a given error. Given a natural line profile convolved with a known instrumental profile and multiplied by a known prefilter profile, knowledge of the ratio of two signals equidistant from a position, is uniquely defined. (See FIG.2.13). If the pre-filter profile is

sufficiently flat, a change in the ratio can be used to infer a small shift.

The method is efficient because a small shift gives a maximum signal change at the point of inflexion. If all the integration time is devoted to these 2 points, maximum possible information is gathered in the shortest possible time.

If the pre-filter profile is not obviously flat enough, simulations must be perfomed by computer to derive the ratio values for all possible shifts. This was in fact performed for the interference filter used as a pre- filter on this project.

The integration time to achieve a given error has been calculated for various chop amplitudes using a gaussian to simulate the detected line shape. The curve has a minimum for points either side just below the inflection points. (FIG.2.14)

Unfortunantely the method has two disadvantages for this application.

Firstly, it is expected that the natural line-shape will be distorted due to the way the various contributions add up along the L.O.S.. The degree of distortion itself contains the same information as the shift. Any structure in the line would give information not contained in the shift, (see ch. 3).

Secondly, the method is very sensitive to the pre-filter profile. Should this drift or change during a run

errors occur. These become significant for the drift brought about by a few degrees temperature change. This effect turned out to be seasonal. In winter the profile drifted so that the natural line position lay near the filter's edge, making the situation worse.

The first objection removes much of the incentive for combating the second.

The chop mode was used with some success, however on the Gegenschein. This L.O.S. is not expected to present a distorted profile and is best observed in the middle of the night when temperature drifts are small.

2.4.1.3 Dynamic Chop Mode.

This is similar to chop mode but the mean position of chop moves so as to null the ratio. It suffers from the same objections as the chop mode and is less efficient.

Although the first one or two ratio measurements can be of comparatively small integration time, the total required to achieve a given precision is still greater.

The fact that it gives an easier job of reduction makes it suitable for bright sources however.

It was not used in the end and is mentioned only for completeness.

2.4.2 Calibration.

2.4.2.1 Absolute Calibration.

Hollow cathode lamps were used for their stability for both absolute and scale calibrations, (the MgI line in emission for absolute and a Zn line ~1. 6Å away for scale calibrations).

The beam is directed via the beam splitter, (flip mirror for the fainter line of the Zn lamp used for scale calbn.), onto a ground glass diffuser. This ensures uniform illumination of the entrance aperture, (FIG.2.15).

Asymmetric illumination results in a partially skew beam through the F-P and thus an asymmetric observed profile, i.e an erroneous calibration.

Absolute calibration was performed continually for 1-2 hours before commencing observation for an evening and repeated before and after every group of scans. The longest period between was thus ~45 mns. , (10 scans).

Since the profile of the emission MgI line from the, (cool), lamp may be thought of as a δ-function, the recorded spectrum is the instrumental function at that wavelength. The mean of the half intensity points was taken for line position.

The peak position therefore gives an indication of profile skewness, (e.g. as may be caused by F-P plate deformation or misalignment).

In this way, absolute calibration was obtained to +/- 0.03 Å, (~2 km/s), precision.

2.4.2.2 Scale Calibration.

Because of the high stability of the F-P controller, the scale calibration was not expected to change significantly.

Throughout the 3 years of use so far no detectable change has occured.

No. of CS100 steps between lines= 62 +/- 0. 5

Difference in wavelength between lines= 1. 623 Å

Hence;

Change in wavelength per step= 0. 262 Å

The instrument scanned from red to blue as the step no. output to the CS100 increased.

Scale calibration was performed nightly on the first two observing trips, but only once on each one subsequent.

2.4.2.3 Dark Count.

The dark count was determined by putting black cloth between the coelostat lens and the coelostat itself and then allowing the instrument to perform ten 10s integrations.

In this way stray light entering the system from the

room was also accounted for. Comparisons revealed, however, that only 1/2 - 1 Hz originated from sources other than dark count.

Dark count would be ~5 Hz at the start of an evening decreasing, after the tube had been cool for 1-2 hours , to 1 - 2 Hz.

This would be performed three times nightly, once it's stability had been established.

100s total integration time gives a standard error of ~ +/- 1 Hz (assuming Poissonian statistics).

2.4.2.4 Pre-Filter Position.

As detailed in section 2.3.5 a scan is required of a white light source, (tungsten filament).

At the end of every group of scans the tungsten lamp was scanned across an entire order.

These data was only used to determine the filter position since it was considered more accurate to use a high resolution filter scan (performed using the Astronomy Group's Ebert spectrometer, see FIG. 2. 16) convolved, by computer, with an Airy function of correct finesse.

The uncertainty in line position resulting from an incorrect filter position constitutes a systematic error on a particular group of scans. However, on combination of many groups of scans it is possible to consider this error random, (see section 2.5.4).

2.5 ERROR SOURCES.

2.5.1 "Shot" Noise.

"Shot" noise is the uncertainty of the result of counting events each having equal probability per unit time of occurence. Such events obey Poissonian statistics.

For large counts, ($N \gg 1$), the distribution of probabilty for obtaining a particular result is very close to a normal distribution of standard deviation;

$$\sigma = N^{\frac{1}{2}}$$

For the effect of the photometric error resulting from shot noise see either section 2.2.3 or 3.5. 2.3.

2.5.2 Calibration Errors.

When results are combined for many groups of scans (frames) the absolute calibration errors add up as random errors. As pointed out in section 2.4. 2.2, the error due to scale calibration is negligible.

2.5.3 Sky Background.

Of the 3 components of sky background, starlight, airglow and scattered light, the first two simply contribute noise since they are sufficiently constant in both time and wavelength. Unfortunately , when taken together they are of similar luminence to the ZL.

From section 2.2.3;

$$T \propto (1+2.\ bg)^2$$

Hence 4X the integration time is required, for a given D/S precision, over the case where the background illumination is negligable.

Scattered light also acts in this way, but it can also vary with time.

This can be due to changes in the scattering material concentration in the L.O.S. or just changes in the L.O.S. with respect to the scattering agent.

For instance when the L.O.S. is near to the horizon, scattering from clouds buildings, haze etc. varies quickly with altitude. The compensation channel offers one way of removing such effects. However, the quality of the data is still reduced because the noise level is no longer constant throughout the scan. Greater reliance was always attributed to data not suffering from this problem.

2.5.4 Systematic Error due to Reduction Method.

The reduction method eventually used when applied to the un-shifted solar Fraunhofer line, produces a small error. This was determined by using the Delbuie atlas for the source profile, convolving it with the instrumental function and applying the reduction program. The result was +0. 052Å (one instrument step) shift, which was subtracted from all results since it constituted a systematic error.

Daysky runs (where the instrument was pointed at the sky via a large wad of Kleenex) confirmed this figure to within +/- 0.03 Å (one instrument step)

2.5.5 Pre-filter Drift.

Simulations using the Astronmy Group's PDP-11 minicomputer facility were undertaken to determine errors due to filter drift. They were of two kinds.

Firstly, the assumption was made that, although it had drifted, its position was known. The error was then purely the result of the filter not being flat-topped. Results are shown in FIG.2.17.

Secondly, it was assumed that the psition of the filter used for dividing out its effect was in error. Results for these runs are shown in FIG.2.18.

The first set of results constitute a systematic error and were accounted for in reduction. They are in any case small compared to statistical errors.

The second set shows a much more serious situation demontrating the need to locate the filter as accurately as possible, (to within +/- 0.2 Å or 1.0 deg.C for our target accuracy of 0.03Å Doppler-shift error).

2.6 OBSERVING TRIPS.

2.6.1 Site and Facilities.

The site used was the Observatorio del Teide, Tenerife in the Canary Islands. At an altitude of ~10,000 feet, it lies above an inversion layer for most of the time.

It's lattitude of ~27 degrees means that the Zodiacal cone lies within a few degrees of the vertical in September, (morning ZL), and April, (evening ZL), at the respective equinox, (see FIG.2.19). The evening ZL is rather more clean than that of the morning since it appears over the sea. The morning ZL rises over the north west coast of Africa which often presents a dusty, cloudy horizon.

Supplies of consumables (gas, food etc.) are within easy reach from this site as are technical facilities at the

Instituto del Astrofisica de Canaries at La Laguna, (20 km).

There are, however, two problems with this site.

Firstly, there is a T.V. station, atop the peak adjacent to the observatory , fitted with anti-terrorist lights of considerable power. Diffuse reflections of these from other buildings and overhead dust raise the scattered light component for low elongation observatons. As a result the majority of the low elongation work was done on the evening ZL which suffered less, (the lights lay to the northeast).

Secondly, large clouds of dust would blow overhead from the mainland deserts. This constitutes a more serious problem for two reasons:

Although not causing serious extinction, it did act as a major source of scattered light, particularly that originating with the T.V. station.

The second reason, and most damning, was that this dust was often patchy giving a scattered light component varying with time and L.O.S. .

Despite these problems, excellent observing conditions often prevailed. A total of 42 nights spent there were usable.

2.6.2 Trips in 1981.

Three trips were made in 1981, each of three weeks duration. The first was in April to install and set-up the

instrument. As a result of some minor modifications and some repair needed to the original photon oounting system used, (Brookdeal 5C1), which was subsequently replaced with the system described in section 2.3.10, relatively few observations were made.

The only other problem encountered of any weight was a drift of the absolute calibration of up to 1/100 th of an order per hour, (~10X that expected).

This did not seriously affect results as calibration was simply performed more often, (wasting some time). It was not possible to attribute the drift to temperature or pressure variation and it remained till July, 1982 to find the cause.

2.6.3 Trips in 1982.

Once again three trips were made in 1982. One in April of three weeks and two, each of two weeks, in July and September.

In April it was found that the acid dust on site, (the region is volcanic), had corroded somewhat the protected silver coatings of all the three coelostat mirrors. After cleaning with a mild soap solution it was found that the observed sky count rate had fallen by only about 10%. The mirrors were returned to England and were recoated.

The F-P seemed not to have wintered too well either.

An extra kink was noticed on rendering the plates parallel while setting up. The finesse was reduced to 23, (from ~28).

The finesse improved towards the end of the trip and was back to normal again in July. This change can be attributed to absorption of moisture by the plate coatings over winter when the site is dampest. The outgassing of moisture from such coatings appears to be rather slow.

Also, in July , it was found that the gas supplied as dry nitrogen was anything but dry. (One bottle even arrived with an Oxygen identity tag!). The matter was taken up with the suppliers via the Institute and no further drift problems have been experienced since.

Drift is now only ~1/600 order per hour, requiring less frequent calibration and thus more integration time.

One further problem encountered in July and, (to a lesser extent), in September was an unusually extensive and high dust cloud overhead. This persisted throughout the July trip but was noted for only about 1/2 the September one. (A change in prevailing wind direction seemed to clear the sky).

The persistance and altitude of the dust was conistent with a volcanic origin. An eruption of a volcano in Mexico early in 1982 may have been responsible.

CHAPTER THREE

DATA REDUCTION

3.1 INTRODUCTION.

This chapter sets out to describe and justify the methodology used to derive from the data quantities which can be tested against models of the Zodiacal dust cloud.

A discussion is included of the effect on results of noise and errors present in the data.

3.2 COMPOSITION AND SCOPE OF DATA.

Virtually all the data is composed of scans of the MgI5183. 6$\mathring{A}$ Fraunhofer line observed along along different elongations. Each scan is composed of 25 points 0. 262 $\mathring{A}$ apart.

The registration, (point corresponding to MgI line position), is recorded digitally together with dark count, integration time, elongation, date, calibration error and pre-filter position. Time and approximate altitude of L.O.S. is also recorded separately in a log book.

Chop data is recorded differently. Chopping was only performed successfully on the Gegenschein and the data was simply recorded in the log book, (one data point merely

consistng of a ratio plus the ancillary information above).

The scope of the data set lay entirely in the ecliptic plane. This is the case most easiy interpreted in terms of the properties of the dust cloud and was thus of most immediate importance.

3.3 RAW DATA PROCESSING.

3.3.1 First Steps.

The data were passed to the digital cassette recorder in the form of a two line header plus twenty-five lines of data. Each header contains the following information;

Run no. ; Elongation; Day; Month; No. of scans; Total dark count; Calibration point; Calibration error; Pre-filter position.

Each following line contains the following information;

Scan position; Sum of signal ch. counts; Sum of compensation ch. counts.

Data were brought back to London in the form of a digital cassette. (They have ~1.0 Mbytes capacity which was

sufficient for any observing trip).

All reduction was eventually done on the Astronomy Group's PDP-11 minicomputer facility.

Although only Fortran 66 is available on the PDP, the latter's ease of use , versatility and availability made the task of reduction far easier and quicker than it would have been using the college mainframe computer.

Transfer of data to the PDP was much simplified since the digital cassette recorder can be connected directly.

An initial "weeding" of the data was performed, using an editor, to remove the occasional mains glitch. From July(1981) onwards mains filters were used on-site which successfully reduced these in number by a factor ~100, (down to a few per trip).

Where a glitch was found it was replaced by the mean of the two points adjacent.

3.3.2 Corrections.

3.3.2.1 Dark Count.

For each frame the dark count is stored in the header. It was thus a simple matter to subtract it from the signal channel count for the whole data set. The first routine in the pre-reduction program listed in FIG.3.1 takes care of this.

3.3.2.2 Extinction/Twilight.

Frames which were acquired from low elongations may need correction for variation in atmospheric extinction and/or twilight onset. This is accomplished in the pre-reduction program by dividing the signal counts by the corresponding comp. ch. counts, (the latter having been normalised).

3.3.2.3 Pre-filter Profile.

The pre-filter position relative to a fixed wavelength is recorded in the header. To remove the effect of the filter profile the signal ch. waveform was simply divided by the filter profile, (see section 2.4.2.4).

The error resulting from uncertainty in the filter's position was determined by simulations, (see section 2.5.4) and combined with the calibration error in the header, (the existing value being the error resulting from drift between absolute calibrations).

3.4 THE REQUIREMENTS OF A REDUCTION METHOD.

3.4.1 Assumptions.

Any assumptions which may safely be made constitutes extra information available and should be used. For example, a good approximation to the natural line profile convolved with the instrumental (Airy) function is a gaussian.

It may also be safely assumed (for the compensated data) that the sky background is constant over the frame. Subtraction of this is unecessary for most purposes since it does nothing to change the s/n ratio. It does prove helpful, however for assessing the line profile by eye.

3.4.2 Output.

Any quantity resulting from a process of reduction must be one which can be tested by theoretical calculations.

In the case of Doppler-shift, it is usually the centre of gravity which is taken as the indicator of position in theoretical calculations. Hence any Doppler-shift derived from the data must be identifiable with that.

It is also essential that the reduction technique include a derivation of the error resulting from the uncertainties inherent in the data. This must refer to a confidence interval for the correctness of the result.

3.5 DOPPLER-SHIFT DERIVATION.

3.5.1 Centres of Gravity.

The centre of gravity can be defined as;

$$\langle\lambda\rangle = \int_{L_1}^{L_2} \lambda . Y_\lambda . d\lambda \; / \; \int_{L_1}^{L_2} Y_\lambda . d\lambda \qquad (Y_\lambda = \text{Intensity at } \lambda)$$

L_1, L_2, are limits chosen to be the extent of the observed line profile for any plausible Doppler-shift.

A routine using finite difference methods in the maths library that forms part of the PDP-11 user system was used for the integrations. The method detailed in section 2.2.3 was used to derive the error.

The technique was used on the solar Fraunhofer line convolved with the instrumental function to determine the true zero of derived Doppler-shift and then applied to the data.

A disadvantage of this derivation is that, to take account of all possible shifts, a bandwidth must be used which is larger than the width of the line. This adds noise and hence increases the error as can be seen from the error treatment given in section 2.2.3.

There are two other major problems with the method:

Firstly, because Y_λ appears twice, the error is root 2X the case where it is only used once.

Secondly, the method fails the criterion set out in section 3.4.1 in that it fails to give weight to points in proportion to s/n ratio.

There is also the objection that 2 integrations take twice as long as one. The extra time taken does not recommend itself to real-time data reduction which it is intended to introduce at a later stage.

The centre of gravity technique has been discussed

here because it was the technique used initially on this project and because it is useful as a standard by which to judge other methods.

3.5.2 Cross-Correlation.

3.5.2.1 Description.

A method is required which uses all the information in the data in the optimum way.

Such a method, known as cross-correlation, defines a quantity $So(\lambda')$ where;

$$So(\lambda') = \int_{-\infty}^{\infty} S(\lambda).F(\lambda-\lambda').d\lambda \qquad (1)$$

where;

$S(\lambda)$ = function to be processed. (Here it refers to the line profile).

$F(\lambda)$ = a function as near equal in shape as possible to $S(\lambda)$, (the reference function).

If $F(\lambda)$ is equal in shape to $S(\lambda)$ then (1) amounts to the same as subjecting $S(\lambda)$ to a matched filter, (one of profile $FT(F(\lambda))$ spatially).

A matched filter is one which maximises the s/n ratio for white noise, where the signal is taken to be;

$$E^{\frac{1}{2}}=\left(\int_{-\infty}^{\infty} S^2(\lambda).d\lambda \right)^{\frac{1}{2}}$$

The filter essentially allows no greater part of the noise spectrum through than is unavoidable in passing the signal.

It is safe to assume the presence of white noise here.

It is important to note that for one value of λ' values of S for all λ are used. They are also made use of each with the optimum weight.

It is quite safe to use the peak of the cross-correlation function as an indicator of line position be cause that one point is arrived at using all the available data in the best possible way.

This method also posesses the advantage that it involves only one integration and is hence both simple and fast to calculate.

Taking account of noise (1) should properly become;

$$So(\lambda') = \int_{-\infty}^{\infty} (S(\lambda) + n(\lambda)).F(\lambda - \lambda').d\lambda \qquad (2)$$

To examine the effect of (photometric) noise, from (2);

$$So(\lambda') = \int_{-\infty}^{\infty}(S(\lambda) + n(\lambda)).F(\lambda - \lambda').d\lambda$$

$$= \int_{-\infty}^{\infty}S(\lambda - \lambda').F(\lambda - \lambda').d\lambda +$$

$$\int_{-\infty}^{\infty}n(\lambda).F(\lambda - \lambda').d\lambda \qquad (3)$$

The second term may be approximated by;

$$\left| \int_{-\infty}^{\infty}n(\lambda).F(\lambda - \lambda').d\lambda \right| \sim \left(\int_{-\infty}^{\infty}\sigma^2.F^2(\lambda - \lambda').d\lambda\right)^{\frac{1}{2}} \qquad (4)$$

where;

σ = standard deviation of $S(\lambda)$.

The problem is that this estimate cannot strictly be used in $So(\lambda')$, arrived at from discrete data, to derive an error in peak position because the nearby values are not sufficiently independant. To do so will overestimate the error.

Since the case was an overestimate and not the reverse this method was originally used. This matter will be returned to in section 3.5.2.3.

3.5.2.2 Choice of Reference Function.

Because the data were only available over a limited range and the integral in (1) is infinite, it is better to choose a reference function which goes to zero in the wings.

This restricts the range of integration needed to that scanned. A gaussian was found to be a close enough approximation and offered ease of computation.

Since a gaussian is symmetric about it's minimum, the cross-correlation is the same as a centre of weight calculation, if $S(\lambda)$ is asymmetric.

The centre of $F(\lambda)$ was chosen to be equal to the position of zero shift. Hence the peak of $S_o(\lambda')$ will be a direct indicator of it's magnitude.

This point was assumed to be equal to the published value for the MgI line, (M.I.T. wavelength tables). A small correction was necessary to the results because of the slight asymmetry in the Fraunhofer line profile. This correction was determined by taking the Fraunhofer profile from the Delbuie solar atlas, convolving it with an appropriate Airy function and then applying the reduction routine.

FIG.3.5 shows a listing of the program for computing both shift and error using this method.

3.5.2.3 Error on Peak Position Resulting from Photometric Noise.

If the second term in equation (3) is considered alone, it can be seen that the matched filter acts as a low-pass spatial filter. (For a spatial frequency such that many ascillations occur over the width of $F(\lambda)$, the second term will be zero. Only spatial frequencies such that incomplete

cycles occur over the width of $F(\lambda)$ can contribute). Only noise of spatial frequency below $\sim 1/\Delta\lambda$ will pass, where $\Delta\lambda$ is the F.W.H.M. of $F(\lambda)$.

This follows from $F(\lambda)$ being a gaussian. The Fourier transform of a gaussian is another one of width approximately the reciprocal of the first.

Another way of looking at this is to first consider the noiseless case and then add in noise of gradually increasing spatial frequency. As each elemental band of frequencies is added the whole $So(\lambda')$ curve moves up or down without altering the position of the peak used to infer the shift.

It is this view which suggested an answer.

Were a shape to be used, different to that of a gaussian, in such a way that the value deduced for the shift did change on addition of noise it is perfectly justifiable to use the uncertainty in So to infer the error in shift.

If the form of $F(\lambda)$ is antisymmetric when it is centred on the centre of weight of $S(\lambda)$, a shift up or down in $So(\lambda')$ due to the introduction of noise will change the zero crossing point and hence the value of the deduced shift, (see FIG 3.20).

The form chosen is just the differential of the gaussian used previously;

$$F'(\lambda) = \frac{dF}{d\lambda} = \frac{2.(\lambda_o - \lambda)}{R^2}.\exp -\frac{(\lambda - \lambda_o)^2}{R^2}$$

where;

$$R = \Delta\lambda / 2.\ (\log_e 2)^{\frac{1}{2}}$$

$\Delta\lambda$ = F.W.H.M. of $F(\lambda)$

To use this function in place of F still is equivalent to use of a matched filter since the result $So'(\lambda')$ can be shown to be equivalent to the differential of $So(\lambda')$, (see Appendix 3.1).

The error on $dSo'(\lambda')$ can be shown to be approximated by ;

$$\varepsilon' = \sigma\left(\int_{-\infty}^{\infty} \frac{dF(\lambda)}{d\lambda}^{2} .\ d\lambda\right)^{\frac{1}{2}}$$

where;

σ = standard deviation of the data.

This presents no computing difficulties, (no singularities etc.).

A program which computes Doppler-shifts and their errors using this method is listed in FIG.3.6.

To summarise the method;

$$So'(\lambda') = \int_{-\infty}^{\infty} S(\lambda).F'(\lambda' - \lambda).d\lambda$$

such that;

$$So'(\lambda'_e) = \sigma\left(\int_{-\infty}^{\infty} F'^{2}(\lambda)\ .d\lambda\right)^{\frac{1}{2}}$$

λ_e is found by a simple search routine, (see listing).

Results are shown in FIG.3.7 to 3.13 inc., and are

tabulated in FIG.3.14 to 3.19 inc..

3.5.3 Derivation of a Doppler-shift from a Chop Ratio.

The chop ratios for various shifts were calculated by computer simulation .

To find the shift corresponding to a particular ratio was then achieved by a simple search and then cubic interpolation.

A program for doing this is listed in FIG.3.21.

3.5.4 Combination of Results.

Since there were many frames , each relating to one elongation, a way to combine these results had to be found.

The principle of least error predicts that the best way to combine a set of results X with associated errors is as follows;

$$X_c = \frac{1}{\sum_n \sigma^{-2}} \cdot \left(\sum_n (X_n / \sigma_n^2) \right)$$

$$\sigma_c = \frac{1}{\sum_n \sigma^{-2}}$$

where X_c and σ_c are the best estimates of the result and it's standard error, (e.g. Barford, 1967).

The frames were combined in two separate ways: First, those of equal elongation on a range 0 to 360 degrees, and second on a range 0 to 180 degrees.

A listing of the program used to perform this function is given in FIG.3.22.

3.6 LINE PROFILE INFORMATION.

A higher photometric accuracy than that acquired to date would be needed to enable estimates of breadth, skewness or chi-squared fits to model predictions to be of much value.

The only purpose to deriving line profiles from the data at present is to look for structure such as may be brought about by, for instance, dust streams or any pronounced inhomogeneities.

Since there were several groups of scans for each elongation, the absolute calibration point being different for each, resampling was necessary in order to recover an overall profile.

If $g'(n.x)$ represents the intensity at each sample point then the continuous spectrum may be given by;

$$g(\lambda) = \sum_{n}^{\infty} g'(n.x).r(\lambda - n.x)$$

where;

$r(\lambda)$ = a sinc function whose zeroes occur at intervals

of x.

This represents the ideal case since it requires an infinite summation

Truncating this summation may result in oscillations in $g(\lambda)$.

However, if a truncated sinc function is used, the summation need only cover it's domain.

The reason the ideal function is a sinc function is that it's Fourier transform is a "top hat" of width 1/x. It thus acts as a low pass filter passing all spatial frequencies less than 1/x. Any frequencies greater than 1/2.x are said to be aliased.

It is therefore necessary to find a function which is in effect a truncated sinc function and has a Fourier transform that includes as much as possible up to spatial frequency 1/x, and as little as possible beyond it.

Such a function has been synthesised for reduction of Landsat data and will serve well, (Bernstein, 1976). This function and it's F.T. are depicted in FIG.3.28 and 3.29 respectively.

A program using this function for recovery of line profiles is listed in FIG.3.27.

Some sample profiles are shown in FIG.3.23 to 3.26 inc..

3.7 COMPUTING.

All the programs were written and run on the Astronomy Group's PDP-11 facility in Fortran 66, (Fortran 4).

All programs were intended to be as self-documenting as possible.

CHAPTER FOUR

INTERPRETATION OF RESULTS

4.1 MODELLING THE ZODIACAL CLOUD.

4.1.1 Preamble.

The net Doppler-shift of a Fraunhofer line observed along a particular L.O.S. depends on many variables, none of which are known with certainty.

Because of this it is necessary to establish models of the Zodiacal cloud against which the results presented in ch.3 may be tested. In order that a fit may be more easily searched for, the model must be parameterised well. It is beneficial if these parameters have a real physical meaning.

It has, however, been found possible to make limited empirical deductions about the particles responsible for the ZL.

Other information present in the data is discussed in section 4.3.

A summary of conclusions made is given in section 4.4.

The models used must define;

i) the distribution of particles in both size and space,

ii) the properties of the particles themselves.

For the present purposes it is not necessary to define the nature of the particles, but merely their properties. For instance, it is necessary to define their VOLUME density but not that of their constituents. Another example will be discussed in section 4.2.4 where it is found to be impractical to calculate the radiation pressure efficiency for a truly realistic particle model. It IS possible, however, to either use an empirical value for this coefficient or a particle model which might have similar optical properties.

Model complexity has been kept no greater than was felt necessary to obtain agreement with observation.

The major simplifying assumption employed has been the independence of particle properties, size distribution and orbital distribution. There is some evidence that this may not be entirely valid, (see section 1.3.3). Such evidence would also be present in the D/S data. None was found however.

An excellent review pertinent to this chapter is given by Burns, Soter and Lamy, (1979).

4.1.2 Parameterisation of Particle Distribution in Space.

The distribution of particles in space may be defined in two ways;

i) the distribution of orbits,

ii) the distribution of number density.

These two are related via the Haug integral, (Haug, 1957);

$$n(\rho,z) = \frac{1}{2\pi^3\rho} \int_a \int_e \int_i \frac{N(a,e,i).da.de.di}{r^2.\left(\frac{a}{r}\right)^{1.5}.\left(2-\frac{r}{a}-\frac{a}{r}.(1-e^2)\right)^{\frac{1}{2}}.\left(\sin^2 i-\frac{z^2}{\rho^2}.\cos^2 i\right)^{\frac{1}{2}}}$$

which reduces to, (see appendix 4.1);

$$dn(r) = r^{-\nu}.\frac{n_i(i).di}{\sin i}.\frac{n_e(e)}{(1-e^2)^{1.5-\nu}}.(1 + e.\cos v)^{1-\nu}.dv.de$$

for particles in the ecliptic plane.

It is clear that, for interpretation of any observations of the Zodiacal cloud (ii) is to be preferred, but any model will be in terms of orbital distribution. This is because any assumptions made about the particles' origin and/or forces acting on them will lead to predictions about the effects on their orbits and not their number density function.

The derivation of (1) has made the assumption that N(a,e,i) is separable such that;

$$N(a,e,i) = n(a).n(e).n(i)$$

and that n (a) obeys a simple power law;

$$n(a) = C_1 r^{2-\nu}$$

where;

C_1 = const.

In order to make calculations as simple as possible, it is of value to make the forms of n (a), n (e) and n (i) no more complex than needed.

Choosing a power law for n (a) has the advantage of implying the same form for n(r). n(r) is a directly measurable quantity now, and this can thus be taken full advantage of.

The form chosen for n (i) was, (Singer & Bandermann, 1967);

$$n(i) = \sin i \cdot \exp(-q.i)$$

i.e. giving a single parameter "q".

Since this means that the number of possible orbits tends to zero as "i" tends to zero, this expression is

reasonable.

A narrow gaussian distribution was chosen for n (e). This might enable an upper limit for eccentricity to be established more easily than if a wide spread were considered, (nothing is known about the form of n (e) in any case).

$$n(e) = \exp -(e-e_m)/0.0144$$

where;

e_m = mean value of "e".

This gives a distribution of F.W.H.M. 0.2.

The parameters required to fully specify the model of particle distribution in space are then;

$$\nu, q, e$$

4.1.3 Parameterisation of particle size distribution.

The publication of lunar micro crater size distributions, (Horz et al., 1975; Morrison & Zinner, 1977; Fechtig, 1976), and their subsequent conversion to those of mass, have led to various interpretations of size distribution, (Giese & Grun, 1976; LeSergeant & Lamy, 1978). The latter differ chiefly in choice of density. In the case of the model of LeSergeant & Lamy a different density is assigned to

submicron, particles which leads to an increase in their predicted number density.

All show that a series of power laws for successive size ranges is a realistic approximation to use.

Hence the parameter set to fully describe a size distribution model is;

$$z\ ,p\ ,c$$

where;

$$dn\ (z) = n\ (z).dz$$

$$= c_i.z^{-p_i} \qquad z_j < z < z_{j+1}$$

is the number of particles with radius between "z" and "z+dz".

4.1.4 Parameterisation of Particle Properties.

The nature of a particle may be fully described by it's;

i) composition,

ii) morphology/shape,

iii) charge.

As will be seen in section 4.2.4 the only properties that affect the prediction of Doppler-shift along the L.O.S.

are;

i) scattering efficiency at the wavelength of observation,

ii) radiation pressure efficiency at the wavelength of observation,

iii) density.

Were the particle a homogeneous sphere (i) and (ii) would be directly calculable, using Mie theory, from complex refractive index.

it now seems very unlikely that homogeneous spheres offer a usable approximation. Much better agreement for the observed volume scattering and polarisation functions is obtained with aggregate structures, (Giese et al., 1978; Greenberg & Gustafson, 1980). These also would share a resemblance to Brownlee particles, (Brownlee, 1978). Evidence for the origin of these is discussed by Bradley, Brownlee and Veblen, (1983).

As a result of all this, there are two possible approaches.

Firstly, there is an empirical one.

The following assumptions must be made;

$$Qsca,\ Qrp = 0 \qquad x < X$$

$$= \text{constant} \qquad x > X$$

where;

Qsca = mean scattering efficiency for the particles.

Qrp = mean radiation pressure efficiency for the particles.

$$x = 2.\pi.z/\lambda$$

λ = wavelength .

In the case of Qsca, λ refers to the wavelength of observation whereas in the case of Qrp it refers to any value.

Hence finding Qsca as a functionof size is easy. To find the effect of Qrp as a function of size, since all wavelengths contribute to the effect of radiation pressure, an integration over the whole solar spectrum would normally be performed;

$$\langle Qrp \rangle(z) = \left(\int_0^\infty Qrp(x).f(\lambda).d\lambda \right)_z$$

where;

$f(\lambda).d\lambda$ = normalised relative intensity of solar output at λ.

Given the above assumption for the radiation pressure efficiency, the expression for $\langle Q_{rp} \rangle(z)$ becomes;

$$\langle Q_{rp} \rangle(z) = Q. \int_0^{2\pi z/X} f(\lambda).d\lambda$$

where;

Q = radiation pressure efficiency for large particles.

Since most of the solar radiation occurs at wavelengths less than one micron, the integral in the above expression approaches unity for large particle sizes.

To use this approximation for Qrp is reasonable if, for the particles responsible for the ZL and the wavelength of observation;

$$X \gg 1$$

(v.d. Hulst suggests x >>10 is sufficient).

FIG.4.1 shows the cumulative brightness as a function of particle size for the size distribution models of Giese & Grun and LeSergeant & Lamy.

This was derived using an approximation for Qsca as follows;

$$Qsca \propto z^2 \qquad x < X$$

$$= \text{constant} \qquad x > X$$

The expression used was;

$$B(z_1) = \frac{\Sigma_i \left(\int_o^{z_1} Qsca(z).z^{2-p_i}.dz \right).c_i}{\Sigma_i \left(\int_o^{\infty} Qsca(z).z^{2-p_i}.dz \right).c_i}$$

A value for X of 2 was chosen from inspection of the results published by Wickramasinghe, (1973), for homogeneous spheres using Mie theory, (see FIG.4.14).

It is clear that only a negligible proportion of the ZL originates from particles with x <10, (z <0.8 m), if either of the Giese & Grun models is correct, whereas in the case of the LeSergeant & Lamy model some 40% does so. It will be shown in section 4.2.3, however that the latter is inconsistent with the results presented in ch.3.

It is clear, then, that the approximation, for either efficiency, is reasonable.

From v.d.Hulst, (1957);

$$Q = 1 - g.\gamma$$

where;

γ = particle geometric albedo

ρ = " volume density

g = mean value for the cosine of the scattering angle.

The parameters needed may be summarised;

$$\gamma , \rho , g$$

The second approach is to define the refractive

index, (c.r.i.), and assume that the particles are optically equivalent to homogeneous spheres. In this case the values for efficiencies may be taken from those published by Wickramasinghe, (1973).

The parameters needed may thus be summarised;

c.r.i, ρ

NOTE: The effect of solar wind is not accounted for here.

The solar wind carries with it only ~0.0001X the momentum of the radiation. On the other hand, if a particle carries a charge it's cross section increases for interaction with another (oppositely) charged particle. This may render the effect important for small particles at least,if the charge carried is sufficient.

Burns, Soter and Lamy, (1979), conclude that this effect is negligible for particles of radius greater than ~0.1 μm. Lafon, Millett and Lamy, (1980), offer the same conclusion, but Mukai & Yamamoto, (1980), believe it to be important for those up to ~100μm.

A conclusion seems unlikely until reliable, comprehensive data on particle charge are available.

4.2 THE PREDICTION OF DOPPLER-SHIFTS FROM VARIOUS MODELS.

4.2.1 Circular,Keplerian Orbits Confined to the Ecliptic Plane.

4.2.1.1 Derivation of the Expression for Doppler-Shift vs Elongation.

The following neglects the effect of radiation pressure.

From FIG.1.2 it may be seen that the Doppler-shift of a particle at distance "r" from the sun,lying along the L.O.S. of elongation is given by;

$$\Delta\lambda = +/-\frac{\lambda}{c}(V_e.\sin\varepsilon - V_p.\sin\theta)$$

where;

Vp = orbital velocity of particle

Ve = orbital velocity of the Earth

+/- refer to the shift in the morning and evening respectively.

Now;

$$Vp = Ve/r^{\frac{1}{2}}$$

if "r" is in A.U. and, from FIG.1.2;

$$r = \sin \varepsilon / \sin \theta$$

So;

$$\Delta\lambda = +/-\frac{\lambda}{c}.\sin \varepsilon.(1 - \sin^{1.5}\theta.\mathrm{cosec}^{1.5}\varepsilon)$$

The expectation value for the Doppler-shift for a particular L.O.S. corresponds to that observed, and may be written;

$$\langle\Delta\lambda\rangle = \frac{\int \Delta\lambda.ds}{\int ds}$$

where dS is the elemental brightness due to particles which have sizes between "z" and "z+dz", and which are found at the point defined by radial distance "r" from the sun, elongation "ε" with scattering angle "θ". dS may be written

$$ds = dn(r).s(\theta).dn_z(z).Qsca.z^2$$

After some reduction, (see appendix 4.1 for expression for n(r)), the expression for $\langle\Delta\lambda\rangle$ for this model is;

$$\langle \Delta\lambda \rangle = +/- \frac{\lambda . V_e . \sin \varepsilon . (1 - \mathrm{cosec}^{1.5} \varepsilon . I_1 / I_2)}{c}$$

where;

$$I_1 = \int_{\varepsilon}^{\pi} \sin \theta . s(\theta) . d\theta$$

$$I_2 = \int_{\varepsilon}^{\pi} \sin \theta . d\theta$$

As may be seen, in this case $\langle \Delta\lambda \rangle$ is only a function of;

i) radial distribution

ii) scattering function

A program written to derive Doppler-shift vs. elongation for this model is shown in FIG.4.2.

4.2.1.2 Dependence on Scattering Function.

FIG.4.3 shows the form of the variation of Doppler-shift with elongation for two different scattering functions;

i) isotropic,

ii) volume scattering function (VSF) derived by Leinert et al., (1976), from Helios data.

In the isotropic case, the Doppler-shift is independent of albedo.

Diffraction is not considered as it is a negligible effect for elongations greater than 25 deg., (see FIG.4.4).

In the second case it has been assumed that all particles have the same scattering function, independent of size, and hence equal to the VSF. This is perhaps not such a bad assumption because it seems, as concluded in section 4.1.4, that the greater part of the ZL originates from particles for which $x>>1$.

Any reasonable form of scattering function will be close to constant over the range $30< \theta <150$ degrees. (An enhancement for backscattering is unimportant for all but the Gegenschein, since the contribution from large scattering angles is always from points farthest from the sun).

4.2.1.3 Dependance on Radial Distribution.

FIG.4.5 shows the form of the Doppler-shift function for three different values of the index ν;

i) 1.3 (Helios results for inner solar system Leinert, (1980)).

ii) 1.0 (Pioneer 10/11 results for outer solar system, (Humes et al., (1974))

iii) 1.5 (for comparison)

It is clear from the diagram that, for reasonable, (in the light of in-situ results), values of ν , the Doppler-shift function is relatively insensitive to the particle radial distribution.

4.2.2 The Mean Particle Velocity Reduction Factor.

4.2.2.1 Definition of χ.

If by some mechanism the velocity, or component of velocity along the direction perpendicular to the solar radius vector, should differ from the Keplerian value, a parameter χ_p may be defined such that;

$$V_T = \chi_p . V_K$$

where; V_K = Keplerian orbital vel. , V_T = Actual perp. component

The expression for the shift for a single particle along the L.O.S. becomes;

$$\Delta\lambda = +/- \frac{\lambda.V_e}{c}.\sin\ \varepsilon.(1 - \chi_p.\mathrm{cosec}^{1.5}\varepsilon.\sin^{1.5}\theta)$$

The effect of such changes on the value for the overall shift observed along a L.O.S. is slightly more subtle. A term in dS, which formerly cancelled, no longer will if χ shares a variable dependance with it.

The physical significance of this lies in the probability of seeing a particular particle along the L.O.S.. For example, the probability "p" of a particle contributing to dS when in an orbit of inclination "i" is given by;

$$p = \frac{di}{\sin i}$$

χ is defined as follows;

$$\langle\Delta\lambda\rangle = +/- \frac{\lambda.V_e}{c}.\sin\ \varepsilon.(1 - \chi.\mathrm{cosec}^{1.5}\varepsilon.I_1/I_2)$$

(A program to derive Doppler-shift vs. elongation for any given constant value of χ is listed in FIG.4.6).

It is possible to invert this relationship to give;

$$\chi = (1 - \frac{\langle\Delta\lambda\rangle.c}{\sin\ \varepsilon.\lambda.V_e}).\frac{I_1}{I_2}.\sin^{1.5}\varepsilon$$

which has a singularity at zero or 180 deg. elongation, so, rearranging;

$$\chi = (\sin^{1.5}\varepsilon - \frac{<\Delta\lambda>.c.\sin^{\frac{1}{2}}\varepsilon}{\lambda.V_e}).\ \frac{I_1}{I_2}$$

If the above expression is used for observed values of shift a parameter is derived, which, if particle sizes and properties are independent of orbits, is independent of elongation. A mean value is a convenient quantity to use in model tests. The mean and it's associated error were derived using the principle of least error, (e.g. Barford, 1967, p.62). The error on χ due to an error on shift, e_λ, is given by;

$$E_\chi = e_\lambda \ /\ \left(\frac{\lambda.V_e.\sin\varepsilon}{c.<\Delta\lambda>} - 1\right)$$

A program written to derive χ and it's mean is listed in FIG.4.7.

The values obtained from the results of ch.3 are depicted in FIG.4.8.

Below is a table of mean values for different combinations of radial distribution and scattering function.

Scattering Function	ν	χ
Isotropic	1.3	0.85
VSF	"	0.88
Isotropic	1.0	0.88
VSF	"	0.91

4.2.2.2 Components of χ.

Three components of χ are treated

i) radiation pressure, η_{rp}

ii) orbital inclination, η_i

iii) Orbital eccentricity, η_e

Neglecting effects due to the solar magnetic field and solar wind;

$$\chi = \eta_e \cdot \eta_i \cdot \eta_{rp}$$

The expressions for $\eta_e, \eta_i, \eta_{rp}$ are derived in appendices 4.3 and 4.4.

The program used for deriving values for η_i, η_e is listed in FIG.4.10. Those for η_{rp} are shown in FIG 4.11 and 4.12. The first employs the approximations described in section

4.1.4 whilst the second uses scattering and radn. press. efficiency functions derived by cubic interpolation from tables of values calculated for homogeneous spheres using Mie theory taken from Wickramasinghe's publication, (1973).

4.2.3 Models with Non-Zero Orbital Eccentricity or Inclination.

From the above it is clear that the three effects are indistinguishable using Doppler-shift data alone.

Hence it was decided, first, to see whether orbital inclination and eccentricity alone could reasonably explain the observations.

Various values of "q" and mean eccentricity, (see section 4.1.2), were investigated, and the results are tabulated in FIG.4.13.

It is useful when using this table to recall that the mean inclination and eccentricity of short period comets are 15 degrees and 0.6 respectively.Those for asteroids are 10 degrees and 0.15. Results from the Helios spacecraft for recorded micrometeoroid encounters are means of 20 degrees and 0.4 resp..

A high value of eccentricity, (0.95), was also tested which produced a value for η_e greater than $\overline{X}$. It is obvious then that a significant, (40%, see section 4.1.4), contribution from particles in hyperbolic trajectories must be ruled out.

Another salient point is that E-M effects will significantly reduce inclination from that of the parent body after ejection. The Helios results are thus somewhat surprising.

In addition to this a set of results for the combination of mean "i" and "e" that would give the observed mean value of χ has been computed. This is shown diagramatically in FIG.4.14. All values of both "i" and "e" consistent with the data presented in ch.3 therefore lie beneath the curve.

4.2.4 Models Including the Effects of Radiation Pressure.

4.2.4.1 Empirical Results.

The program listed in FIG.4.10 was run to find the values of Q, (Qrp for large x), and density required to produce the observed with two plausible combinations of mean inclination and eccentricity, and the Max. size distribution model of Giese & Grun. Isotropic scattering was assumed together with a radial distribution index of 1.3.The results are tabulated below;

For mean "i" of 20 degrees and mean "e" of 0.6;

Q	ρ	
1.0	0.31	g/cc
0.8	0.23	"
0.6	0.16	"
0.4	0.10	"
0.2	0.04	"

For mean "i" of 10 degrees and mean "e" of 0.4;

Q	ρ	
1.0	0.13	g/cc
0.8	0.10	"
0.6	0.07	"
0.4	0.04	"
0.2	0.02	"

The conclusion from this work is then clear. If the Giese & Grun size distributions are correct the density MUST be < 1.0 g/cc.

An alternative explanation may be possible part way between the models of Giese & Grun and LeSergeant & Lamy.

Investigations are being carried out by the author at present.

It should also be made clear that low albedo values are favoured since, from section 4.1.4;

$$Q = 1 - g.\gamma$$

If the VSF portrayed in FIG.4.4 is correct then $g \sim 1$. Hence;

$$Q = 1 - \gamma$$

When attempting to fit albedo and density to this type of data, a higher density forces a higher albedo, (almost linearly). In the same situation with brightness data the opposite is the case. Combining the two should be of great value.

Leinert et al., (1976), found agreement with their VSF and the Giese & Grun Max. model using a density of 3.0 g/cc and an effective albedo of 0.5 +/- 0.2. Giese & Grun, (1976), find an albedo of a few tenths and density of 3.0 g/cc will produce the observed ZL brightness.

Cook, (1978), found a value of 0.006 in the same way, only this time with a density of 0.18 g/cc derived from photographic meteor data. (He also finds evidence for a strong radial dependance of albedo). Hanner, on the other hand believes this to be too low. Using the value of 3.0 g/cc

preferred on the basis of lunar microcrater depth diameter ratios, Hanner, (1980), finds an albedo of ~0.24.

Brownlee particles exhibit densities typically between 1 and 3 g/cc but ~20%, (cp meteorites) are believed to have pre-impact densities of <0.1 up to 1.5 g/cc.

It would seem that the evidence to date does not preclude densities <1.0 g/cc nor small albedos. The point where the albedo vs. density functions for both brightness and Doppler-shift data cross would appear to be with Cook's results, (0.18 g/cc,0.0006).

To be more sure of the meaning of Doppler-shift data requires better knowledge of their optical properties.

4.2.4.2 Restrictions on Usable Particle Models.

As discussed in section 4.1.4, reliable theory exists for computing Qsca(x) and Qrp(x) for homogeneous spheres.

Unfortunately, as a result of the laboratory microwave simulation work, (Giese et al., 1978 and Greenberg & Gustafson, 1980), it would appear that a realistic particle model is that of a conglomerate of smaller shapes, (spheres, needles or plates). These are required to explain the shape of the VSF and polarisation function as mentioned earlier.

This type of particle model is also required for consistence with the morphology and shape of Brownlee particles.

The fact that more than one mineral may be present

would not be aproblem if the particle were homogeneous. However this does not seem to be the case.

Irregularity of shape may be expected to increase absorption due to multiple reflections as will surface blackening.

4.2.4.3 Homogeneous Spherical Particles of Various Compositions.

Because the effect of radiation pressure is greatest over the size range where both scattering and radn. press. efficiencies are changing most quickly, the properties of particles of size close to one micron can make a significant difference to the observed Doppler-shift.

It was decided inspite of the dubious applicability of Mie theory to investigate the density and c.r.i. required for homogeneous spherical particles to explain the shifts observed.

A table is presented below of some typical results using the Giese & Grun Max. model, (corrected for choice of density), with the program listed in FIG.4.12.

c.r.i.	ρ	η_{rp}
1.7-0.0i	3.0,1.0	0.97,0.91
1.7-0.2i	3.0,1.0	0.97,0.88
1.1-0.0i	3.0,1.0	0.997,0.996
1.1-0.2i	3.0,1.0	0.98,0.94
1.5-0.0i	1.0	0.93
1.5-0.4i	3.0,1.0	0.97,0.90

It would seem that the results of section 4.2.4.1 underestimate the effect of radiation pressure to some effect and hence require a lower density to be assumed.

If Mie theory applied to homogeneous dielectric spheres represents an acceptable model then either a density of no greater than 1g/cc with non-absorbing particles,or some absorption, (imaginary part >0.0), together with a slightly higher density, (1.0g/cc< ρ < 3.0g/cc), is demanded to explain the results of ch.3. An increase in the real part of the refractive index, it must be noted, has a similar effect to incresing the absorption.

4.3 OTHER INFORMATION EXTRACTED FROM THE DATA.

4.3.1 Line profiles.

There is no evidence of structure in the recovered profiles, as might arise from dust streaming for example.

As stated previously, line profiles contain less information on the same quantities as the shifts. No conclusions can be drawn from the profiles observed.

4.3.2 Seasonal Variations.

Data were collected in significantly greater quantity for elongations 40 and 180 degrees with the aim of detecting any seasonal variation occurring in either the inner or outer solar system.

Doppler-shifts vs. season are presented in FIG.4.15 for both elongations.

Possible causes might be tidal interaction with Jupiter, E-M effects, (Parthasarathy, 1978), or enhancements due to meteor streams or sun-grazing comets.

No such effect may be concluded from the data.

4.3.3 The Recession of the Gegenschein.

From the data presented in ch.3 a value for the Doppler-shift of the Gegenschein may be given;

$$\langle \Delta\lambda \rangle_G = 0.082 \pm 0.026$$

where the error refers to one standard deviation.

It would seem therefore that the positive shift recorded by Hicks et al., (1974), is real, (see FIG.1.4).

4.3.4 The Form of $\chi(\epsilon)$.

If $\chi(\epsilon)$ were found not to be constant with elongation, this would be strong evidence for a radial dependence of particle properties such as size distribution, or albedo or a change in the distribution of orbital eccentricities or inclinations.

No such effect may be concluded from the data at this stage.

More data on low elongations is, however, obviously very desirable.

4.4 CONCLUSIONS.

4.4.1 The Results of Fried, (1978).

Fried's results are depicted together with those of ch.3 in FIG.3.13.

Clearly they are not consistent and require radically different explanations, (principally size distribution).

In fact no self consistent explanation of Fried's results has been published. The model of LeSergeant and Lomy might explain the hyperbolic velocities of the low elongations but not the flatness between 60 deg. and 300 deg. elongation. (For a full discussion see ch. 1)

The possibility that Fried witnessed a temporary phenomenon is possible, although it seems unlikely in the view of the number of different occasions on which the present data was gathered.

4.4.2 Orbits.

If all the particles responsible for the Zodiacal light were unaffected by radiation pressure a curve may be drawn of $\bar{i}$ vs. $\bar{e}$ and is presented in FIG.4.13.

A significant contribution to the ZL from particles in high eccentricity (or hyperbolic) orbit may be ruled out.

4.4.3 Size Distribution.

Either of the two models of Giese & Grun, (1976), are consistent with the results, (see section 4.1.4).

As in section 4.4.2, the model of LeSergeant & Lamy is found inconsistent with the results.

4.4.4 Particle Properties.

Empirical results for the values of density and albedo have been determined making the assumption that the particles are large, ($x>>1$), and that the Giese & Grun Max. model gives the correct relative number density with size.

Models where constant values of Q are presumed seem, (on the basis of using Mie theory results for homogeneous spheres), to underestimatethe integrated effect of radiation pressure on the dust cloud and thus require both low density and albedo for the dust.

Were the Mie results to apply, then it could be concluded that either low density, ($\rho<1$g/cc), non-absorbing or medium density, (1g/cc$<\rho<3$g/cc), slightly absorbing particles in orbits of mean inclination and eccentricity ~20deg. and ~0.4 respectively would suffice to produce the observed shifts, given the relative size distribution from the Giese Max. model and the various assumptions specified in this chapter.

CHAPTER FIVE

FUTURE PROSPECTS

5.1 ACHIEVEMENTS TO DATE.

A scanning, microprocessor controlled servo-stabilised Fabry-Perot interferometer has been built and installed at the Observatorio del Teide, Tenerife.

Five observing trips, giving a total of 42 nights successful observation, have been made. Sufficient coverage has been achieved to give a Doppler-shift data base of the highest reliable precision to date for the ecliptic plane from +/-25 degrees out to the Gegenschein.

The results are consistent with those of Hicks et al., (1974), but at variance with those of Fried, (1978).

Some empirical deductions about the particle albedo and density have been possible.

The framework for interpreting radial velocity measurements in terms of orbital distributions has been improved, and one established for doing so in terms of density and optical properties.

No evidence for either seasonal changes or radial dependance of particle properties can be concluded from the data as yet, but it has been shown that improvements in both precision and coverage would yield such information.

An upper limit has been set for the Doppler-shift of the Gegenschein which seems to confirm a small recessional velocity, (~3km/s), suggested by previous radial velocity work,

(Hicks et al., 1974).

5.2 THE REQUIREMENT FOR FURTHER GROUND-BASED WORK.

Some comparatively minor modifications to the existing instrument, together with the use of a better observing site, should enable uncertainties to be reduced by as much as a factor 4 with the same integraton time.

The observatory in Tenerife now, unfortunately, suffers from light pollution which is significant for a source as faint as the ZL. Frequent dust clouds blowing in from the mainland accentuate the problem.

Sites in both Hawaii and Bolivia have been recommended in discussions with other ZL observers. If finances permit, further observations will be carried out from one of these.

Another problem with Tenerife is the frequent pollution with dust and cloud of the eastern horizon. This has the effect of reducing the coverage of the all important low elongations.

Better low elongation coverage is needed to investigate the radial dependance of particle properties/orbits.

Given a site of sufficient quality, off ecliptic meaurements would be possible. These would be of limited coverage because of the long integration times expected. From section 2.2.3 the integration time T obeys;

$$T \quad (1 + 2.bg)^2$$

where;

bg = sky background illumination as a fraction of ZL brightness.

If bg >1 then T $\propto$ bg. This will be the case for such observations. A moderate improvement in site would therefore imply a considerable one for efficiency.

Off ecliptic observations could go some way to delineate orbital effects on Doppler-shift from those of radiation pressure.

An improvement in efficiency would also lead to a better chance of observing any seasonal effects since these require a lot of information on only one or two elongations.

5.3 THE CASE FOR MAKING RADIAL VELOCITY OBSERVATIONS FROM SPACE.

As discussed in section 1.3.6.4 the behaviour of dust in the solar neighbourhood is of great importance in understanding the Zodiacal cloud as a whole. The work of Beavers, Cook et al., (1980), has shown what can be achieved using radial velocity measurements.

The question of the existence of dust free zones could, once and for all, be settled. If they do exist, their

radii could be determined, from which information could be gained on their composition and the mechanisms bringing about their destruction, e.g. collisions, (Zook & Berg, 1975), sputtering, (Beard, 1979), or rotational bursting, (paddack & Rhee, (1976).

Even given a cloudless sky at an eclipse observable from a favourable site sufficient data could not be gathered, in the time available, for a full analysis. It may take ten such events.

Thus it seems that a spaceborne experiment is justified on these grounds alone.

It follows from the remarks made in the last section that off ecliptic coverage could be much better achieved from space where the background illumination will be reduced by ~50% to that of diffuse starlight alone. Continuous operation would allow total coverage of the sky.

There are no major technical problems envisaged associated with building such an instrument to work in space. In fact there are arguments to suggest that it's operation would have fewer problems, and it's performancebe better than on the ground, (e.g. no drift problems due to changes in the optical thickness of F-P the gap, if operated in vacuum).

5.4 LABORATORY SUPPORT.

As discussed in section 4.1.4 there is now

considerable evidence in favour Of conglomerate, composite particle models, (Giese, 1980; Greenberg & Gustafson, 1980; Brownlee, 1978).

There is to date no means of calculating, or experimental information on, the optical efficiencies implied by such models. These are needed to properly interpret radial velocity measurements.

It is expected that such data will become available from the laboratory microwave simulation experiments of Giese et al. and Grenberg/Gustafson, (see references above). These are, however only being undertaken for a limited range of particle sizes, compositions and constructions. What seems to be needed is an understanding of the optical effects of a body being irregular in shape, composition and construction in general. (For instance, the effect of surface roughness is to enhance absorption as a result of multiple reflections).

Because the effects of radiation pressure are observable via Doppler-shift measurements, such information would enable tests of realistic particle models to be made.

It is intended to carry out studies along these lines.

ACKNOWLEDGEMENTS.

I would like to thank Prof. Jim Ring, Dr. Paul Atherton, Colin Perry and Dr. Ken Reay, (my supervisor), for many helpful discussions, Joe, Jack Crabtree and Denis for turning silly ideas into practical mechanical success, Dr. Andy Forrest for enlightening me, (and everyone else for miles around), concerning the wonders of microprocessors, Nic for tea, pizza, typing and keeping me together whilst producing this thesis, my parents for inspiring me in the first place, (contrary to the effects of school), and, most of all, Dr. Ken Reay for giving me the chance to do it.

APPENDICES

APPENDIX 3.1.

FUNCTIONAL DEPENDANCE OF $So(\lambda')$ ON $So'(\lambda')$.

Given the two cross-correlation functions;

$$\begin{aligned} So(\lambda') &= \int_{-\infty}^{\infty} S(\lambda).F(\lambda-\lambda').d\lambda \\ So'(\lambda') &= \int_{-\infty}^{\infty} S(\lambda).\frac{dF(\lambda-\lambda')}{d\lambda}.d\lambda \end{aligned} \qquad (1)$$

the connection between $\frac{dSo(\lambda')}{d\lambda}$ and $So'(\lambda')$ is to be investigated under the two following conditions;

i) $S(\lambda)$ is symmetric about some point,

ii) $F(\lambda) = \alpha.S(\lambda)$. i.e. the condition for a matched filter. (α = constant).

Differentiating $So(\lambda')$;

$$\frac{dSo(\lambda')}{d\lambda} = \int_{-\infty}^{\infty} \frac{dS(\lambda)}{d\lambda}.F(\lambda-\lambda').d\lambda + \int_{-\infty}^{\infty} S(\lambda).\frac{dF(\lambda-\lambda')}{d\lambda}.d\lambda$$

$$= So'(\lambda') + \int_{-\infty}^{\infty} \frac{dS(\lambda)}{d\lambda}.F(\lambda-\lambda').d\lambda$$

Now from condition (i);

$$\int_{-\infty}^{\infty} \frac{dS(\lambda).F(\lambda-\lambda')}{d\lambda}.d\lambda = \int_{-\infty}^{\infty} \frac{dS(\lambda-\lambda').F(\lambda)}{d\lambda}.d\lambda$$

and from condition (ii);

$$\int_{-\infty}^{\infty} \frac{dS(\lambda-\lambda').F(\lambda)}{d\lambda}.d\lambda = \int_{-\infty}^{\infty} 1/\alpha . \frac{dF(\lambda-\lambda')_{\alpha}}{d\lambda}.S(\lambda).d\lambda$$

$$= \int_{-\infty}^{\infty} \frac{S(\lambda).dF(\lambda-\lambda')}{d\lambda}.d\lambda$$

$$= So'(\lambda)$$

Hence;

$$\frac{dSo(\lambda')}{d\lambda} = 2.So'(\lambda') \qquad (2)$$

Note that $S(\lambda)$ could be replaced by a noisy signal $s(\lambda) + n(\lambda)$. The results from using the differential of $So(\lambda')$ or $So'(\lambda')$ would be equal but for a factor 2 for both the noiseless and the noisy cases.

It thus follows that the s/n is the same in either case. Hence both methods costitute the use of a matched filter.

APPENDIX 4.1.

DERIVATION OF RADIAL DISTRIBUTION OF NUMBER DENSITY FROM THE ORBITAL DISTRIBUTION.

The Haug integral, (Haug, 1958), relating spatial distribution of number density to the distribution of orbits, was originally defined using cylindrical polar co-ordinates;

$$n(\rho,z)= \frac{1}{2.\pi^3.\rho} \iiint_{a\ e\ i} \frac{N(a,\ e,\ i).da.de.di}{r^2.(a/r)^{3/2}.[(2-r/a-a/r.(1-e^2)).(\sin^2 i-z^2/\rho^2.\cos^2 i)]^{\frac{1}{2}}}$$

Restricting interest to the ecliptic plane only;

$$n(r) = \frac{1}{2.\pi^3.r} \iiint_{a\ e\ i} \frac{N(a,\ e,\ i).da.de.di}{r^2.(a/r)^{3/2}.\sin i.[2-r/a-a/r.(1-e^2)]^{\frac{1}{2}}} \qquad (1)$$

The ranges for integration are;

$$0 < i < \pi/2 \qquad \text{(prograde orbits only).}$$

$$0 < e < 1$$

$$\frac{r}{1+e} < a < \frac{r}{1-e}$$

The changes of variables used by Briggs in his 1962 publication to perform the integration were cumbersome and rather opaque.

That given by Bandermann & Wolstencroft, (1969), resulted in a singularity and was more complicated than necessary.

The need to integrate over "a" is removed altogether if instead the orbital phase "v" is introduced via;

$$r/a = \frac{(1-e^2)}{1 + e.\cos v}$$

First, a change of variable;

$$x = a/r \quad \text{hence,} \quad dx = da/r$$

Equation (1) becomes;

$$n(r) = \frac{1}{r^2} \iiint_{x\ e\ i} \frac{N(a, e, i).da.de.di}{x.(e^2.x^2-(x-1)^2)^{\frac{1}{2}}}$$

Assuming N(a, e, i) is separable;

$$N(a, e, i) = n_a(a).n_e(e).n_i(i)$$

and that;

$$n_a(a) = C_1.a^{2-\nu}$$

then;

$$n(r) = r^{-\nu} \int_0^{\pi/2} \frac{n_i(i).di}{\sin i} . \int_0^1 n_e(e). \int_{1/1+e}^{1/1-e} \frac{x^{1-\nu}.dx.de}{(e^2.x^2-(x-1)^2)^{\frac{1}{2}}}$$

Now;

$$x = \frac{1 + e.\cos v}{1 - e^2}$$

Hence;

$$dx = \frac{-e \quad .\sin v.dv}{1 - e^{-2}}$$

After some reduction;

$$n(r) = r^{-\nu} \int_{o}^{\pi/2} \frac{n_i(i).di}{\sin i} \int_{o}^{1} n_e(e).(1-e^2)^{\nu-3/2} \int (1+e.\cos v)^{1-\nu}.dv.de$$

The upper limit for the phase integral is thus;

$$1/1+e = 1 + e.\cos v/1 - e^2$$

$$1 - e = 1 + e.\cos v$$

$$\cos v = -1$$

$$v = \pi$$

Similarly the lower limit can be shown to be 0.

So dn(r), the element of n(r) where the orbital parameters lie between i and i+di, e and e+de, v and v+dv respectively, is given by;

$$dn(r) = r^{-\nu}.n_i(i).di.n_e(e).(1-e^2)^{\nu-3/2}.(1+e.\cos v)^{1-\nu}.dv.de$$

APPENDIX 4.2

THE RADIATION PRESSURE FACTOR.

A4.2.1 Radiation Pressure.

If the radiative energy output from the sun is Erad ergs/ster.sec then the force experienced by the particle due to radiation pressure is;

$$Frp = \frac{Erad.\pi z^2}{c} \cdot \frac{1}{r^2} \int_0^\infty Qrp(z,\lambda).f(\lambda).d\lambda$$

where;

z = particle radius.

c = velocity of light.

r = solar distance.

$Qrp(z,\lambda)$ = radiation pressure efficiency coefficient.

$f(\lambda).d\lambda$ = intensity of solar radiation between λ and $\lambda + d\lambda$, normalised to unity.

Qrp is sometimes reffered to as Qpr since an identical factor pertains to the treatment of the Poynting-Robertson effect.

For convenience;

$$Qrp(z,\lambda).f(\lambda).d\lambda = \langle Qrp \rangle$$

(See text for discussion of the properties of $\langle Qrp \rangle$).

A4.2.2 Definition of "β".

"μ" is defined as the ratio of the force due to radiation pressure to that of gravity;

$$\beta = \frac{Frp}{Fg} = \frac{Erad.\pi z^2.\langle Qrp \rangle}{c} . \frac{r^2}{r^2} \cdot \frac{r^2}{GMsun.4/3.\rho.\pi.z^3}$$

$$= \frac{3.Erad}{4.GMsun.c} . \frac{\langle Qrp \rangle}{\rho.z}$$

$$= \frac{C.\langle Qrp \rangle}{\rho.z} \qquad (1)$$

A4.2.3 Definition of "μ".

Because Frp has sign opposite to that of Fg it reduces the effect of gravity, (and, as a result, increases the total energy of the particle). This may be interpreted as equivalent, (for the particle), to a reduction in solar mass by

a factor "μ", given by;

$$\mu^2 .Fg = Fg - Frp$$
$$= 1 - Frp/Fg$$
$$= 1 - \beta \qquad (2)$$

The velocity of a particle, not experiencing radiation pressure, found in an orbit of eccentricity "e" and semi-major axis "a", and at a solar distance "r" is given by;

$$Vp = GMsun.(2/r - 1/a) \quad \text{(ptcle. mass << Msun)}$$

where;

v = orbital phase measured away from perihelion.

Accounting for radiation pressure therefore the orbital velocity will be Vp′ such that;

$$Vp' = \mu .Vp$$

NOTE:

This treatment DOES NOT account for the effect of radiation pressure in changing orbits, it simply defines the velocity of a particle under it's influence found already in a particular orbit.

APPENDIX 4.3

DERIVATION OF COMPONENT OF "χ" DUE TO ORBITAL ECCENTRICITY AND INCLINATION.

A4.3.1 The Component of the Velocity Vector Parallel to Vc.

For inclined, eccentric orbits the component of orbital velocity, Vp, along the direction perpendicular to the solar radius vector in the ecliptic plane, Vpc, is given by;

$$Vpc = Vp.\cos i.\sin \phi$$

where;

i = orbital inclination.

ϕ = angle between solar radius vector and particle velocity vector for a given eccentricity "e".

Now;

$$Vp^2 = \frac{(GMsun)}{r} . \frac{(2.a - r)}{a} \qquad (\text{ptcle. mass} << \text{Msun})$$

(e.g. McNally, 1974)

where;

a = semi-major axis.

r = solar distance.

Hence;

$$Vpc = Vc.\cos i.[a/r.(1-e^2)]^{\frac{1}{2}}$$

where;

Vc = orbital velocity in circular Keplerian case, $(= (GMsun/r)^{\frac{1}{2}})$.

Instead of expressing Vpc as a function of "r" it is prefferable to do so as a function of "v", the orbital phase, (as will be seen later);

$$r = \frac{a.(1-e^2)}{1 + e.\cos v}$$

$$Vpc = \frac{Vc.(1 + e.\cos v)^{\frac{1}{2}}.\cos i}{}$$

A4.3.2 Definitions of "η_i","η_e" .

In the expression for the Doppler-shift for circular orbits, (see text), the terms in "i", "e" and "v" in the expression for dn(r) cancel, (see appendix 4.1). They no longer do, but since separable from those in "θ", will now form part of "χ".

The expressions for the components of "χ" are thus as follows.

$$\eta_i = \frac{\int_0^{\pi} n_i(i).\cos i.di \,/\, \sin i}{\int_0^{\pi} n_i(i).di \,/\, \sin i}$$

$$\eta_e = \frac{\int_0^{1} (1-e^2)^{\nu-3/2}.n_e(e).\int_0^{\pi} (1+e.\cos v)^{3/2-\nu}.dv.de}{\int_0^{1} (1-e^2)^{\nu-3/2}.n_e(e).\int_0^{\pi} (1+e.\cos v)^{1-\nu}.dv.de}$$

APPENDIX 4.4

THE CONTRIBUTION OF RADIATION PRESSURE TO "$\mathcal{X}$".

In appendix 4.2 it was shown that;

$$Vp' = \mu . Vp$$

where Vp′ and Vp are the orbital velocities for particles experiencing and not experiencing radiation pressure respectively.

It is then clear that the expression used to evaluate " η_e" in appendix 4.3 must be multiplied by "μ".

Hence the Doppler-shift of an individual particle is now a function of "z". As a result the terms in "z" in the expression for dS, (see text), no longer cancel in the expression for L.O.S. Doppler-shift. Since they are separable from terms in "θ", "e", "i" and "v" another separate factor of "χ" may be defined;

$$\eta_{rp} = \frac{\int_0^\infty n_z(z).\mu.Qsca(z).z^2.dz}{\int_0^\infty n_z(z).Qsca(z).z^2.dz}$$

This is equivalent to the expectation value of "μ" over that part of the size distribution which contributes to

the ZL. It is important to note that if it is decided that a given size distribution is correct in the relative sense but whose absolute values must be corrected for some reason, then the size range responsible for the ZL will change. Hence so will the effect of radiation pressure predicted from it.

NOTE:

This treatment clearly requires "μ" to be real and hence "β" <1. For a particle this implies bound orbits only.

A different treatment would be required for hyperbolic trajectories, (see text for discusion).

FIGURE LIST

1.1 The Zodiacal Light from Observatorio del Teide, Tenerife.

1.2 Viewing Geometry for Zodiacal Light Observations.

1.3 The Interplanetary Dust Size Distribution at 1 A.U. as Interpreted by Giese & Grun, (1976), and LeSergeant & Lamy, (1978) from Lunar Microcrater Statistics.

1.4 The Doppler-Shift Results of Fried, (1978).

1.5 The Doppler-Shift Results of Hicks et.al. (1974).

1.6 The Spatial Distribution of a Particle of Any Given Size with Solar Distance.(Beard, 1978).

2.1 Demonstrating the Ideal Bandwidth for Detecting a Frequency Shift $\Delta\nu$.

2.2 The MgI5183.618A Absorption (Fraunhofer) Line (From Delbuie Atlas of the Solar Spectrum).

2.3 Input Optics.

2.4 Detector Optics.

2.5 S/N us.EHT for RCA 31043A-02 PMT used.

2.6 Pulse Height Distribution for RCA31403A-02 PMT Used, (culmulative).

2.7 Instrument Housing.

2.8 Block Diagram of Electronics.

2.9 Optical Overview.

2.10 Top Down Task Analysis.

2.11 Flow Chart for Basic Program.

2.12 Listing of Basic Program.

2.13 The Chopping Technique.

2.14 Integration Time vs. Chop Amplitude.

2.15 Calibration Optics.

2.16 Interference Filter Profile.

2.17 Error Resulting from Division of Signal by Interference Filter Profile.

2.18 As for Fig. 2.17 but with Incorrect Filter Profile Position.

2.19 Geometry Defining Orientation of Zodiacal Cone.

3.1 Pre-Reduction Program.

3.2 Centre of Gravity Reduction Program.

3.3 Centre of Gravity Results Folded into π Radians.

3.4 Table of C. of G. Results Combined from Whole Data Set Folded into π Radians.

3.5 Cross-Correlation Reduction Program. (XCOL).

3.6 Cross-Correlaton Reduction Program; Improved Version. (XCOL2).

3.7 XCOL2 Results for July 1981.

3.8 XCOL2 Results for Sept. 1981.

3.9 XCOL2 Results for April 1982.

3.10 XCOL2 Results for July 1982.

3.11 XCOL2 Results for Sept. 1982.

3.12 XCOL2 Results for Whole Data Set.

3.13 XCOL2 Results for Whole Data Set Folded into π Radians.

3.14 Table of XCOL2 Results for July and Sept. 1981.

3.15 Table of XCOL2 Results for April 1982.

3.16 Table of XCOL2 Results for July 1982.

3.17 Table of XCOL2 Results for Sept. 1982.

3.18 Table of XCOL2 Results for Whole Data Set.

3.19 Table of XCOL2 Results for Whole Data Set Folded into π Radians.

3.20 Form of $S(\lambda)$ with Antisymmetric $F(\lambda)$, (see section 3.5.2.3).

3.21 Program for Finding a Doppler-Shift from a Chop Ratio.

3.22 Program for Combining Results from Different Frames.

3.23 Measured Profile from 30deg. Elongation.

3.24 Measured Profile for 110deg. Elongation.

3.25 Measured Profile for 180deg. Elongation.

3.26 Measured Profile for 40deg. Elongation.

3.27 Program for Recovery of Observed Line Profile.

3.28 Resampling Function Used.

3.29 Fourier Transform of Resampling Function Used, together with the Ideal Case, (Top Hat).

4.1 Cumulative Brightness as a Function of Size for the Size Distributions of Giese & Grun, (1976), and LeSergeant & Lamy, (1978).

4.2 Listing of Program Used to Derive Doppler-Shift vs Elongation for Circular Keplerian Orbits.

4.3 Doppler-Shift vs Elongation for Two Different Scattering Functions, (Circular, Keplerian Orbits).

4.4 The Two Scattering Functions Used for FIG.4.3. Also Shown is the Contribution Diffraction Would Make, (Giese & Grun Max. Model Used).

4.5 Doppler-Shift vs. Elongation for Three Different Radial Distribution Indeces. (Circular, Keplerian Orbits).

4.6 Listing of Program Used to Derive Doppler-Shift vs. Elongation for Any Constant Value of the Particle Velocity Reduction Factor.

4.7 Program Used to Derive Particle Velocity Reduction Factor from Given Doppler-Shifts.

4.8 Results from Applying Program of FIG.4.7 to the Results of Ch.3.

4.9 Doppler-Shift vs. Elongation for Mean Value of Observed Particle Velocity Reduction Factor, (Using the Program Listed in FIG.4.6).

4.10 Listing of Program Used for Deriving η_i, η_e from Given Mean Orbital Inclination and Eccentricity.

4.11 Program for Estimating η_{rp} from Observed Mean χ and Given Size Distribution.

4.12 Program Used to Derive η_{rp} from Given C.R.I. and Density.

4.13 Table of η_e, η_i for Various Values of Mean Inclination and Eccentricity.

4.14 Curves of Mean Eccentricity vs. Inclination for Orbital Parameters Alone to Produce Observed χ.

4.15 Examples of Qsca and Qrp Taken from Wickramasinghe, (1973),showing Approximation Employed.

4.16 Doppler-Shift vs. Season Observed for Elongations 40deg. and 180deg..

REFERENCES

(Alphabetical Order).

Adney: 1973; NASA, UMASS-ARF-73-284.

Bandermann: 1972; MNRAS, 160, 321.

Bandermann & Wolstencroft: 1969; Nature, 221, 251.

Barford: 1967; Experimental Measurements: Precision, Error and Truth, Addison-Wesley.

Beard: 1979; Astrophys.J., 234, 696.

Beavers et al.: 1980; Astrophys. J.,238, 349.

Beggs et al.: 1964; MNRAS, 127, 329.

Berg and Grun: 1973; Spa. Res. XIII, 1046.

Blackwell: 1952; MNRAS, 112, 652.

Blackwell and Petford: 1966; MNRAS, 131, 383, 399.

Blackwell and Ingham: 1961; MNRAS, 122, 113.

Blackwell et al.: 1967; Adv.Astron.Astrophys., 5, 1.

Blackwell et al.: 1967; MNRAS, 136, 313.

Blanchard: 1972; J.Geophys.Res., 77, 2442.

Bradley,Brownlee and Veblen: 1983; Nature, 301, 473.

Briggs: 1962; Astron. J.,67,710.

Briotta et al.: 1976; AFGL, TR-76-0236.

Brownlee: 1978; Cosmic Dust, J.Wiley & Son, 295

Burns,Soter and Lamy: 1979; Icarus, 40, 1.

Calbert and Beard: 1972; Astrophys.J.,176, 497.

Cassini: 1730; Mem.Acad.Roy.Sci., Tome VIII, (1666-1699). Comp. Libraires, Paris, 119.

Ceplecha: 1976; Lect.Notes in Phys., 48, 385.

Clarke et al.: 1967; Modern Astrophys., (ed. M. Hack), Gauthiers-Villars, Paris.Cook: 1978; Icarus, 33, 349.

Delsemme: 1976; Lect.Notes in Phys., 48, 314,481.

Dohnanyi: 1976; Lect.Notes in Phys., 48, 251.

Dohnanyi: 1969; J.Geophys.Res., 74, 2531.

Dohnanyi: 1971; Science, 173, 558.

Dohnanyi: 1970; J.Geophys.Res., 75, 3468.

Dohnanyi: 1967; NASA, SP-150, 315.

Dohnanyi: 1978; Cosmic Dust, J. Wiley & Son,527.

Dumont: 1972; Comp.Rend.Acad.Sci., Paris, 275, 765.

Dumont: 1973; Plan.Spa.Sci., 21, 2149.

Dumont: 1976; Lect.Notes in Phys., 48, 85 and 115.

Dumont and Sanchez-Martinez: 1973; Astron. & Astrophys., 22, 321.

Dumont and Sanchez-Martinez: 1975; Astron. & Astrophys., 38, 405.

Elsasser: 1958; Die-Sterne, 34, no.9-10, 166

Fechtig et al.: 1978; Cosmic Dust, J.Wiley & Son, 607.

Fechtig et al.: 1974; Proc.Fifth Lun.Sci.Conf., Geochem. & Cosmochem. Acta, Suppl. 5, 3, 2463.

Finkelman: 1972; Marine Tech.Soc.J., 6, 34.

Frey et al.: Astron. & Astrophys., 36, 447.

Fried: 1978; Astron. & Astrophys., 68, 259.

Giese: 1980; I.A.U.Symp.no.90, 81

Giese: 1973; Plan.Spa.Sci., 21,513.

Giese & Grun: 1976; Lect.Notes in Phys., 48, 135.

Gillett: 1967; NASA SP-150, 9.

Greenberg: 1980; I.A.U.Symp.no.90, 343.

Greenberg & Gustafson: 1981; Astron. & Astrophys., 93, 35.

Grotrian: 1934; Z.Astrophys., 8, 124.

Grun et al.: 1973; Spa.Res.XIII, 1046.

Grun and Zook: 1980; I.A.U.Symp.no.90, 293.

Haug: 1958; Z.Astrophys., 44, 71.

Hanner: 1980; Icarus, 43, 373.

Hanner et al.: 1976; Lect.Notes in Phys., 48, 29.

Hemenway: 1976; Lect.Notes in Phys., 48, 251.

Hicks: 1974; Phd Thesis, Univ. of London.

Hicks et al: 1974; MNRAS, 166,439.

Hodge et al.: 1964; J.Geophys.Res., 69, 2919.

Horz et al.: 1975; Pla.Spa.Sci., 23, 151.

Hulbert: 1930; Phys.Rev., 35, 1098.

Hulst v.d.: 1947; Astrophys. J., 105, 471.

Hulst v.d.: 1949; Recherches Astron.Obs.Utrecht, 11, pt.2.

Hulst v.d.: 1957; Light Scattering by Small Particles, J.Wiley & Son.

Humes et al.: 1974; J.Geophys.Res., 79, 3677.

Huruhata: 1951; Publ.Astron.Soc.Jap., 2,156.

Ingham: 1961; MNRAS, 122, 157.

Jacquinot: 1954; Opt.Soc.Am., 44, 761.

James: 1969; MNRAS, 142, 45.

James & Smeethe: 1970; Nature, 227, 589.

Kornblum: 1969; J.Geophys.Res., 74, 1893.

Kresak: 1980; I.A.U. Symp.no.90, 211.

Kresak: 1976; Bull.Astron.Inst.Czechosl., 27, 35.

Kresak: 1978; Bull.Astron.Inst.Czechosl., 29, 114.

Kurt and Syunyev: 1967; Cosmic Res., 5, 496.

Lafon,Lamy and Millett: 1980; I.A.U.Symp.no.90, 303.

Leinert: 1976; Astron. & Astrophys., 47, 221.

Leinert: 1978; Astron. & Astrophys., 64, 119.

Leinert: 1978; Die Rumliche Vertailung des Interplanetaren Staubes nach Zodiakallichtbeobachtungen von Helios 1,2, Ruprecht-Karl-Universitat Heidelberg.

Leinert et al.: 1980; I.A.U.Symp.no.90, 15.

Leinert et al.: 1974; Astron. & Astrophys., 30, 411.

Lena et al.: 1974; Astron. & Astrophys., 37, 81.

LeSergeant & Lamy: 1978; Nature, 276, 800.

LeSergeant & Lamy: 1980; I.A.U.Symp.no.90, 289.

Levasseur-Regourd and Dumont: 1978; Comptes Rend des Journees de Planetologie, Paris.

Lillie: 1972; The Scientific Results from OAO-2, (A.O.Code ed.), NASA SP-311, 95.

Lopez-Rodriguez and Sanchez-Magro: 1977; Astron. & Astrophys., 64, 161.

Lyot: 1929; Annales de l'Observatoire de Paris, Section de Meudon, VIII, No.1.

MacQueen: 1968; Astrophys.J., 154, 1059.

MacQueen and Poland: 1977; Solar Phys.,55, 143.

Marvin and Einaudi: 1967; Geochem.Cosmochem Acta, 31, 1871.

Maucherat et al.: 1976; Absolute U.V. Photometry of the Zodiacal Light from the ELZ experiment on the D2B-AURA Sattelite, I.A.U. General Assy., Grenoble.

McDonnell: 1978; Cosmic Dust, J.Wiley & Son, 337.

McDonnell: 1975; Plan.Spa.Sci., 23, 205.

McNally: 1974; Positional Astronomy, Muller, 286.

Mercer et al.: 1973; ZL Photography, Apollo 17, Prelim.Sci.Rep., NASA SP-330, 34-1.

Millard and Finkelman: 1970; J.Geophys.Res., 75, 2125.

Morfill and Grun: 1979; Plan.Spa.Sci., 27, 1269.

Morfill and Grun: 1979; Plan.Spa.Sci., 27, 1283.

Morrison and Zinner: 1977; Proc.8th Lun.Sci.Conf., 841.

Mukai and Yamamoto: 1982; Astron. & Astrophys., 107, 97.

Mullen: 1977; Astron. & Astrophys., 61, 369.

Mutch: 1966; Earth Plan.Sci.Lett., 1, 325.

Ney: 1974; Astrophys.J., 189, L141. Icarus, 23, 551.

Opik: 1937; Pub.Univ.Tartu., 29, 51.

Parkin et al.: 1968; Science,
159, 936.

Parthasarathy: 1978; Astron.J., 83, 1235.

Peterson: 1963; Astrophys.J., 138, 1218.

Peterson: 1967; Astrophys.J, 148, L37-39.

Peterson: 1967; NASA SP-150, 23.

Pitz et al.: 1976; Ultraviolet Observations of the Zodiacal LIght with the Astro-7 Rocket Experiment, I.A.U. Gen.Assy.,

Grenoble.

Pitz: 1980; I.A.U.Symp.no.90, 29.

Probstein: 1969; Problems of Hydrodynamics and Cont. Mechanics. Soc.Indust.Appl.Math., Philadelphia.

Reay: 1969; Nature, 224, 54.

Reay and Ring: 1968; Nature, 219, 710.

Rhee: 1976; Lect.Notes in Phys., 48, 238.

Ring et al.: 1964; Nature, 202, 167.

Robley: 1962; Ann.Geophys., 18, 341.

Roser and Staude: 1978; Astron. & Astrophys., 67, 381.

Roser and Staude: 1979; Astron. & Astrophys., 71, 269.

Roser and Staude: 1980; I.A.U.Symp.no.90, 81.

Sandford et al.: 1973; Astrophys.J., 181, L15-17.

Schwehm: 1976; Lect.Notes in Phys., 48, 459.

Selby: 1982; Preprint.

Schmid: 1935; Beitr.Geophys., 45, 5.

Singer and Bandermann: 1967; NASA SP-150, 379.

Shima and Kimoto: 1966; Chem.Geol., 1, 77.

Soifer et al.: 1971; Astrophys.J., 168, L73-78.

Soter et al.: 1977; Comets, Asteroids, Meteorites, Univ.of Toledo, 121.

Vegard: 1938; Ergeben.Exact.Naturwiss., 17, 229.

Weinberg: 1964; Annales d'Astrophys., 27, 718.

Weinberg and Sparrow: 1978; Cosmic Dust, J.Wiley & Son, 75.

Whipple: 1950; Proc.Nat.Acad.Sci., 36, 687.

Whipple: 1951; Proc.Nat.Acad.Sci., 37, 19.

Whipple: 1976; Lect.Notes in Phys., 48, 403.

Whipple and Gossner: 1949; Astrophys.J., 109, 380.

Wickramasinghe: 1973; Light Scattering Functions for Small Particles, J.Wiley & Son.

Wolstencroft and Brandt: 1967; NASA SP-150, 57.

Wolstencroft and Rose: 1967; Astrophys.J., 147, 271.

Wyatt and Whipple: 1950; Astrophys.J., 111, 134.

Zook: 1975; Plan.Spa.Sci., 23, 1391.

Zook and Berg: 1975; Plan.Spa.Sci., 23, 183.

FIGURES

FIG.1.1 The Zodiacal Light from Observatorio del Teide, Tenerife. (Photo by Chris Bell).

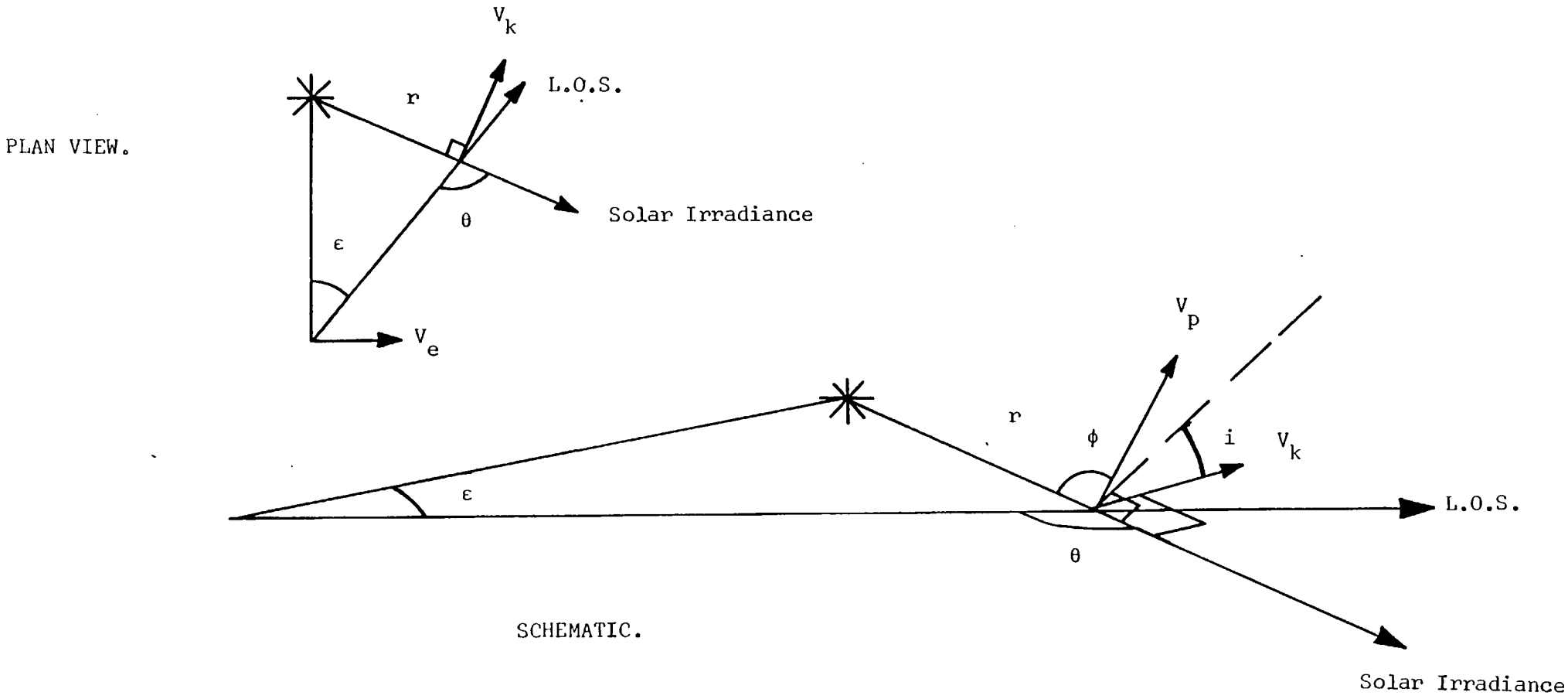

FIG.1.2 Viewing Geometry for ZL Observations.

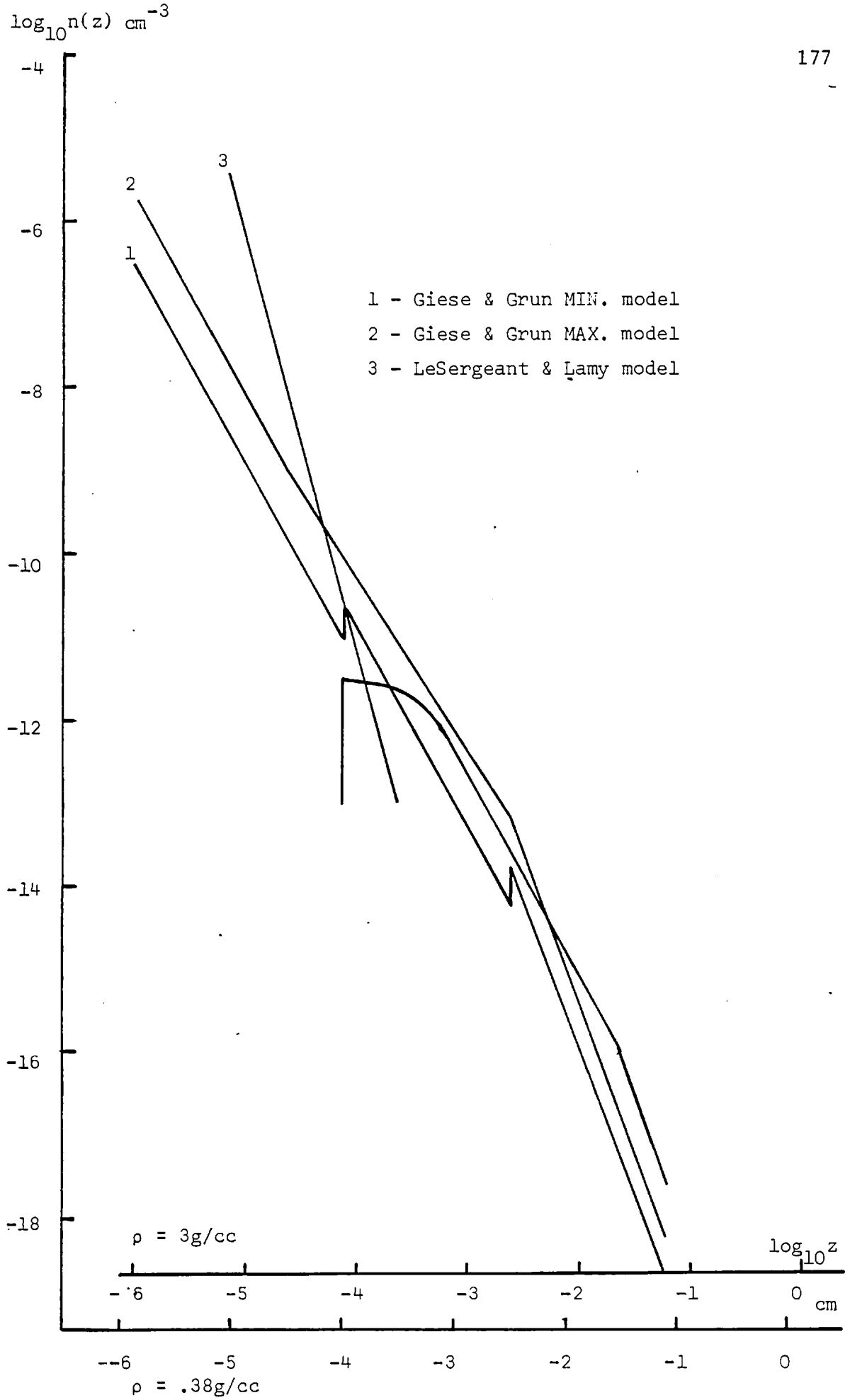

FIG.1.3 The Size Distributions at 1A.U. as Interpreted from Lunar Micro-crater Statistics.

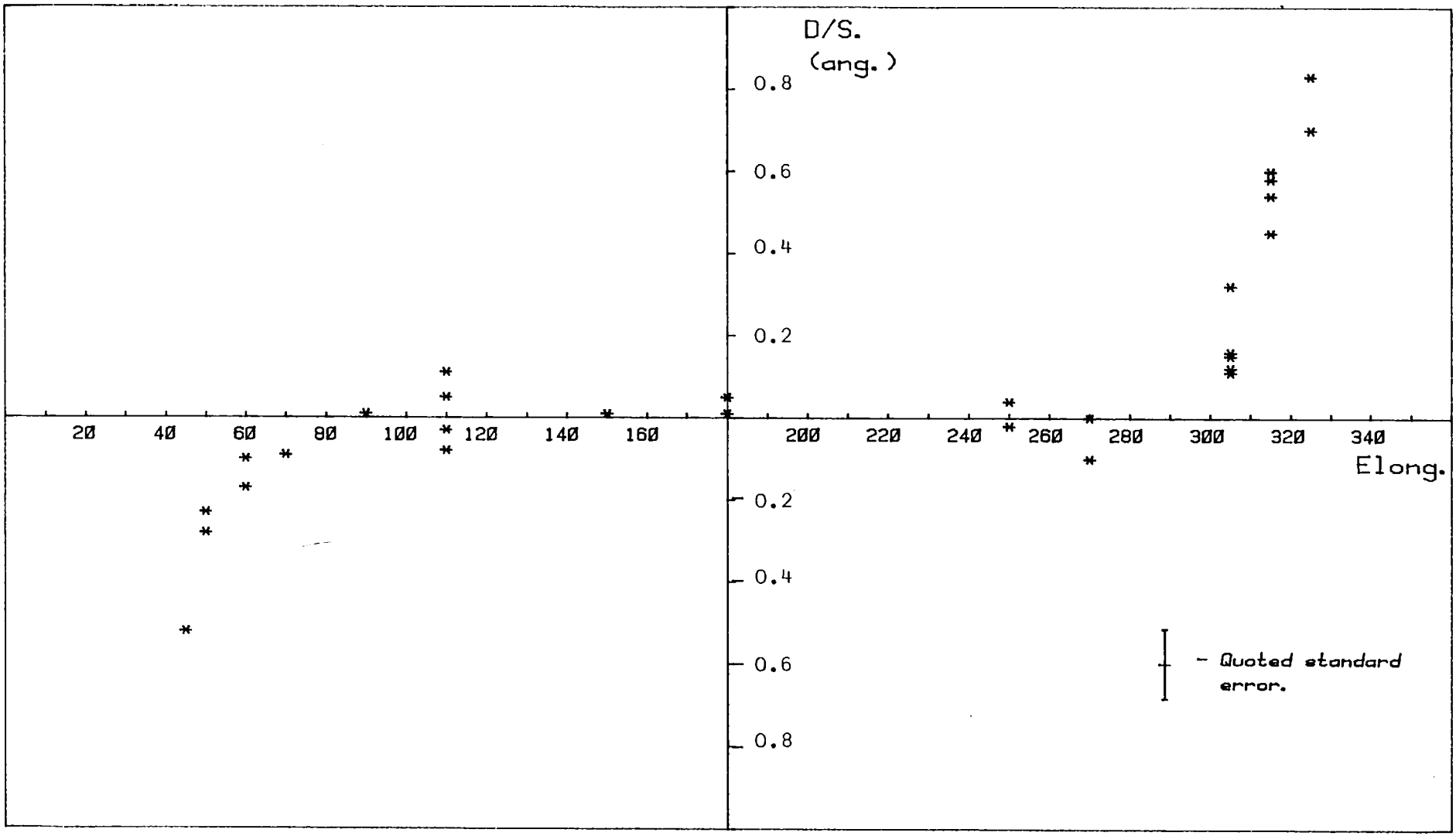

FIG. 1.4 The Doppler-Shift Results of Fried, (1978).

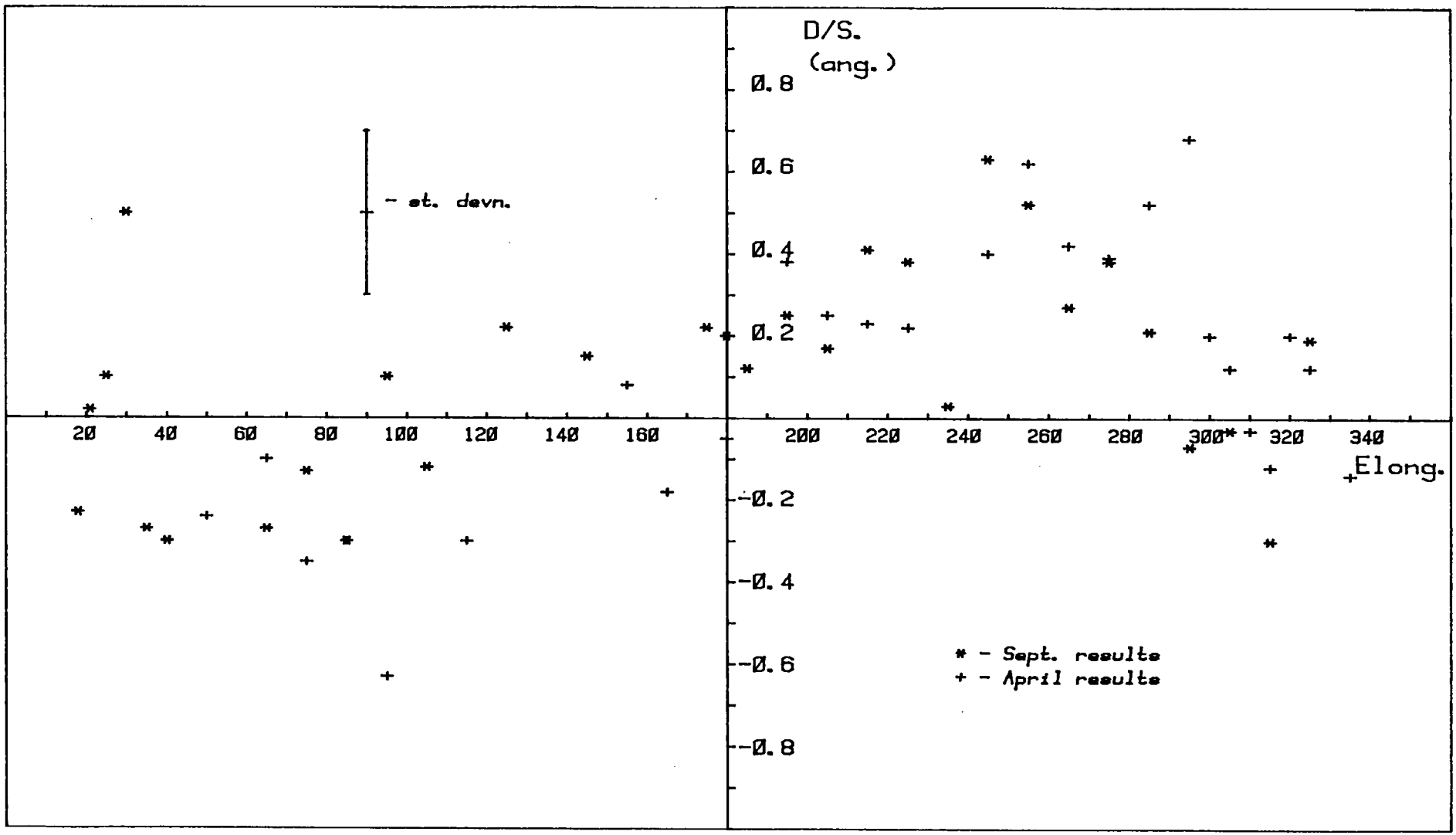

FIG. 1.5 The Doppler-Shift Results of Hicks et al., (1974).

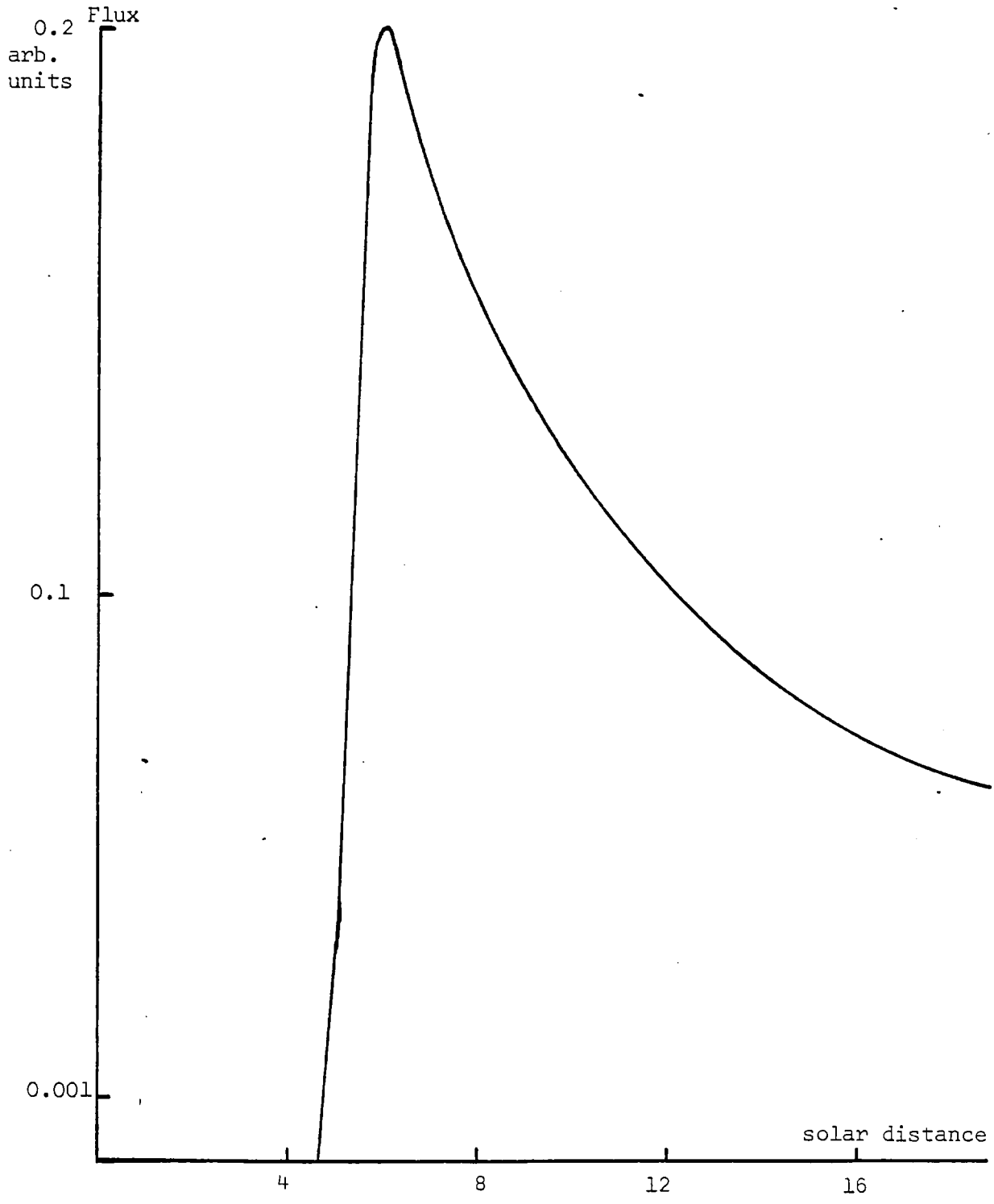

FIG.1.6 The Spatial Distribution of a Particle of any Given Size if Sputtering Alone acts to Reduce Particle Dimensions.

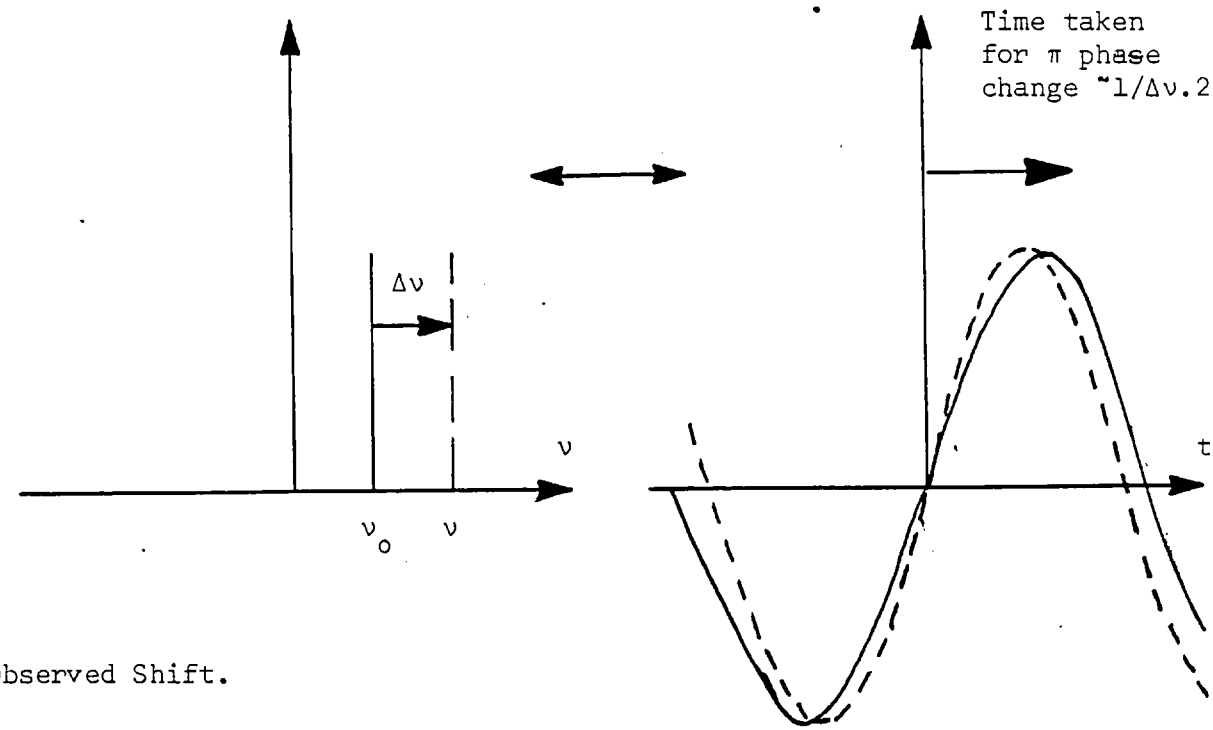

Observed Shift.

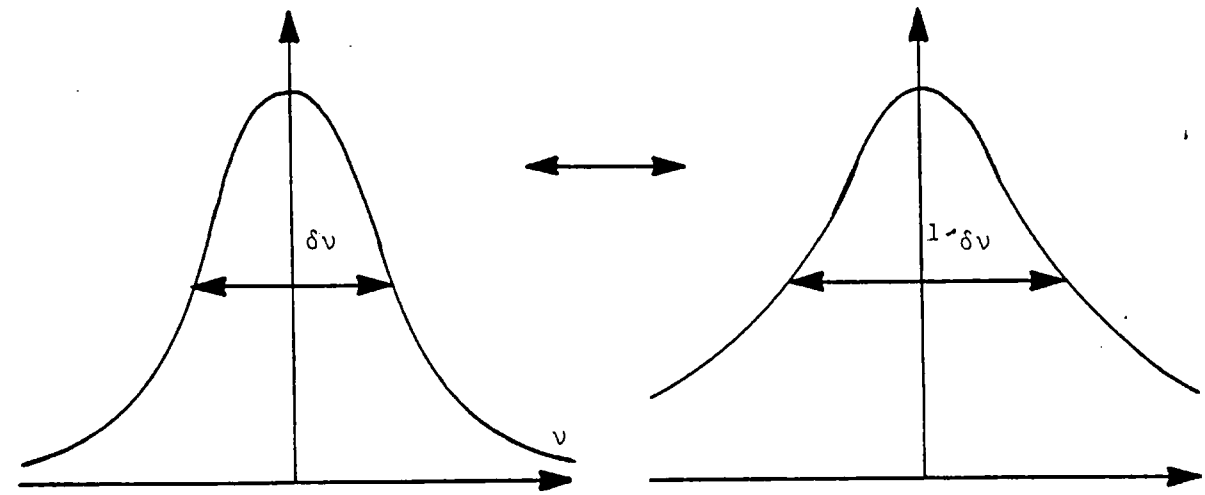

Instrumental Function.

Hence; $\delta\nu \quad \Delta\nu$

FIG.2.1 Demonstrating the Ideal Bandwidth for Detecting a Frequency Shift of $\Delta\nu$.

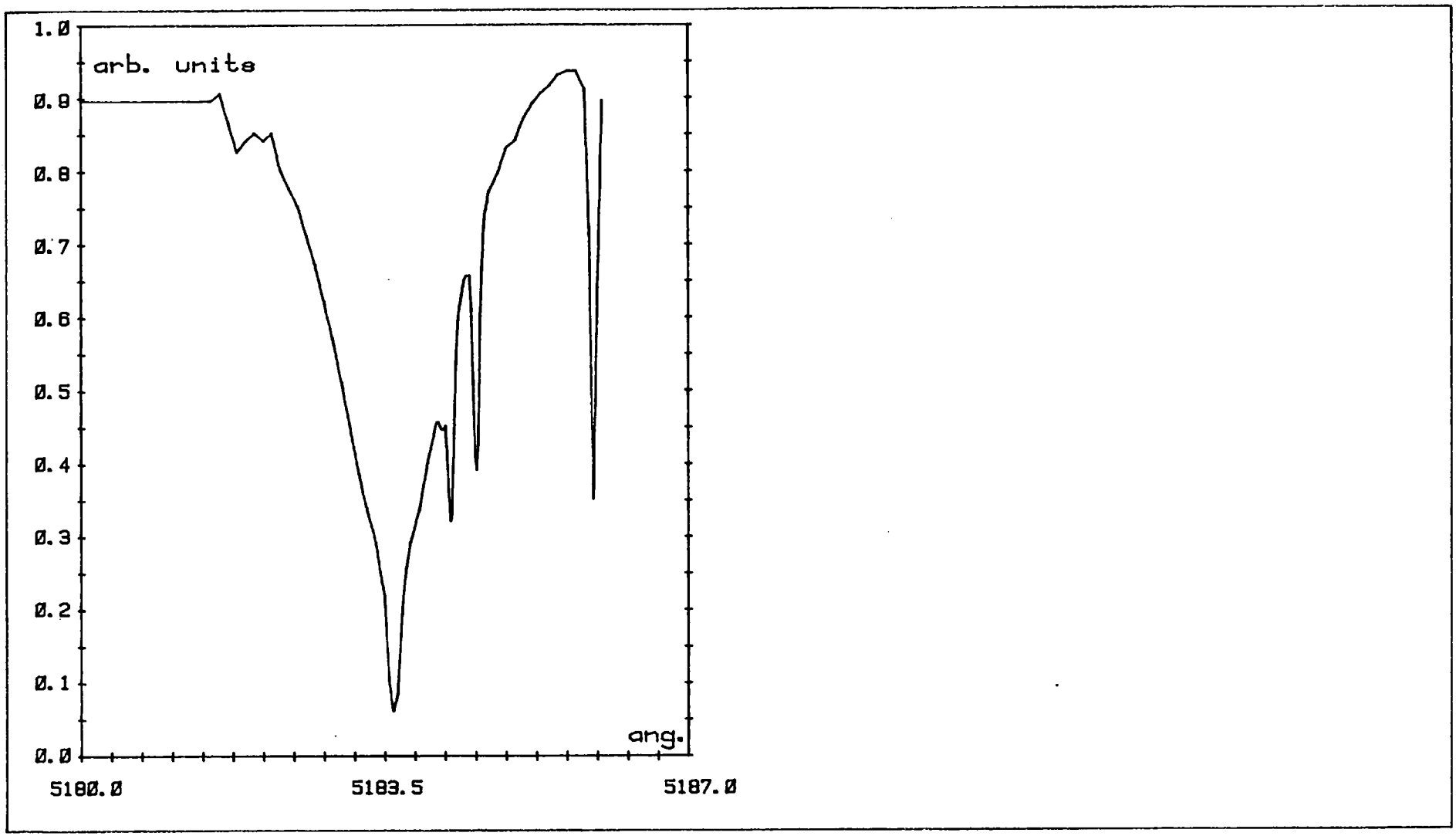

FIG. 2.2 The MgI5183.618A Fraunhofer Absorption Line.

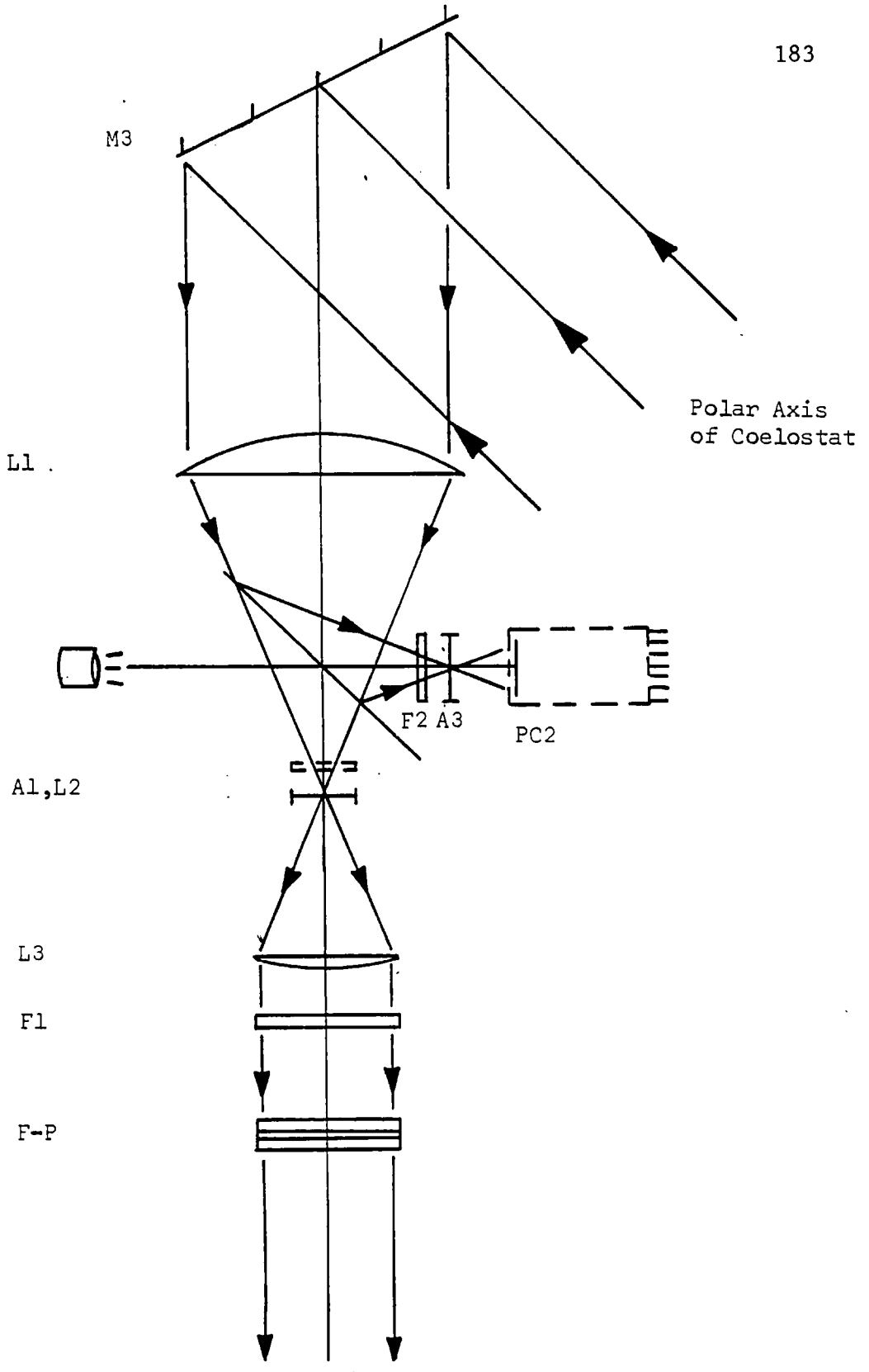

FIG.2.3 Input Optics.

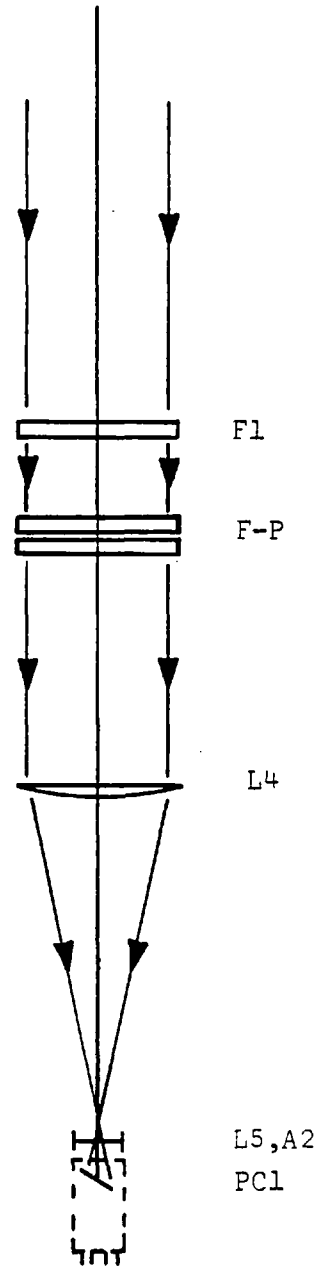

FIG.2.4 Detector Optics.(See FIG.2 .9 for key).

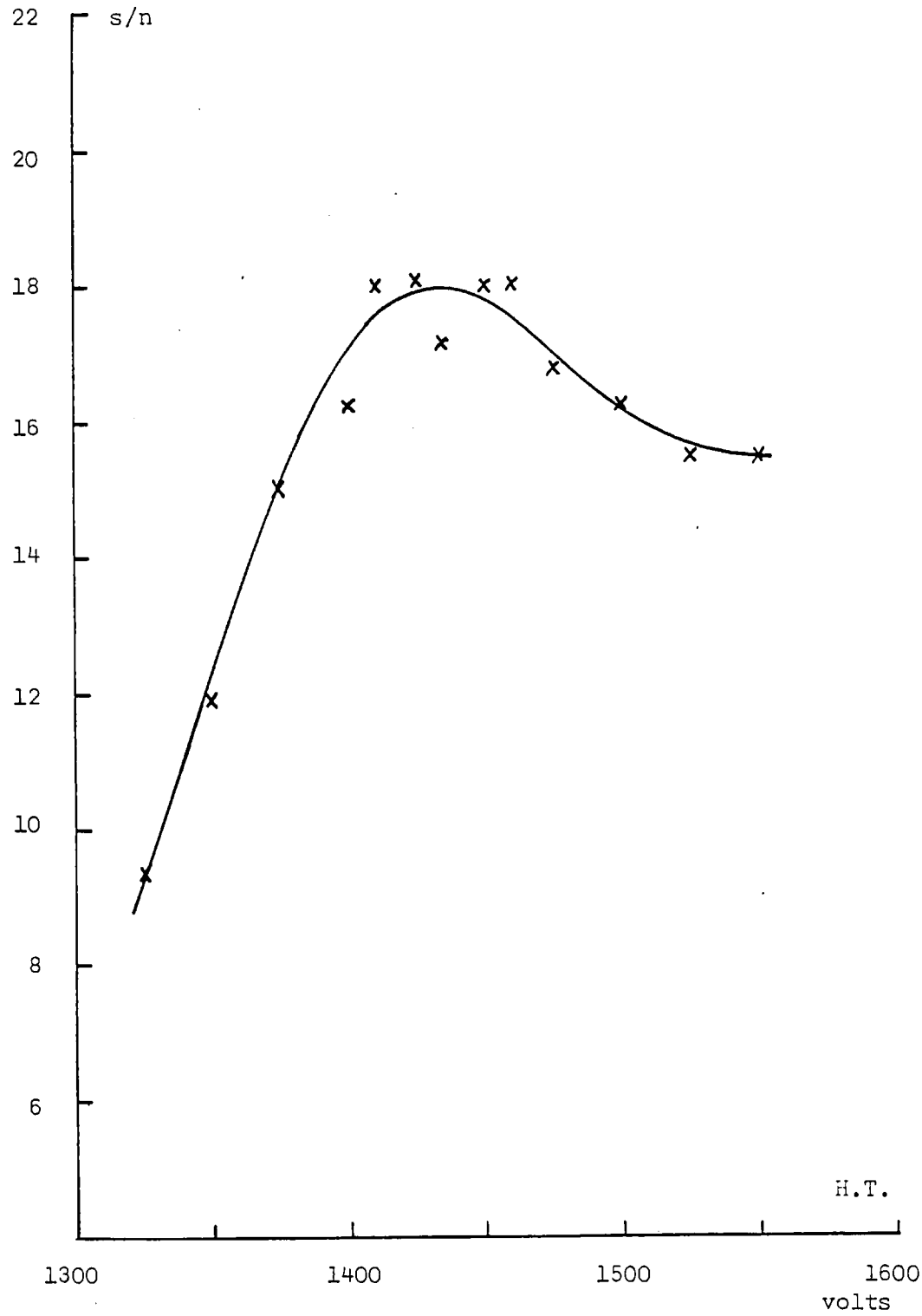

FIG.2.5 s/n Ratio vs. H.T. for RCA 31043A-02 PMT Used.

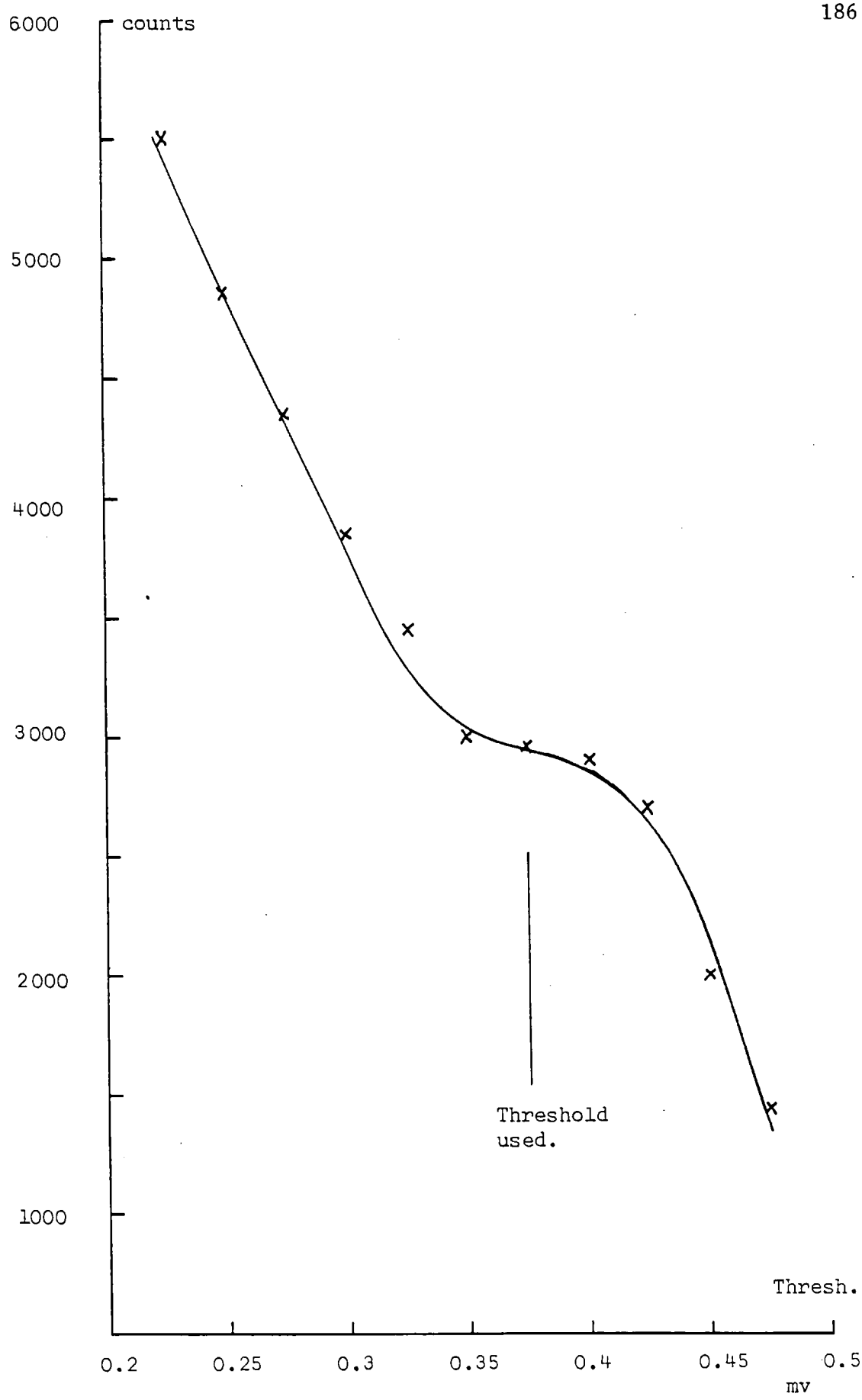

FIG.2.6 Pulse Height Distribution for RCA 31043A-02 PMT Used. (Cumulative).

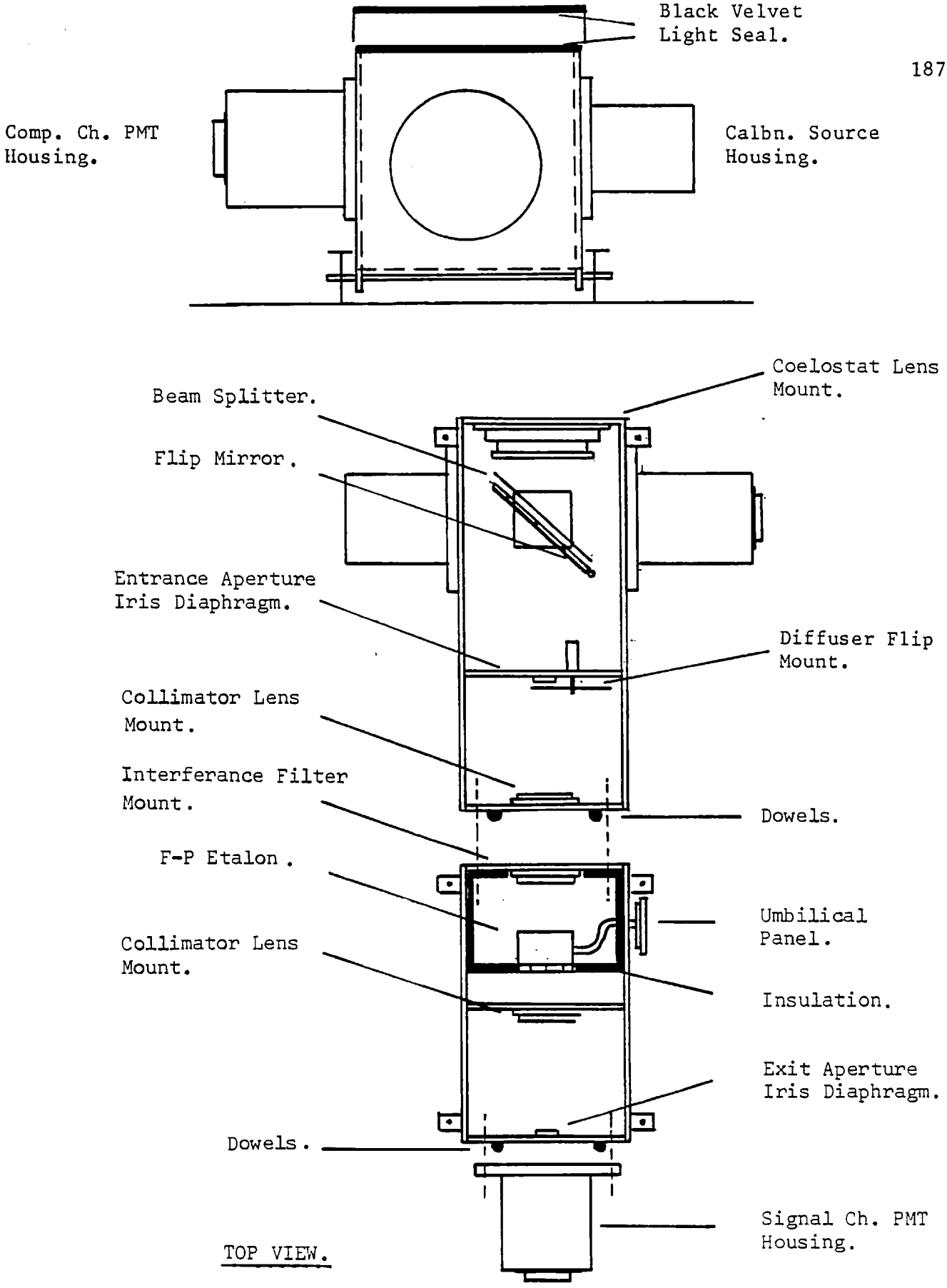

FIG.2.7 Instrument Housing.

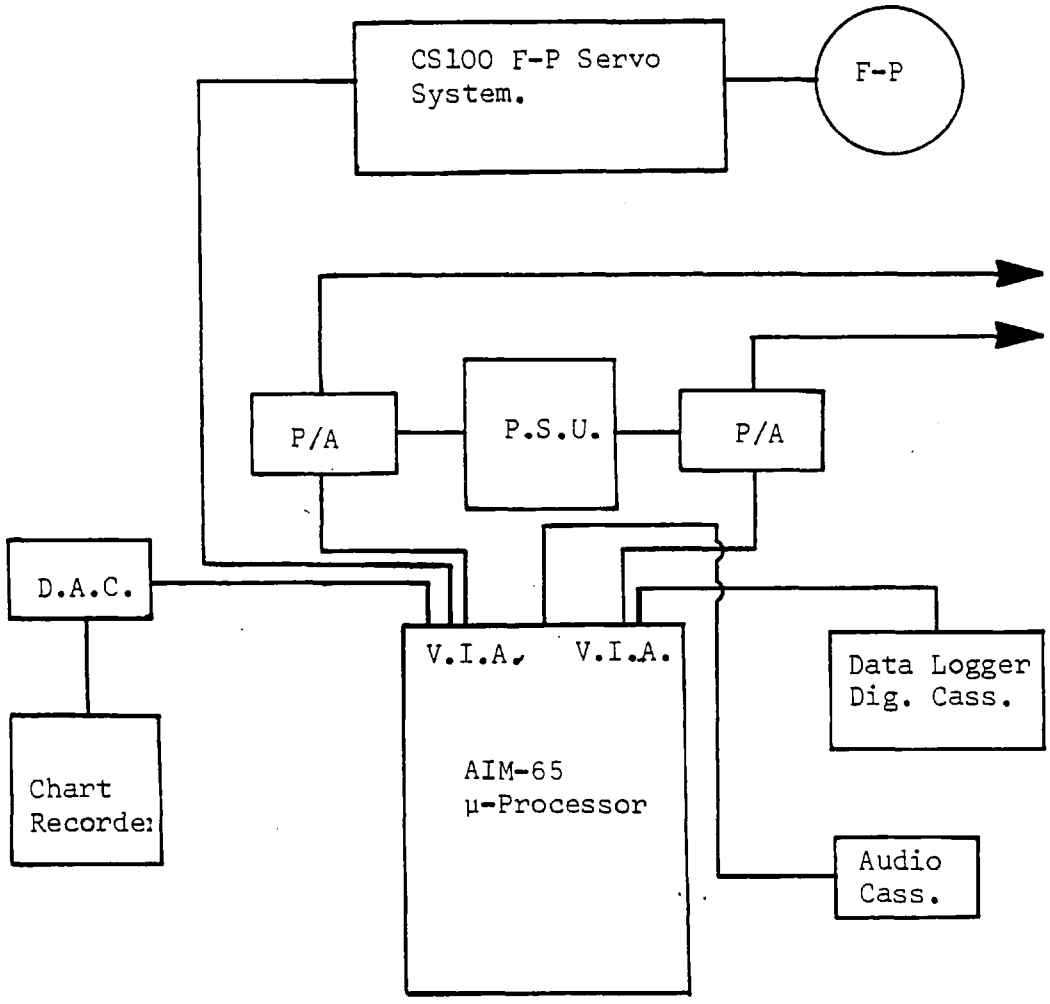

FIG.2.8 Block Diagram of Electronics.

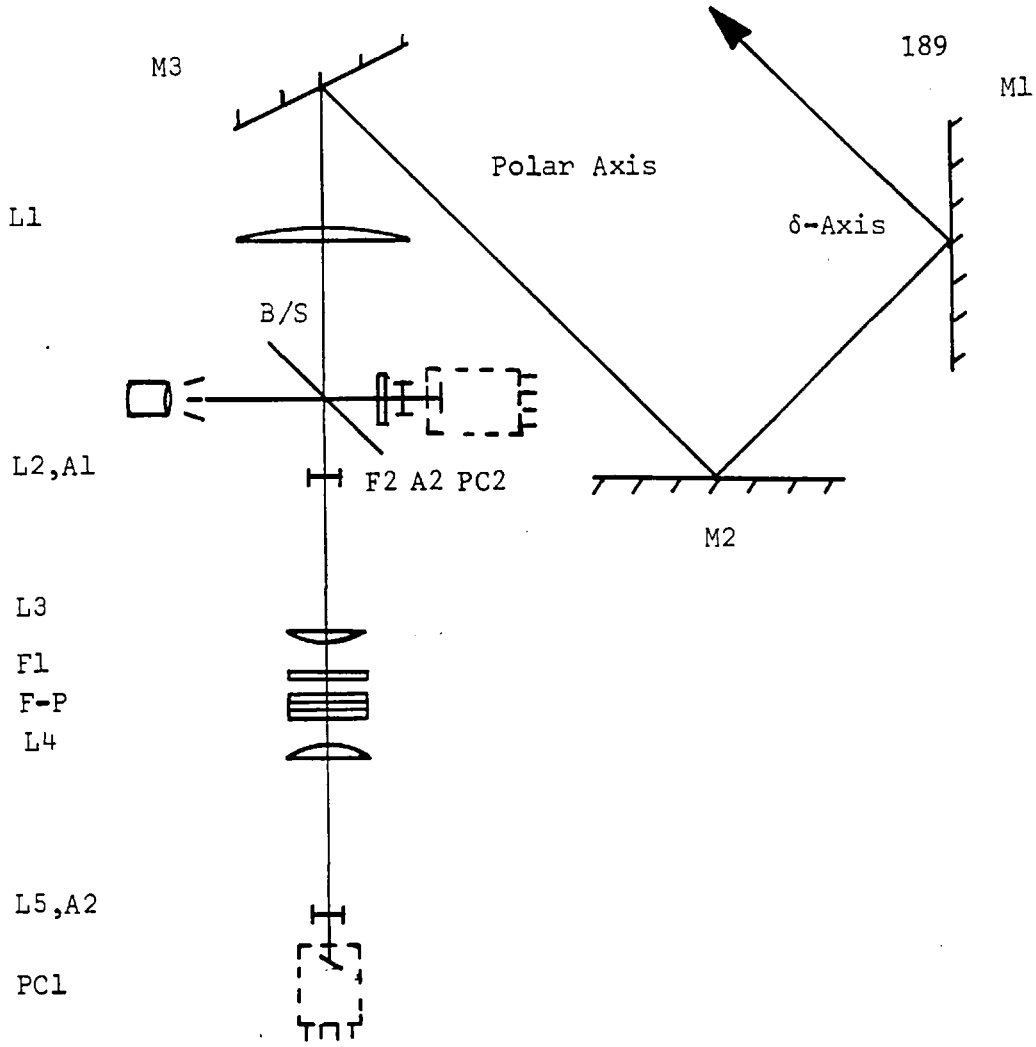

KEY:

L1;Coelostat Lens.
L2;Field Lens.
L3;Collimating Lens.
L4; " " .
L5;Field Lens.
A1;Entrance Aperture.
A2;Exit Aperture.
F1;Premonochromater.10A F.W.H.I. 3-Cavity Interferance Filter.
F2;Wide Band Filter.300A Single Cavity Interferance Filter Centred on 5000A.
PC1;Signal Channel Photocathode.
PC2;Comp. Channel Photocathode.
M1-3;Coelostat Mirrors.Silvered Coated + Protective "Hard" MnF12 Coating.

FIG.2.9 Optical Overview.

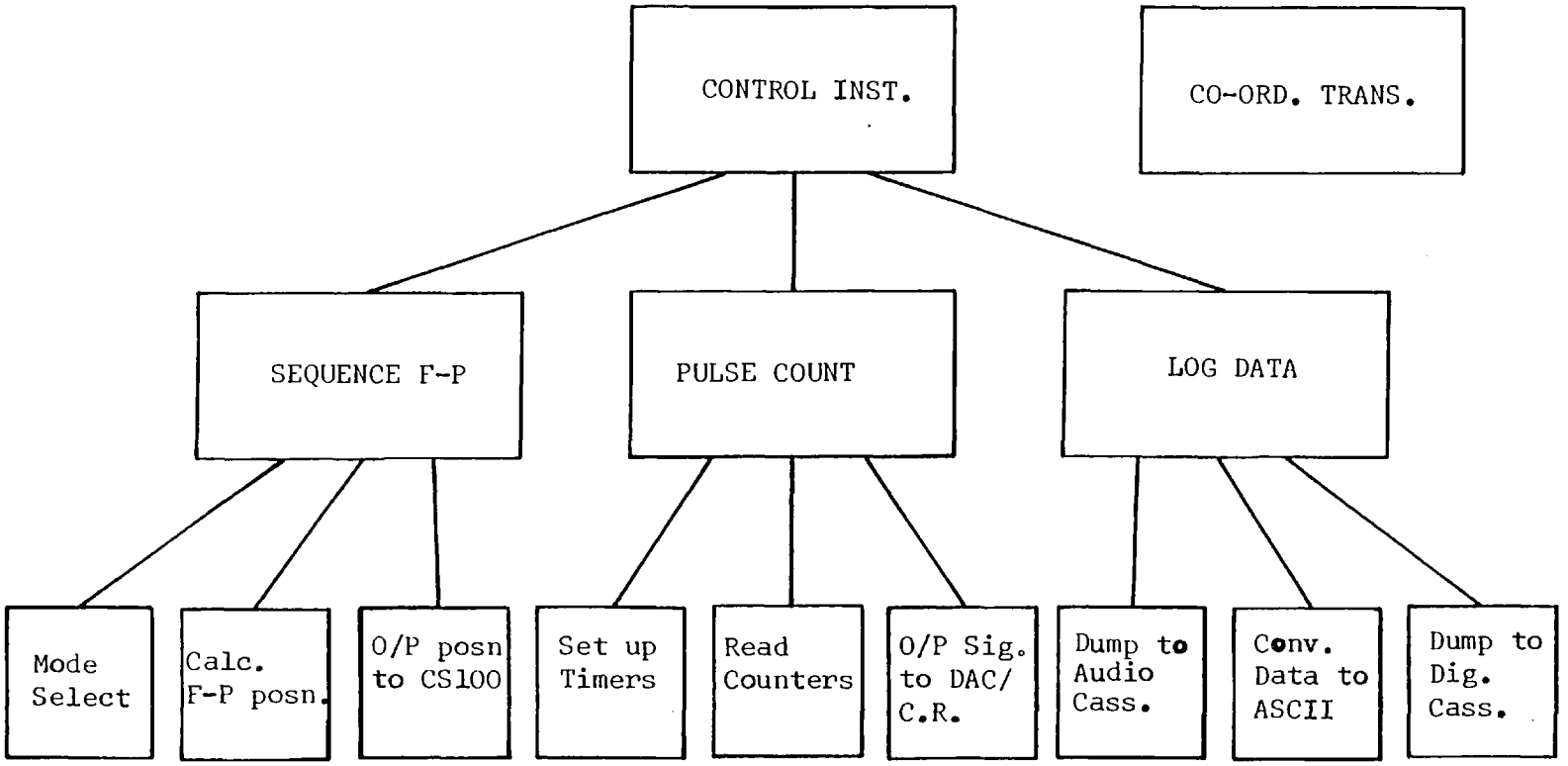

FIG.2.10 Top Down Task Analysis for Microprocessor.

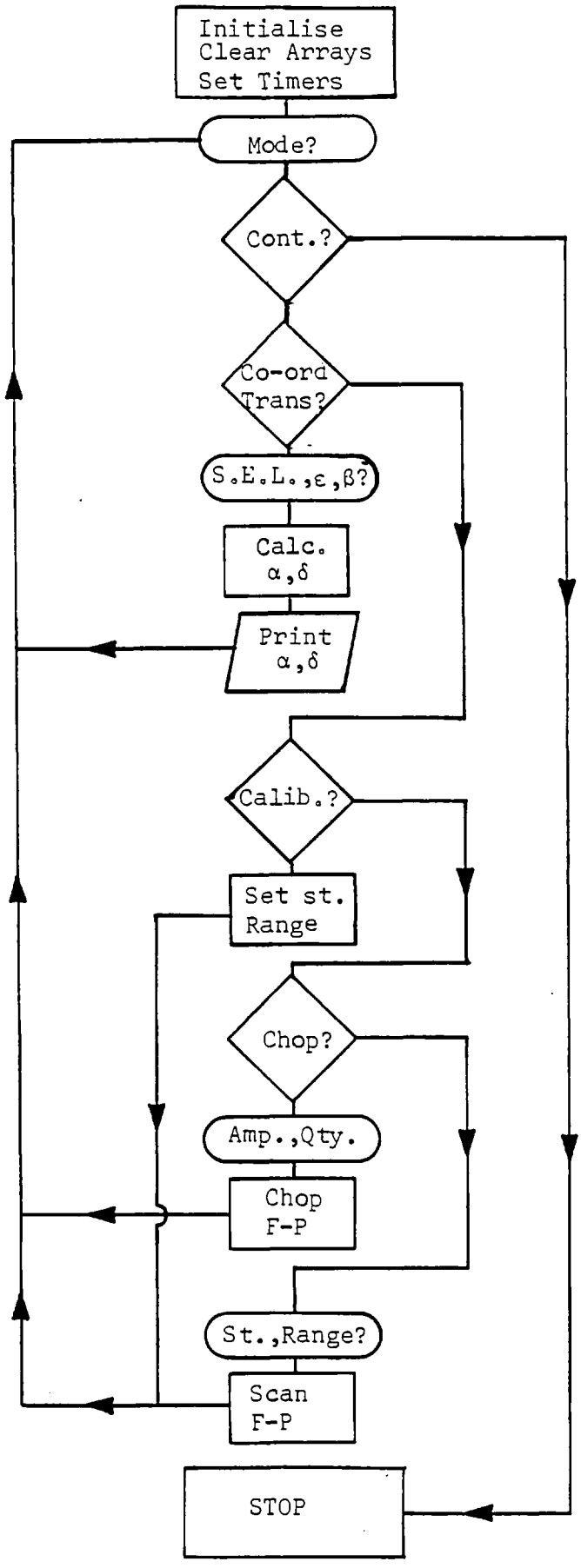

FIG.2.11 Flow Chart For BASIC Program.

```
LIST

 10 DIMA(10),T1(130),T2(130)
 20 FORI=0TO130
 23 T1(I)=0:T2(I)=0
 25 NEXTI
 30 POKE4,210:M=0
 40 POKE5,30
 50 POKE188,88
 60 POKE189,30
 70 POKE40962,135
 80 POKE36866,0
 90 POKE40963,255
 100 POKE36867,255
 105 PRINT"SELECT"
 110 INPUTA$
 115 IFA$="SCAN"THENGOSUB1910
 120 IFA$="CAL"THENGOSUB1860
 125 IFA$="POSN.CAL"THENGOSUB1370
 130 IFA$="CALCHOP"THENGOSUB1990
 135 IFA$="CHOP"THENGOSUB2020
 137 IFA$="DAYSKY"THENGOSUB2050
 138 IFA$="SKYCAL"THENGOSUB3010
 140 GOTO105
 150 GOTO190
 155 PRINT"NO.,EL.,DAY,MNTH.,DC,CAL."
 157 INPUTA(1),AA,A(4),A(5),AB,A(9)
 160 RETURN
 190 IFR=1THEN220
 200 IFR=2THEN510
 210 IFR=3THEN530
 220 PRINT"SCAN!"
 305 A(6)=TT
 325 IS=II
 330 II=(II-1)*J
 360 IFK=0THEN385
 370 BN=0
 380 POKE8146,0:GOSUB1220
 385 JJ=0
 390 FORN=PTOP+IISTEPJ
 400 GOSUB1280
 410 GOSUB1100
 415 T1(JJ)=T1(JJ)+Y
```

FIG.2.12 Listing of BASIC Program.

```
417 T2(JJ)=T2(JJ)+INT(B/100)
418 JJ=JJ+1
420 NEXTN
430 TT=TT-1
440 GOSUB810
450 IFTT>0THEN385
451 IFK=0THEN460
452 GOSUB1830
453 IFIS>25THEN460
455 GOSUB1610
460 RETURN
510 PRINT"CHOP!"
520 GOTO560
530 PRINT"CALCHOP"
560 K=0:Y1=0
570 Y2=0
590 PRINT"CE,DL,SL?"
600 INPUTCE,DL,SL
610 PRINT"QTY?"
620 INPUTI
622 PRINT"DC"
624 INPUTDC
625 IFR=2THEN630
626 CE=CE-8
627 FORJJ=1TO15
628 CE=CE+1
629 Y1=0:Y2=0
630 FORJ=1TOI
631 N=CE+(DL/2)
635 GOSUB1280
640 GOSUB1100
650 Y1=Y1+Y
660 N=CE-(DL/2)
670 GOSUB1280
680 GOSUB1100
690 Y2=Y2+Y
700 NEXTJ
710 DC=DC*IS
720 Y1=Y1-DC
730 Y2=Y2-DC
740 SN=SQR(Y1+Y2)/(Y1+Y2)
750 E=(Y1-Y2)/(Y1+Y2)
760 PRINT"CE=";CE
```

(FIG. 2.12 cont.)

```
770 PRINT"E=";E
780 PRINT"NOISE EQ.E=";SN
784 IFR=2THEN790
786 NEXTJJ
790 PRINT"AGAIN"
800 INPUTJ
804 IFJ=1THEN590
806 GOTO160
810 PRINT"DUNNIT!"
820 IFK=0THEN1030
830 IFM<73THEN880
840 FORI=MTO79
850 POKE8015+I,0
860 NEXTI
870 GOSUB1220
880 POKE8015+M,240
890 POKE8016+M,240
910 POKE8018+M,R
920 POKE8019+M,L
930 POKE8020+M,240
940 POKE8021+M,240
950 FORI=MTO72
960 POKE8022+I,0
970 NEXTI
980 GOSUB1220
990 FORI=0TO79
1000 POKE8015+I,0
1010 NEXTI
1020 GOSUB1220
1030 PRINT"RUN;";A(1)
1040 PRINTBN;"BLKS TAPED!"
1050 RETURN
1100 Y=PEEK(8013)+256*PEEK(8012)
1110 B=PEEK(8011)+256*PEEK(8010)
1120 PRINTN;Y;B
1130 IFK=0THEN1210
1140 POKE8015+M,PEEK(8012)
1150 POKE8016+M,PEEK(8013)
1160 POKE8017+M,PEEK(8010)
1170 POKE8018+M,PEEK(8011)
1180 M=M+4
1190 IFM<80THEN1210
1200 GOSUB1220
```

(FIG.2.12 cont.)

```
 1210 RETURN
 1220 PRINT"TAPING!"
 1230 POKE4,211:POKE5,31
 1240 X=USR(0):M=0
 1250 POKE4,210:POKE5,30
 1260 BN=BN+1
 1270 RETURN
 1280 IFN<4095THEN1310
 1290 PRINT">RANGE!"
 1300 GOTO1360
 1310 CH=INT(N/256)
 1320 CL=N-256*CH
 1330 POKE40961,CL
 1340 POKE40960,CH
 1350 X=USR(0)
 1360 RETURN
 1370 PI=3.141592654
 1380 PRINT"SEL,EP,BE"
 1390 INPUTSEL,EP,BE
 1400 EP=EP+SEL
 1410 EP=(EP/180)*PI
 1420 BE=(BE/180)*PI
 1430 RR=23.466*PI/180
 1440 SDEL=COS(RR)*SIN(BE)+SIN(RR)*COS(BE)*SIN(EP)
 1450 TDEL=SDEL/SQR(1-(SDEL*SDEL))
 1460 DEL=ATN(TDEL)*180/PI
 1470 CALF=COS(BE)*COS(EP)/SQR(1-(SDEL*SDEL))
 1480 CDEL=SQR(1-(SDEL*SDEL))
 1490 SALF=((COS(RR)*COS(BE)*SIN(EP))-(SIN(RR)*SIN(
BE)))/CDEL
 1500 ALF=ATN(SALF/CALF)
 1510 IFCALF>0THEN1540
 1520 ALF=ALF+PI
 1530 GOTO1560
 1540 IFSALF>0THEN1560
 1550 ALF=ALF+2*PI
 1560 ALF=ALF*180/PI
 1570 HRS=INT(ALF/15)
 1580 MNS=(ALF*4)-HRS*60
 1590 PRINTHRS;MNS;DEL
 1600 RETURN
 1610 A(3)=INT(AA/256)
 1620 A(2)=AA-256*A(3)
```

(FIG.2.12 cont.)

```
1630 A(8)=INT(AB/256)
1640 A(7)=AB-256*A(8)
1650 FORI=1TO9
1670 POKE7023+I,A(I)
1680 NEXTI
1690 FORI=0TO(4*IS)-4STEP4
1700 J=I/4
1710 POKE8015+I,INT(T1(J)/256)
1720 POKE8016+I,T1(J)-256*INT(T1(J)/256)
1730 POKE8017+I,INT(T2(J)/256)
1740 POKE8018+I,T2(J)-256*INT(T2(J)/256)
1750 NEXTI
1760 IFIS=25THEN1790
1770 FORI=1TO(25-IS)*4
1780 POKE8014+4*IS+I,0
1785 NEXTI
1790 POKE4,128:POKE5,27
1800 X=USR(0)
1810 POKE4,210:POKE5,30
1820 RETURN
1830 FORKL=0TOIS-1
1835 ZX=P+(KL*J)
1840 PRINTZX;T1(KL);T2(KL)
1845 NEXTKL
1850 RETURN
1860 R=1
1865 P=100
1870 POKE8009,20
1880 II=30:J=2
1890 K=0
1900 GOSUB220
1905 RETURN
1910 R=1:K=1
1920 P=0
1922 FORI=0TO130
1924 T1(I)=0:T2(I)=0
1926 NEXTI
1940 POKE8009,200
1950 II=25:J=10
1960 PRINT"NO.OF SCANS"
1962 INPUTTT
1970 GOSUB155
1975 GOSUB220
```

(FIG.2.12 cont.)

```
1980 RETURN
1990 R=3
1995 POKE8009,240
2000 GOSUB530
2010 STOP
2020 R=2
2025 POKE8009,200
2030 GOSUB510
2040 RETURN
2050 TT=10
2055 R=1
2060 POKE8009,60
2070 II=55:J=10
2080 P=480:K=1
2090 GOSUB220
3000 RETURN
3010 K=0:P=670
3020 POKE8009,20
3030 II=30:J=2
3040 R=1:GOSUB220
3050 RETURN
```

(FIG.2.12 cont.)

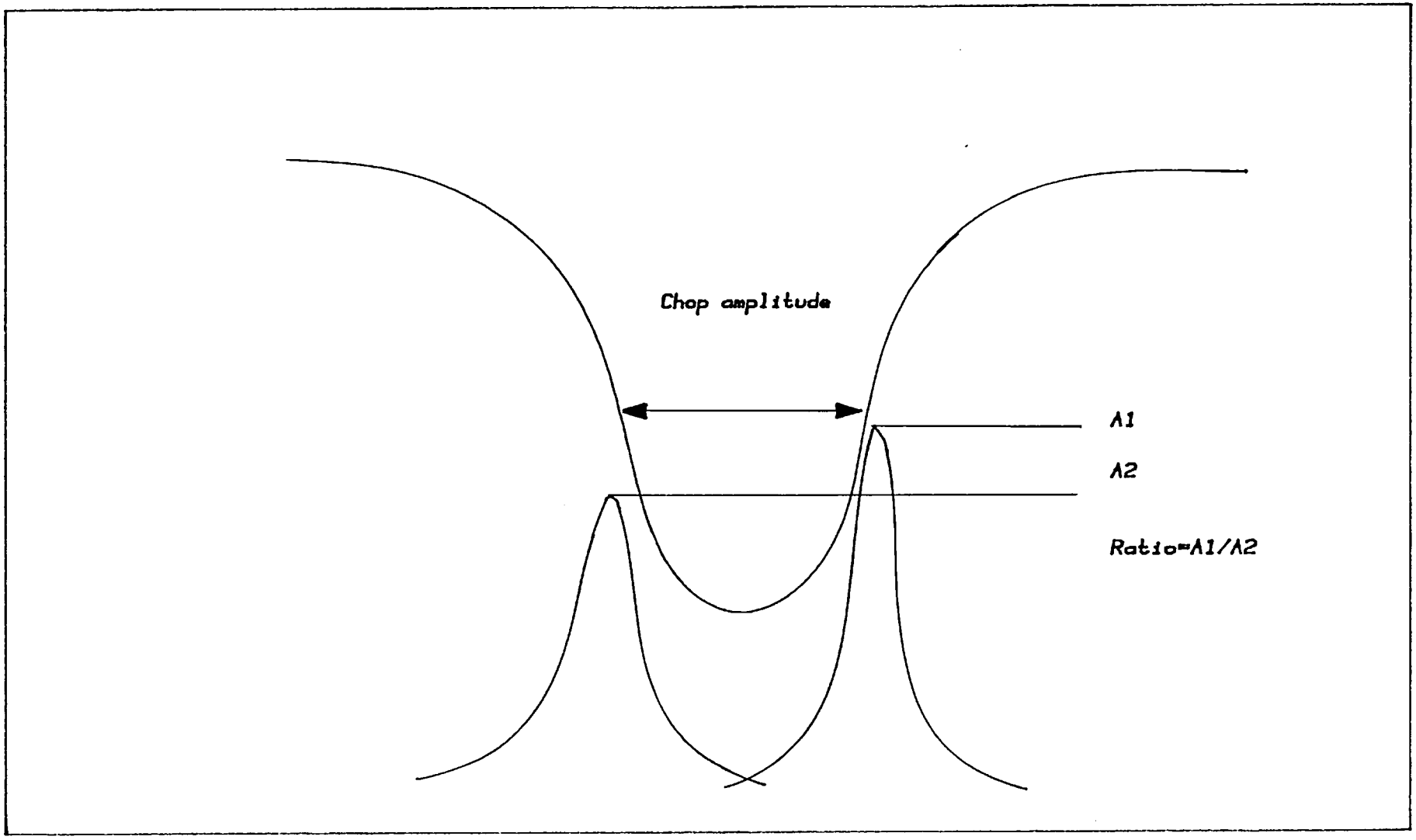

FIG. 2. 13 The Chopping Technique.

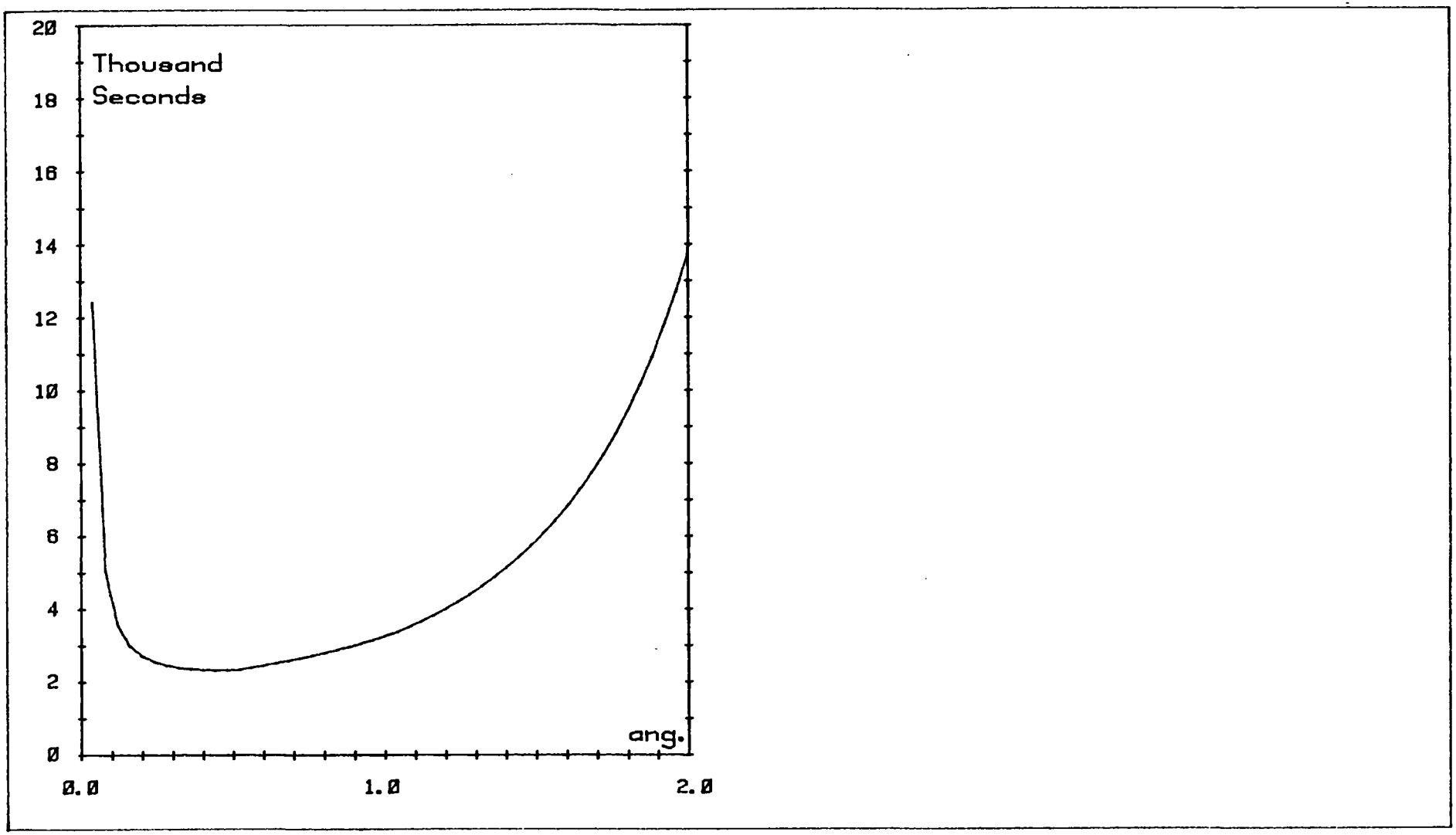

FIG. 2.14 Integration Time vs. Chop Amplitude.

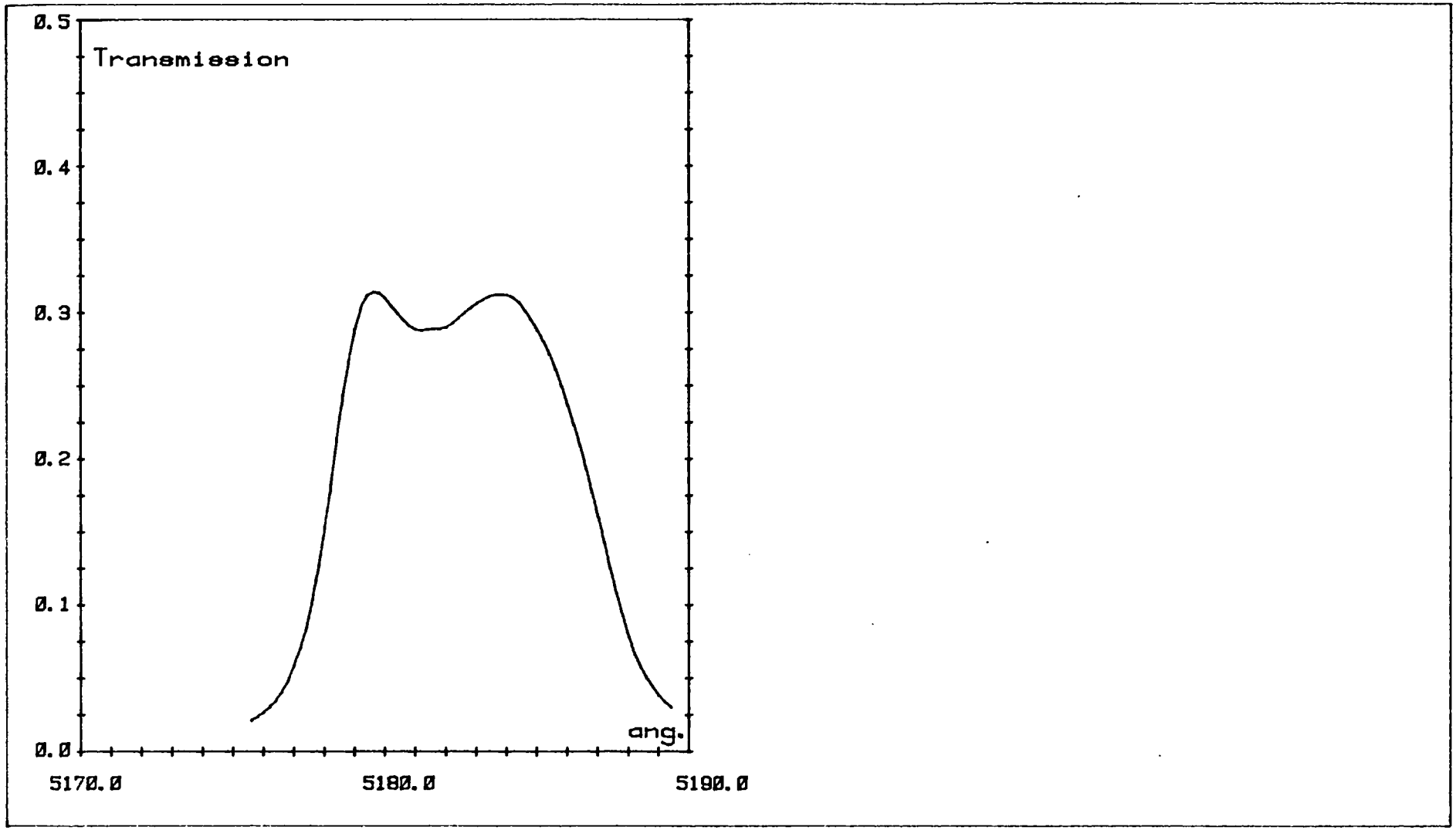

FIG. 2.15 The Interference Filter Profile.

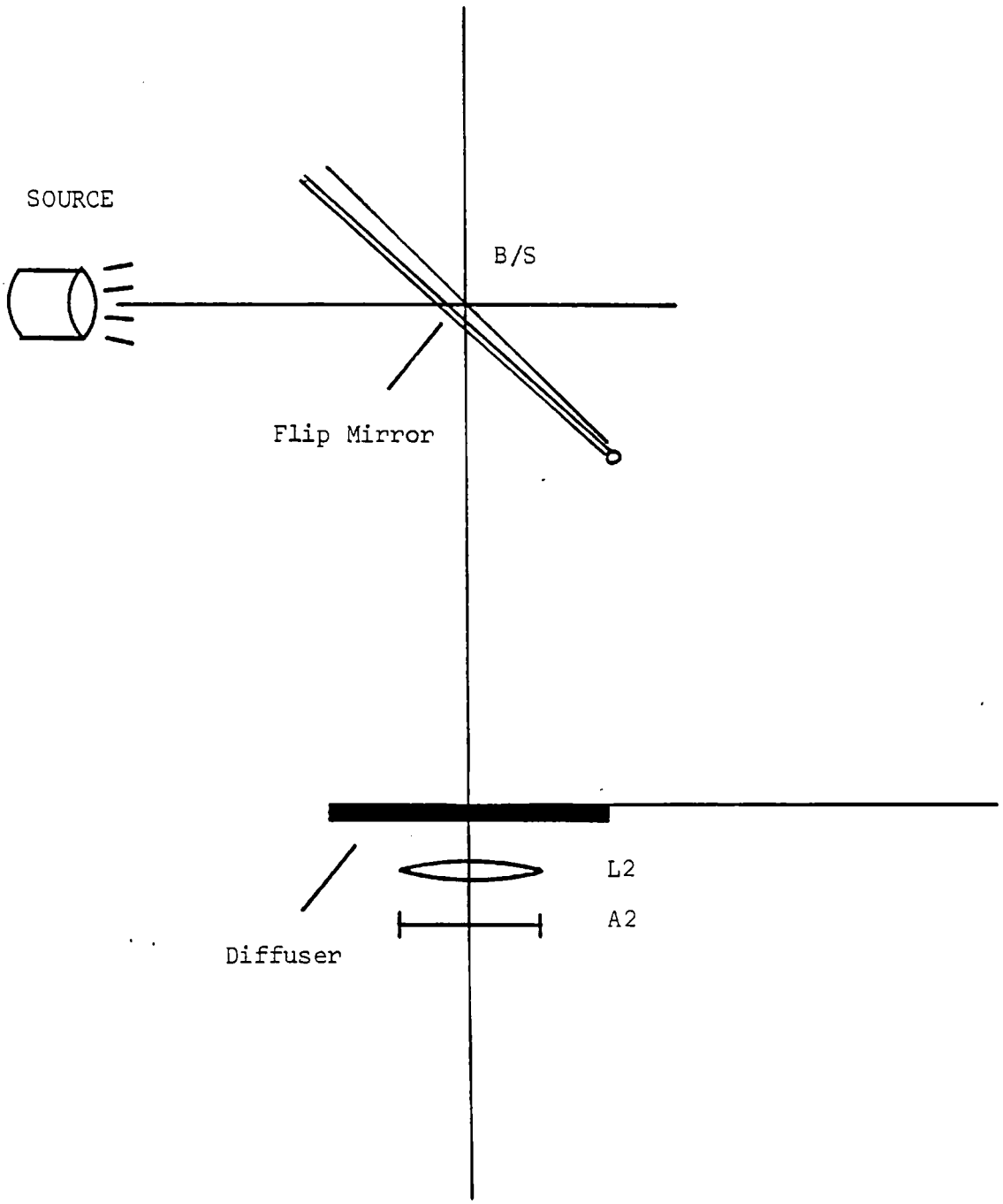

FIG.2.16 Calibration Optics.

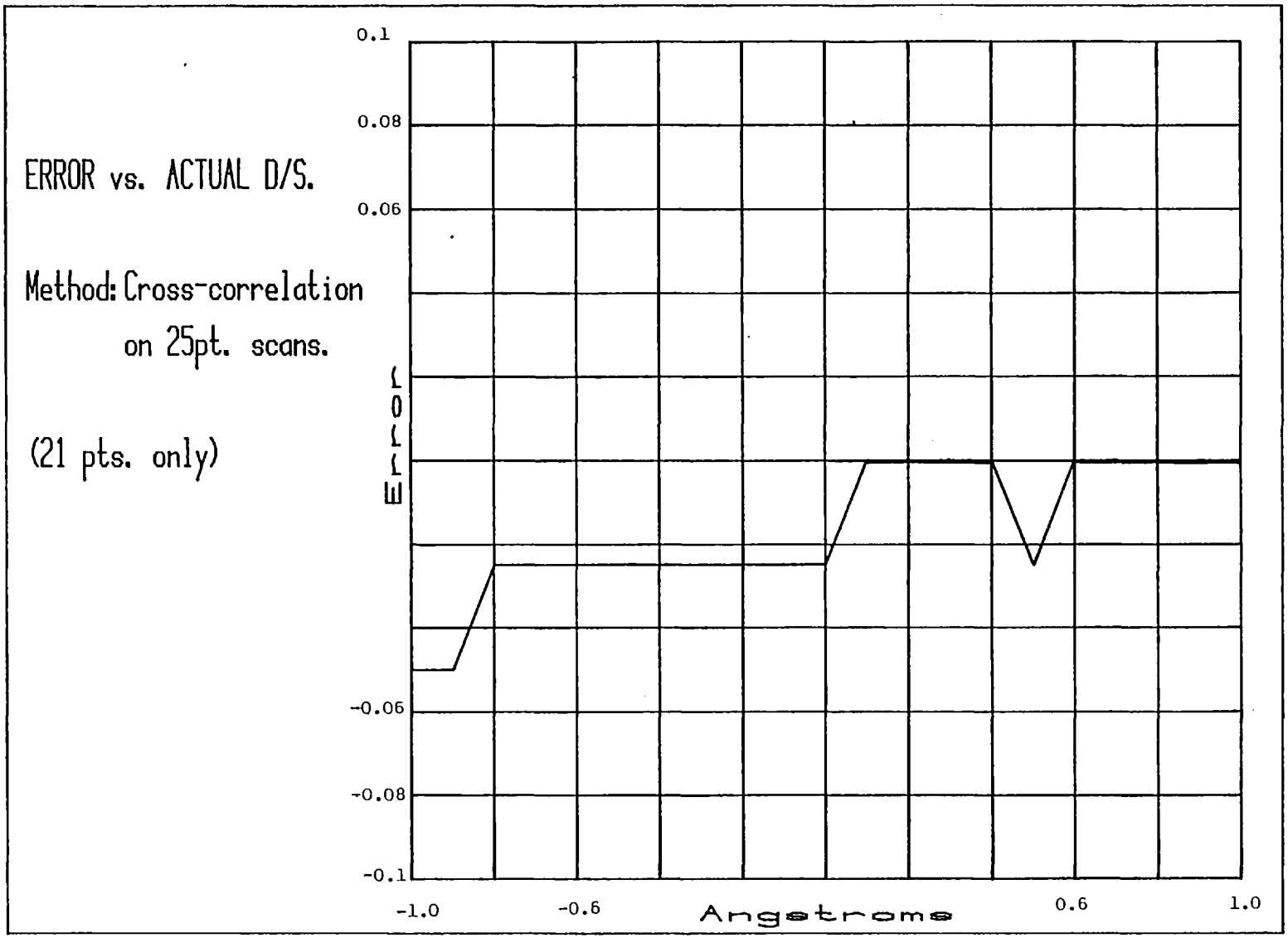

FIG.2.17 Error Resulting From Division of Signal by Int. Filter Profile.

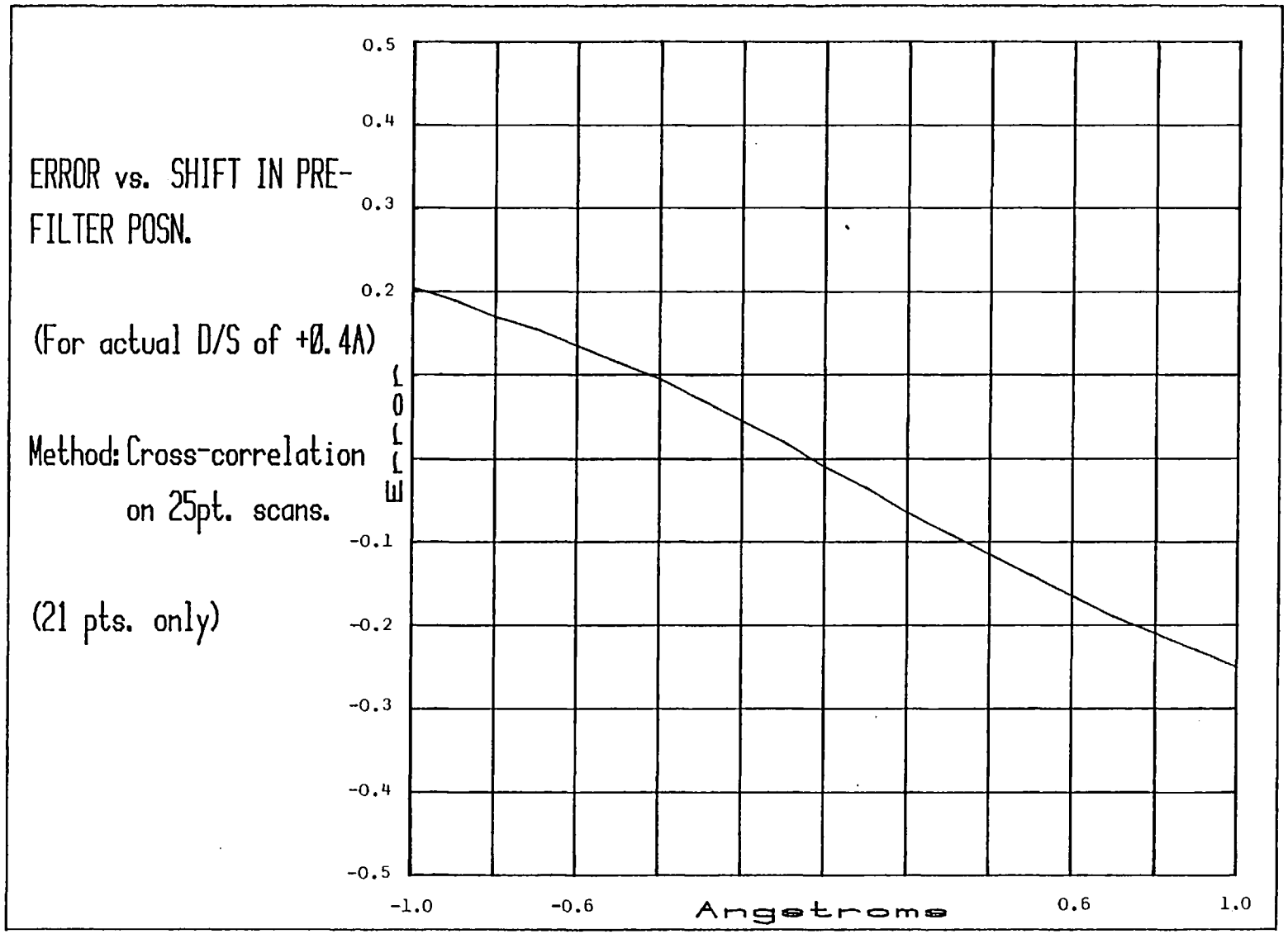

FIG.2.18 As FIG.2.17 but with incorrect Filter Posn..

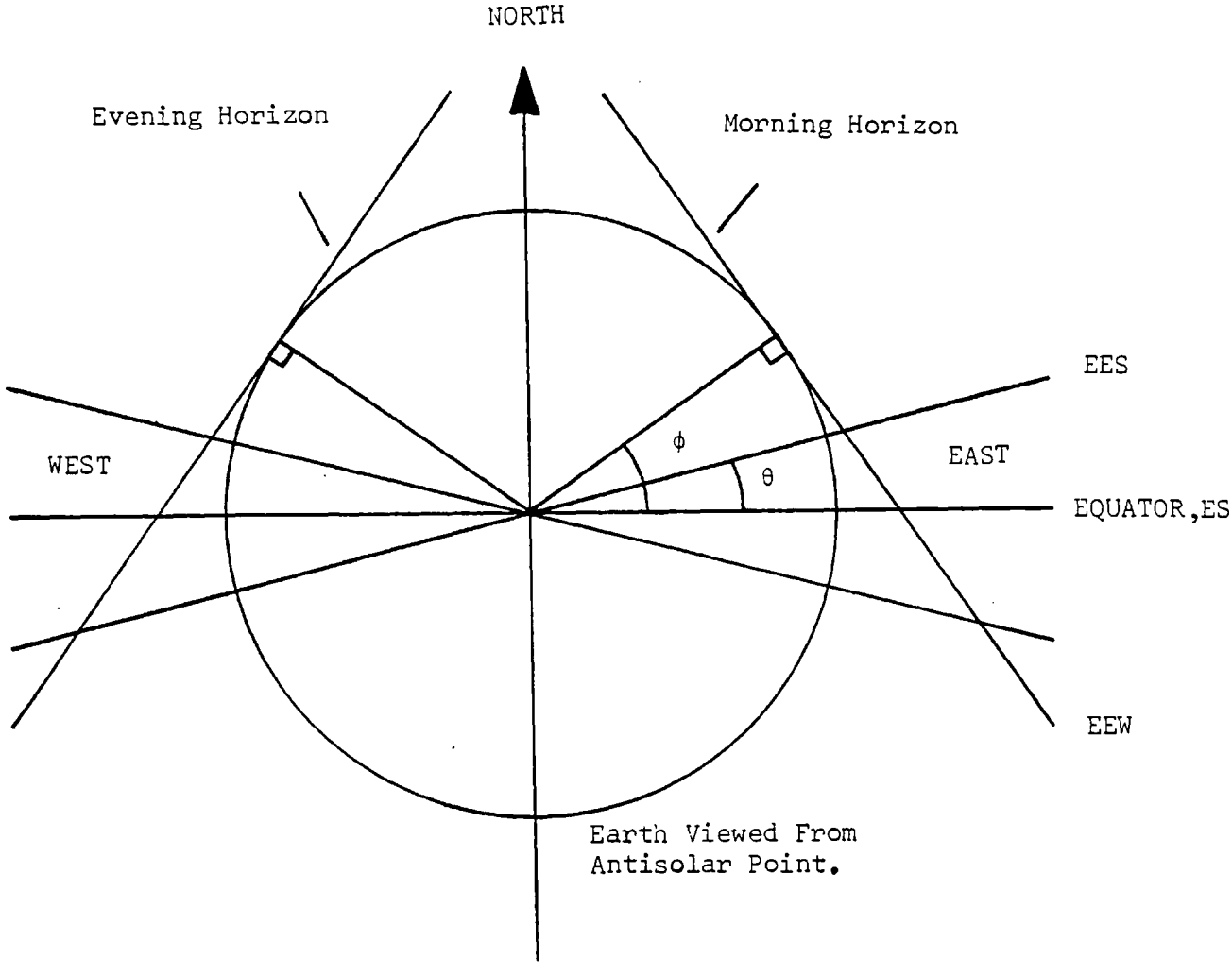

ϕ =lattitude.
θ =Earth's axial tilt.
EES =ecliptic plane for summer equinox.
EEW =ecliptic plane for winter equinox.
ES =ecliptic plane for either solstace.

FIG.2.20 Geometry Defining Orientation of ZL Cone.

```
      program predux
c*************************************************************************
c**                                                                     *
c**       PRE REDUCTION PROGRAM                                         *
c**                                                                     *
c**                                                                     *
c**       ACTIONS:                                                      *
c**               1.Delete unwanted frames.                             *
c**               2.Subtract dark count.                                *
c**               3.Correct for extinction/twilight effects.            *
c**               4.Correct for pre-filter profile.                     *
c**               5.Assess photometric error.                           *
c**                                                                     *
c*************************************************************************
      real a(20),b(20),x1(25),y1(25),h1(10),h2(10),f(280),w1(25)
      real z(25),xf(280)
c**READ IN FILTER PROFILE:
      call assign(10,'ifs.ire')
      do 5 i=1,280
5     read(10,*)xf(i),f(i)
c**ENTER INPUT AND OUTPUT FILE NAMES:
      type *,'INPUT DATA FILE NAME?'
      type *,
      call assign(8,'fname1.ire',-1)
      type *,
      type *,'OUTPUT DATA FILE NAME?'
      type *,
      call assign(9,'fname2.ire',-1)
      type *,
c**
c**ENTER PARAMETERS:
      type *,'No. of frames,no. to be deleted and no. for comp.'
      accept *,n,m1,m2
      if(m1.eq.0.)go to 12
      type *,'Enter the frame no.s to be deleted.'
      do 10 i=1,m1
10          accept *,a(i)
12          if(m2.eq.0)go to 20
      type *,'Enter the frames requiring comp.'
      do 15 i=1,m2
15          accept *,b(i)
c**
c**START LOOP:
20          do 100 ii=1,n
      i=ii
c**
c**READ IN HEADER:
      read(8,*)h1(1),h1(2),h1(3),h1(4),h1(5)
      read(8,*)h2(1),h2(2),h2(3),h2(4)
c**
c**READ IN DATA,SUMMING COUNTS,ASSESSING PHOTOMETRIC ERROR:
      sum=0.
      sum1=0.
```

FIG.3.1 Pre-reduction Program.

```
  ers=0.
  do 40 j=1,25
  read(8,*)w1(j),x1(j),y1(j)
  x1(j)=x1(j)-h2(1)
  sum=sum+y1(j)
  sum1=sum1+x1(j)
40        ers=ers+sqrt(x1(j)+(2.*h2(1)))
  ers=ers/25
  calz=h2(2)
  kfs=h2(4)
  h2(4)=ers
c**TEMP. MOD. TO INCLUDE ERROR DUE TO FILTER POSN. UNCERTAINTY:
  h2(3)=sqrt(((h2(3)*0.0261)**2)+0.01)
  call xzt(calz,z)
  call prefil(z,f,kfs,x1,xf)
c**
c**OUTPUT PARAMETERS TO DISPLAY:
  type *,'FRAME no.',i
  type *,'P/M ERROR=',h2(4)
  type *,'D/C=',h2(1)
  type *,'CALBN. ERROR=',h2(3)
  type *,
c**
c**DELETE?
  t=0
  do 50 j=1,m1
50        if(i.eq.a(j))t=1
  if(t.eq.1)go to 100
c**
c**COMPENSATE?
  t=0
  do 60 j=1,m2
60        if(i.eq.b(j))t=1
  if(t.eq.0)go to 70
  call comp(x1,y1,sum)
  type *,'FRAME NO.',i,'COMPENSATED!'
c**
c**OUTPUT:
70        write(9,*)h1(1),h1(2),h1(3),h1(4),h1(5)
  write(9,*)h2(1),h2(2),h2(3),h2(4)
  do 90 j=1,25
  jj=j
90        write(9,*)w1(jj),x1(jj)
100       continue
  type *,'Pre-reduction complete!'
  stop
  end
c**
c**COMPENSATION SUBROUTINE:
  subroutine comp(x1,y1,sum)
  real x1(25),y1(25)
  do 10 i=1,25
10        y1(i)=y1(i)/sum
```

(FIG.3.1 cont.)

```
  do 20 i=1,25
20        x1(i)=x1(i)/25
  return
  end
c**
c**PRE-FILTER CORRECTION SUBROUTINE:
  subroutine prefil(z,f,kfs,x1,xf)
  real f(280),x1(25),z(25),xf(280)
  do 50 J=1,25
  k=1
10        if(xf(k).le.z(J))go to 30
  k=k+1
  if(k+kfs.le.280)go to 10
30        if(k+kfs.lt.1.or.k+kfs.gt.280)type *,'Out of range!'
  if(k+kfs.gt.280)k=280-kfs
  if(k+kfs.lt.1)k=1-kfs
50        x1(J)=x1(J)/f(k+kfs)
  return
  end
c**
c**WAVELENGTH DETERMINATION:
  subroutine xzt(calz,z)
  real z(25)
  calz=calz/10
  do 10 i=1,25
10        z(i)=((calz-(i-1))*0.261)+5183.618
  return
  end
```

(FIG.3.1 cont.)

```
      program cs
c*************************************************
c**                                              *
c**        CALCULATES CENTRE OF GRAVITY OF LINES.*
c**                                              *
c*************************************************
      real x(25),z(25),z1(25),f(280),xz(25),xf(280),e(100),zx(25)
     1     ,eri(100)
      call assign(4,'cs.ire')
      write(7,5)
5     format(3x,20hno. of pts.,sky D/S?)
      accept *,npt,os
c***Read in filter profile data.
      call assign(2,'ifs.ire')
      do 10 i=1,280
10    read(2,*)xf(i),f(i)
c***Open loop.
      write(6,15)
15    format(6x,3hno.,10x,4hdate,8x,6helong.,10x,4hD/S.,6x,10herror est.
     1     ,2x,12hno. of scans,4x,10hcalbn. pt.)
      do 100 m=1,npt
      i=m
      read(3,*)n,e(i),md,mm,ns
      read(3,*)dc,calz,erc,kfs
      calz=calz/10.
      call xzt(calz,xz)
      do 35 j=1,25
      read(3,*)nj,z(j)
      z(j)=z(j)-dc
c***DIVISION by filter function.!!!!!!
      k=1
30    if(xf(k).le.xz(j))go to 32
      k=k+1
      if(k+kfs.le.280)go to 30
32    if((k+kfs).lt.1.or.(k+kfs).gt.280)write(6,33)
33    format(3x,15hout of range!!!)
      if((k+kfs).gt.280)k=280-kfs
      if((k+kfs).lt.1)k=1-kfs
35    z(j)=z(j)/f(k+kfs)
c***Subtract scan from continuum estimate!!!
      con=(z(1)+z(2))/2
      do 40 j=1,25
      z1(j)=con-z(j)
      xzd=xz(j)-5180.0
40    zx(j)=xzd*z1(j)
c***Now do centre of gravity calculation!!!!!!!!
      call gsf(0.261,zx,x,25)
      x1=x(25)
      call gsf(0.261,z1,x,25)
      x2=x(25)
      dop=(x1/x2)-os-3.618
c***Compute statistical error.(upper limit for one sigma!!!!!
```

FIG.3.2. Listing of Centre of Gravity program.

```
      sum=0.
      do 50 j=1,25
   50 sum=sum+sqrt(z(j)+(2.*dc))
      er=0.261*sum/5.
      erc=erc*0.0261
      er=(er/x2)*2.*(x1/x2)
      er=sqrt((er**2)+(erc**2))
   c***Output!!!!!
   65 write(4,*)e(i),x1,x2,dop,er
      write(6,70)i,md,mm,e(i),dop,er,ns,calz
   70 format(4x,i4,10x,i2,1x,i2,4x,f10.1,4x,f10.3,4x,f10.3,4x,i4,9x,
        1     f10.3)
   100        continue
      stop
      end
      subroutine xzt(calz,xz)
      real xz(25)
      do 10 i=1,25
   10 xz(i)=((calz-float(i-1))*0.261)+5183.618
      return
      end
```

(FIG.3.2. cont.)

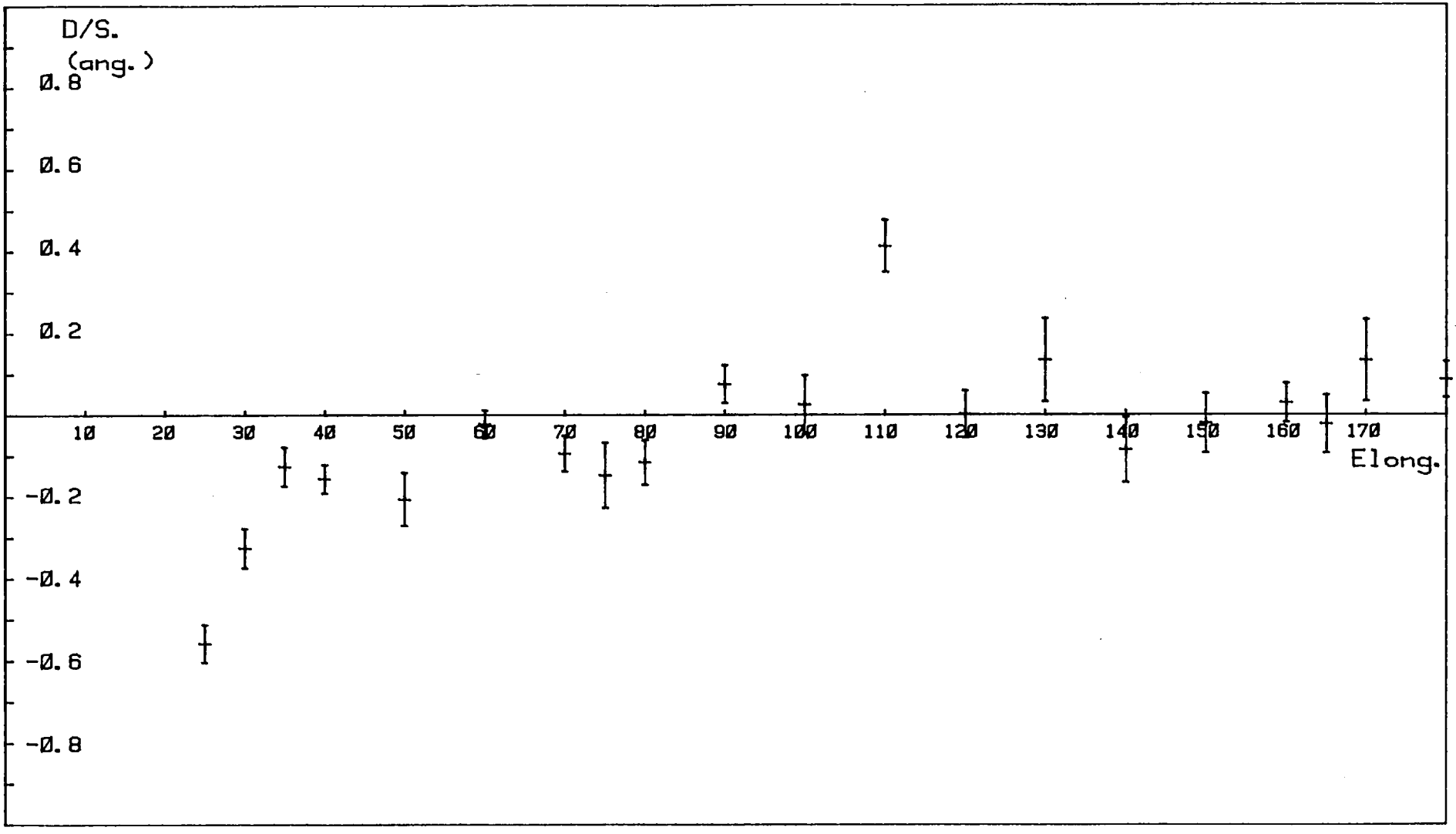

FIG. 3.3 Centre of Gravity Results for Whole Data Set Folded into 180 deg..

ELONGATION	D/S.	ERROR ESTIMATE
25.0	-0.543	0.046
30.0	-0.310	0.048
35.0	-0.111	0.048
40.0	-0.141	0.035
50.0	-0.191	0.065
60.0	-0.007	0.034
70.0	-0.080	0.044
75.0	-0.132	0.080
80.0	-0.101	0.055
90.0	0.090	0.046
100.0	0.040	0.072
110.0	0.426	0.064
120.0	0.017	0.058
130.0	0.149	0.102
140.0	-0.070	0.080
150.0	-0.005	0.073
160.0	0.044	0.048
165.0	-0.008	0.071
170.0	0.148	0.100
180.0	0.101	0.044

COMBINED RESULTS FOLDED INTO 180 DEG.

FIG.3.4 C of G Results Combined from Whole Data Set Folded into 180des..

```
  program xcol
c**************************************************************************
c**                                                                      *
c**                                                                      *
c**        CALCULATES SHIFT OF PEAK OF CROSS-CORRELATION OF              *
c**        LINES WITH GAUSSIAN OF WIDTH EQUAL TO NATURAL                 *
c**        LINE WIDTH AT NATURAL CENTRE.                                 *
c**                                                                      *
c**************************************************************************
  real x(100),s(37),z(25),ds(100),xz(25)
  type *,'Enter filename for results'
  type *,
  call assign(4,'fname1.ire',-1)
  type *,'Enter data filename'
  type*,
  call assign(3,'fname2.ire',-1)
  write(7,5)
5 format(3x,20hno. of pts.,sky D/S?)
  accept *,npt,os
c***Open loop.
  write(6,15)
15        format(6x,3hno.,10x,4hdate,8x,6helong.,10x,4hD/S.,6x,10herror es
t.
     1    ,2x,12hno. of scans,4x,10hcalbn. pt.)
  do 100 m=1,npt
  i=m
  read(3,*)n,e,md,mm,ns
  read(3,*)dc,calz,erc,ers
  calz=calz/10.
  call xzt(calz,xz)
  do 35 j=1,25
35        read(3,*)nj,z(j)
c***Cross-correlate!!!!!!!!!!
  call saus2(s,xz)
  call crass(s,z,25,6,x,0.261)
c***Cross-correlation established.Now for d/s.
  do 40 j=-6,6
  ds(j+7)=(-float(j))*0.261
40        continue
c***Find peak by cubic interpolation.
  k=1
  top=x(1)
  do 50 j=1,13
  if(x(j).le.top)go to 50
  top=x(j)
  k=j
50        continue
  if(k.gt.2)go to 55
  dop=1.566
  go to 65
55        a=x(k-2)
  b=x(k-1)
  c=x(k)
```

FIG.3.5 Cross-Correlation Reduction Program.

```
  d=x(k+1)
  top=x(1)
  do 60 J=0,20
  p=1.+(float(J)*0.1)
  if(cubint(a,b,c,d,p).le.top)go to 60
  top=cubint(a,b,c,d,p)
  pos=p*0.261
  a=p
60        continue
c**CALL ERROR ROUTINE:
  call erf(g,x,ers,top,a,a,b,c,d,err)
  err=sqrt((err**2)+(erc**2))
  dop=ds(k-2)-pos-os
c***Output!!!!!
65        write(4,*)e,dop,err
  write(6,70)i,md,mm,e,dop,err,ns,calz
70        format(4x,i4,10x,i2,1x,i2,4x,f10.1,4x,f10.3,4x,f10.3,4x,i4,9x,
     1    f10.3)
100       continue
  stop
  end
c**CUBIC INTERPOLATION:
  function cubint (a,b,c,d,p)
  cubint=-(p-1.0)*(p-2.0)*(p-3.0)*a/6.0
     1    +p*(p-2.0)*(p-3.0)*b/2.0-p*(p-1.0)*(p-3.0)*c/2.0
     1    +p*(p-1.0)*(p-2.0)*d/6.0
  end
c**WAVELENGTH DETERMINATION:
  subroutine xzt(calz,xz)
  real xz(25)
  do 10 i=1,25
10        xz(i)=((calz-float(i-1))*0.261)+5183.618
  return
  end
c**GAUSSIAN GENERATION:
  subroutine gaus2(g,xz)
  real g(37),xz(25)
  do 10 i=1,37
  J=i
  w1=xz(1)-((J-7)*0.261)
10        g(i)=-100.*exp(-1.2323*((w1-5183.618)**2))
  return
  end
c**ERROR ROUTINE:
  subroutine erf(g,x,ers,top,a,a,b,c,d,err)
  real g(37),x(13)
  do 10 i=1,25
10        g(i)=g(i)**2
  call asf(0.261,g,g,37)
  err=top-ers*sqrt(abs(g(37)))
  p1=a-0.1
15        if(cubint(a,b,c,d,p1).le.err)go to 30
  p1=p1-0.1
```

(FIG.3.5 cont.)

```
  if(p1.ge.0.)go to 15
30        err=(a-p1)*0.261
  return
  end
  subroutine acn3(d,c,fin)
c*************************************************************
c**       CONVOLVES B WITH AIRY FN.                          *
c**                                                          *
C**       ONE CALL ONLY TO AIRY SO BEWARE OF OUTER           *
C**       ORDERS!!!!!                                        *
c*************************************************************
  real d(25),a(561),c(25),b(321),c1(321)
c**
c**INTERPOLATE 241 VALUES:
  do 2 m=1,22,3
  j=m
  a1=d(j)
  a2=d(j+1)
  a3=d(j+2)
  a4=d(j+3)
  do 2 k=0,29
  p=k*0.1
  i=41+((j-1)*10)+k
2 b(i)=cubint(a1,a2,a3,a4,p)
  b(281)=d(25)
c**
c**synthesise continuum:
  do 3 j=1,40
3 b(j)=b(41)
  do 4 j=282,321
4 b(j)=b(281)
c**
c**generate airy fn. and convolve:
5 call airy2(a,5183.618,fin)
  do 20 j=-120,120,10
  do 10 i=1,321
10        c1(i)=a(i+120-j)*b(i)
  call asf(0.0261,c1,c1,321)
  l=j/10
20        c(l+13)=c1(321)
  return
  end
  subroutine airy(a,cen,fin)
  real*8 sap,sam1,pi
  real a(800)
  pi=3.14159265
  tor=0.7
  sap=347.*cen/2.
  sm1=5203.618
  deltal=0.05
  do 300 j=1,800
  sam1=sm1-(float(j-1)*deltal)
  a(j)=tor/(1.0+0.4053*(sin(2.*pi*sap/sam1)**2)*(fin**2))

300    continue
  return
  end
```

(FIG.3.5 cont.)

```
  program xcol2
c**********************************************************************
c**                                                                   *
c**                                                                   *
c**       CALCULATES SHIFT OF PEAK OF CROSS-CORRELATION OF            *
c**       LINES WITH GAUSSIAN OF WIDTH EQUAL TO NATURAL               *
c**       LINE WIDTH AT NATURAL CENTRE.                               *
c**                                                                   *
c**       UPDATE:                                                     *
c**              USES DIFFERENTIAL OF A GAUSSIAN AS REF.              *
c**              FUNCTION.WHILST GIVING THE SAME SHIFT                *
c**              BETTER ALLOWS ERROR HANDLING.                        *
c**                                                                   *
c**                                                                   *
c**********************************************************************
  real x(13),s(37),z(25),ds(100),xz(25)
  type *,'Enter filename for results'
  type *,
  call assign(4,'fname1.ire',-1)
  type *,'Enter data filename'
  type *,
  call assign(3,'fname2.ire',-1)
  write(7,5)
5 format(3x,20hno. of pts.,sky D/S?)
  accept *,npt,os
c***Open loop.
  write(6,15)
15        format(6x,3hno.,10x,4hdate,8x,6helong.,10x,4hD/S.,6x,10herror es
t.
     1    ,2x,12hno. of scans,4x,10hcalbn. pt.)
  do 100 m=1,npt
  i=m
  read(3,*)n,e,md,mm,ns
  read(3,*)dc,calz,erc,ers
  calz=calz/10.
  call xzt(calz,xz)
  do 35 j=1,25
35        read(3,*)nj,z(j)
c***Cross-correlate!!!!!!!!!!
  call dsaus(s,xz)
  call cross(s,z,25,6,x,0.261)
c***Cross-correlation established.Now for d/s.
  do 40 j=-6,6
  ds(j+7)=-j*0.261
40        continue
c***Find zero by cubic interpolation.
  k=4
45        try1=sign(1,x(k))
  try2=sign(1,x(k-1))
  if(try1.ne.try2)go to 55
  k=k+1
  if(k.le.11)go to 45
55        a=x(k-2)
```

FIG.3.6 Cross-Correlation Reduction Program; Improved Version.

```
  b=x(k-1)
  c=x(k)
  d=x(k+1)
  do 60 j=0,20
  p=1
57        try1=sign(1,cubint(a,b,c,d,p))
  try2=sign(1,cubint(a,b,c,d,p+0.1))
  if(try1.ne.try2)go to 60
  p=p+0.1
  if(p.le.2.0)go to 57
60        pos=p*0.261
c**CALL ERROR ESTIMATE ROUTINE:
  call erf(g,x,ers,p,a,b,c,d,err)
  err=sqrt((err**2)+(erc**2))
  dop=ds(k-2)-pos-os
c***Output!!!!!
65        write(4,*)e,dop,err
  write(6,70)i,md,mm,e,dop,err,ns,calz
70        format(4x,i4,10x,i2,1x,i2,4x,f10.1,4x,f10.3,4x,f10.3,4x,i4,9x,
     1    f10.3)
100       continue
  stop
  end
c**CUBIC INTERPOLATION:
  function cubint (a,b,c,d,p)
  cubint=-(p-1.0)*(p-2.0)*(p-3.0)*a/6.0
     1    +p*(p-2.0)*(p-3.0)*b/2.0-p*(p-1.0)*(p-3.0)*c/2.0
     1    +p*(p-1.0)*(p-2.0)*d/6.0
  end
c**CALC. LAMBDA FOR EACH POINT:
  subroutine xzt(calz,xz)
  real xz(25)
  do 10 i=1,25
10        xz(i)=((calz-(i-1))*0.261)+5183.618
  return
  end
c**GENERATION OF THE DIFFERENTIAL OF A GAUSSIAN:
  subroutine dsaus(g,xz)
  real g(37),xz(25)
  do 10 i=1,37
  j=i
  w1=xz(1)-((j-7)*0.261)
  bum=w1-5183.618
10        g(i)=200.*bum*exp(-1.2323*(bum**2))
  return
  end
c**ERROR ESTIMATE SUBROUTINE:
  subroutine erf(g,x,ers,p,a,b,c,d,err)
  real g(37),x(13)
  do 10 i=1,37
10        g(i)=g(i)**2
  call asf(0.261,g,g,37)
  err=ers*sqrt(abs(g(37)))
```

(FIG.3.6 cont.)

```
  p1=p
15        try=abs(cubint(a,b,c,d,p1))
  if(try.ge.err)go to 30
  p1=p1+0.1
  if(p1.le.2)go to 15
30        err=(p-p1)*0.261
  return
  end
  subroutine acn3(d,c,fin)
c*************************************************************
c**       CONVOLVES B WITH AIRY FN.                          *
c**                                                          *
C**       ONE CALL ONLY TO AIRY SO BEWARE OF OUTER           *
C**       ORDERS!!!!!                                        *
c*************************************************************
  real d(25),a(561),c(25),b(321),c1(321)
c**
c**INTERPOLATE 241 VALUES:
  do 2 m=1,22,3
  j=m
  a1=d(j)
  a2=d(j+1)
  a3=d(j+2)
  a4=d(j+3)
  do 2 k=0,29
  p=k*0.1
  i=41+((j-1)*10)+k
2 b(i)=cubint(a1,a2,a3,a4,p)
  b(281)=d(25)
c**
c**synthesise continuum:
  do 3 j=1,40
3 b(j)=b(41)
  do 4 j=282,321
4 b(j)=b(281)
c**
c**generate airy fn. and convolve:
5 call airy2(a,5183.618,fin)
  do 20 j=-120,120,10
  do 10 i=1,321
10        c1(i)=a(i+120-j)*b(i)
  call gsf(0.0261,c1,c1,321)
  l=j/10
20        c(l+13)=c1(321)
  return
  end
  subroutine airy(a,cen,fin)
  real*8 gap,sam1,pi
  real a(800)
  pi=3.14159265
  tor=0.7
  gap=347.*cen/2.
  sm1=5203.618
```

(FIG.3.6. cont.)

```
  deltal=0.05
  do 300 j=1,800
  saml=sml-(float(j-1)*deltal)
  a(j)=tor/(1.0+0.4053*(sin(2.*pi*sap/saml)**2)*(fin**2))
300       continue
  return
  end
```

(FIG.3.6 cont.)

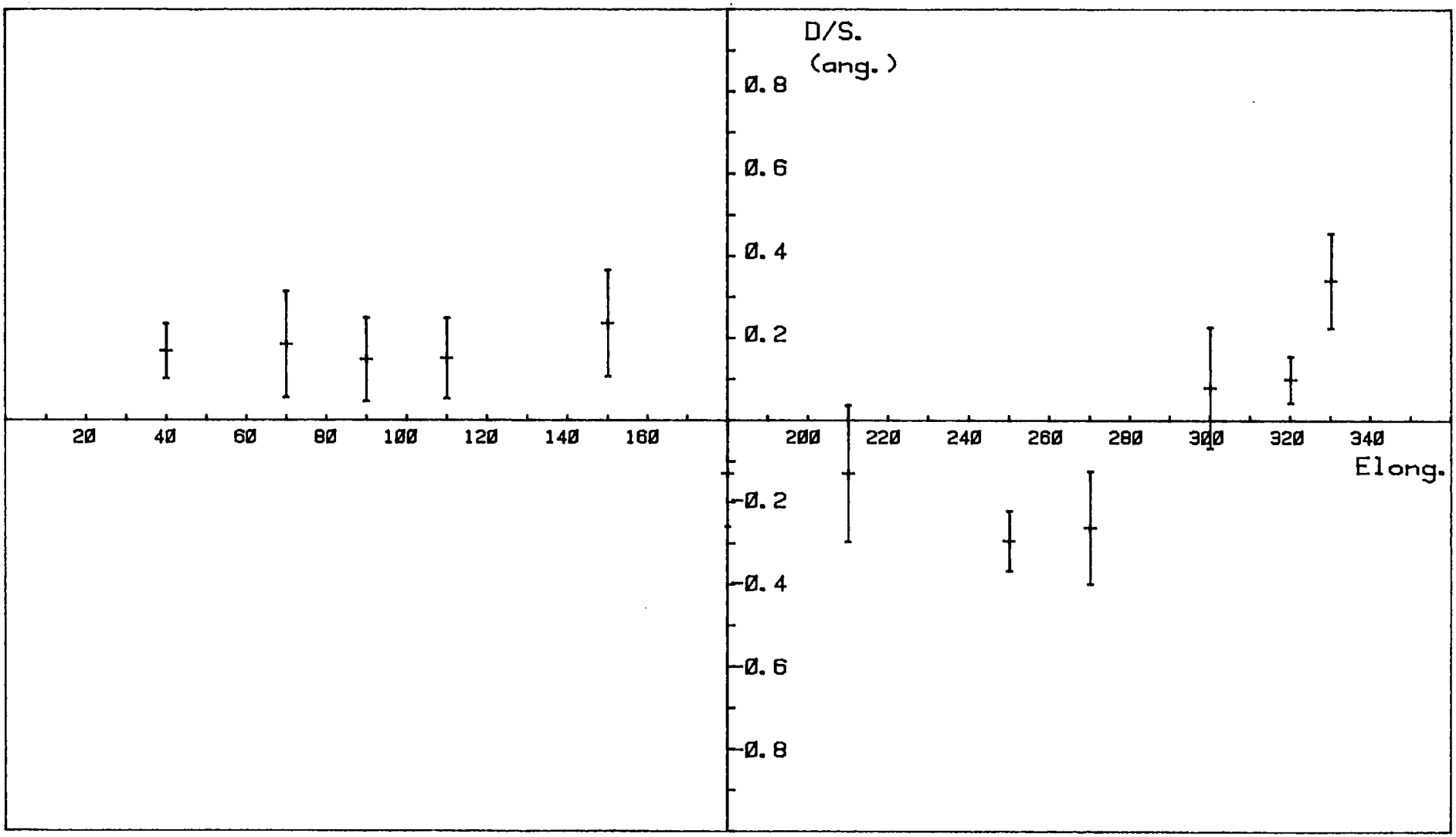

FIG. 3.7 Cross-Correlation Results for July 1981.

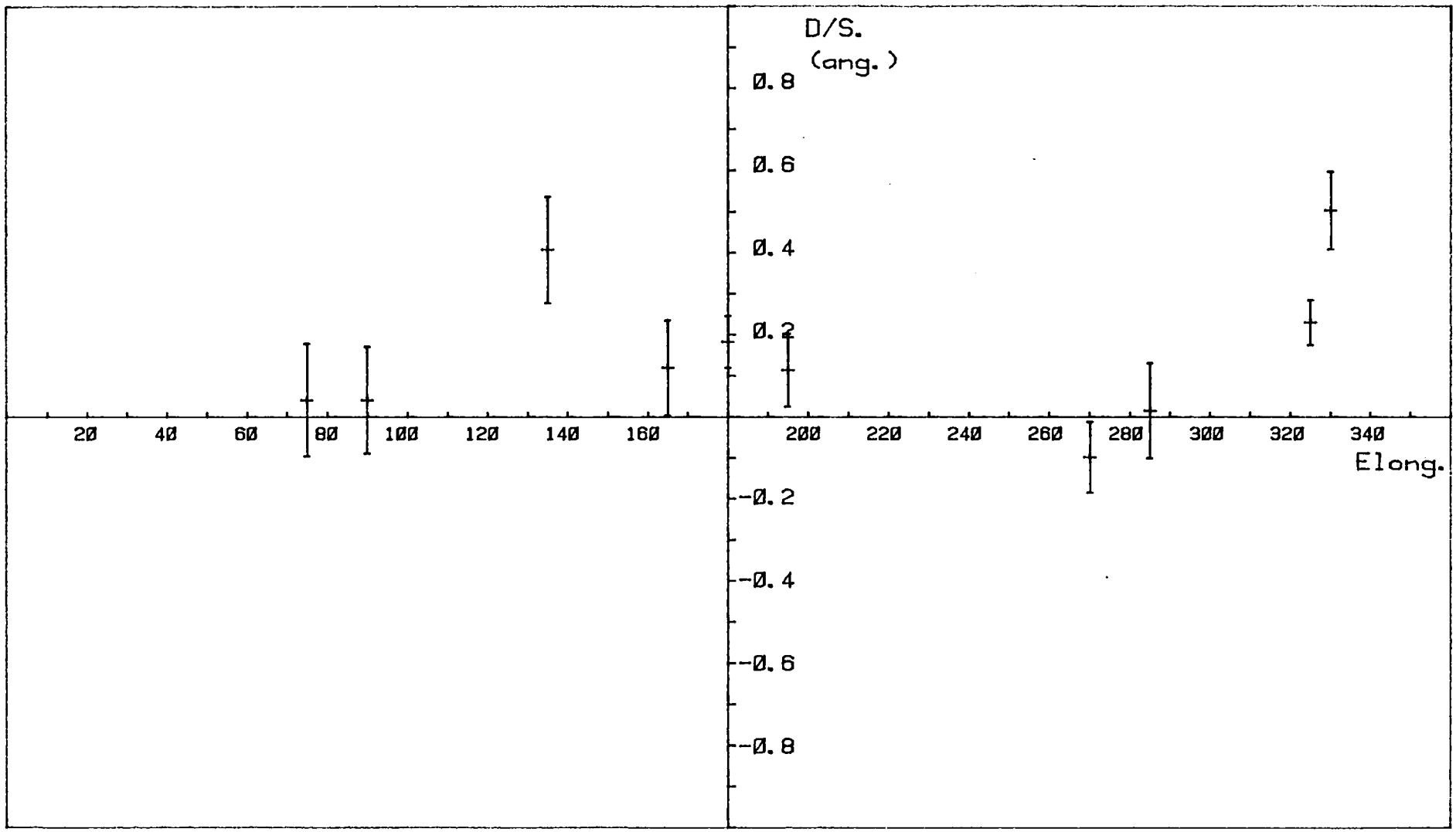

FIG. 3.8 Cross-Correlation Results for September 1981.

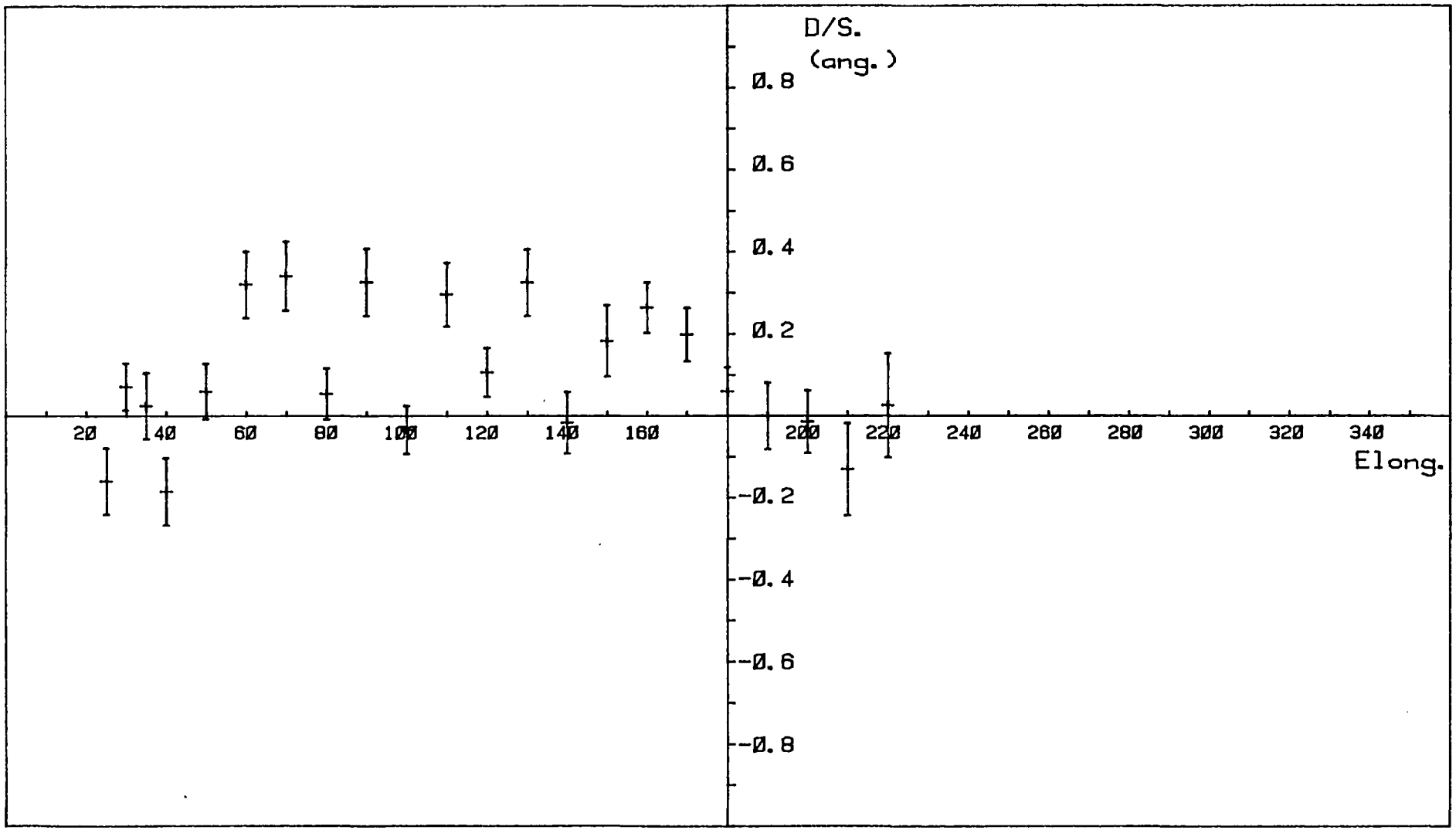

FIG. 3.9 Cross-Correlation Results for April 1982.

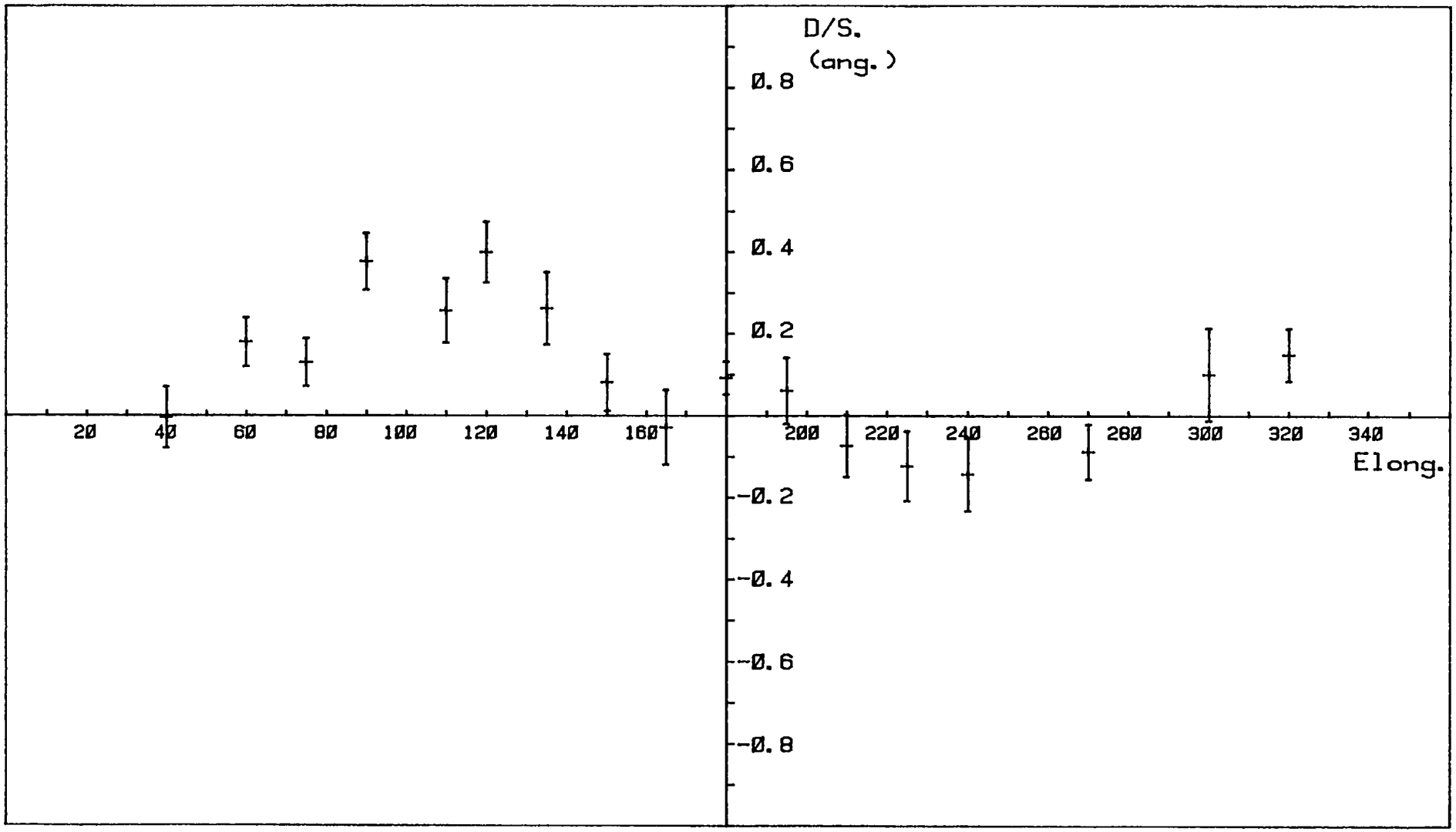

FIG. 3.10 Cross-Correlation Results for July 1982.

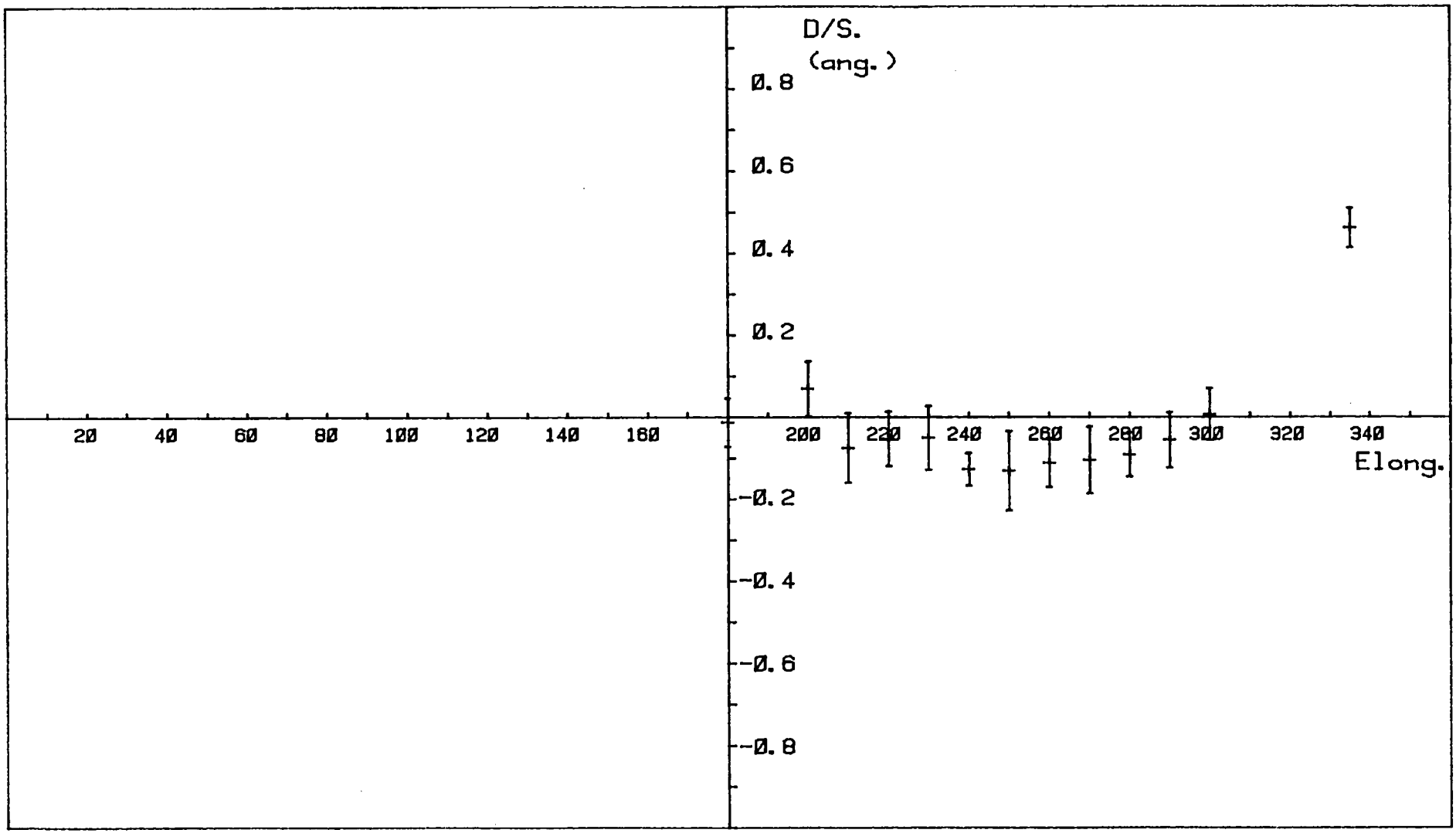

FIG. 3.11 Cross-Correlation Results for September 1982.

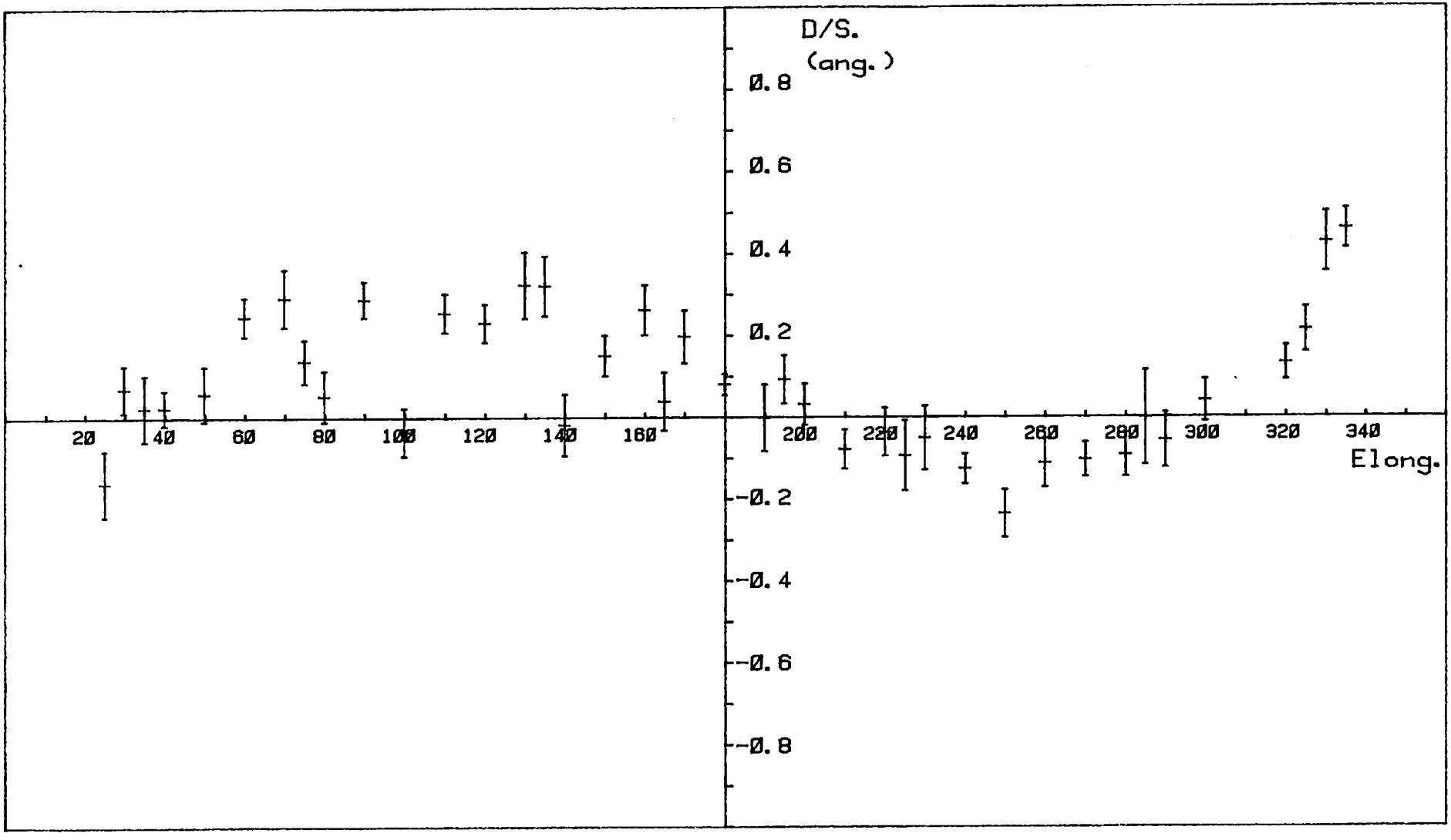

FIG. 3.12 Cross-Correlation Results for Whole Data Set.

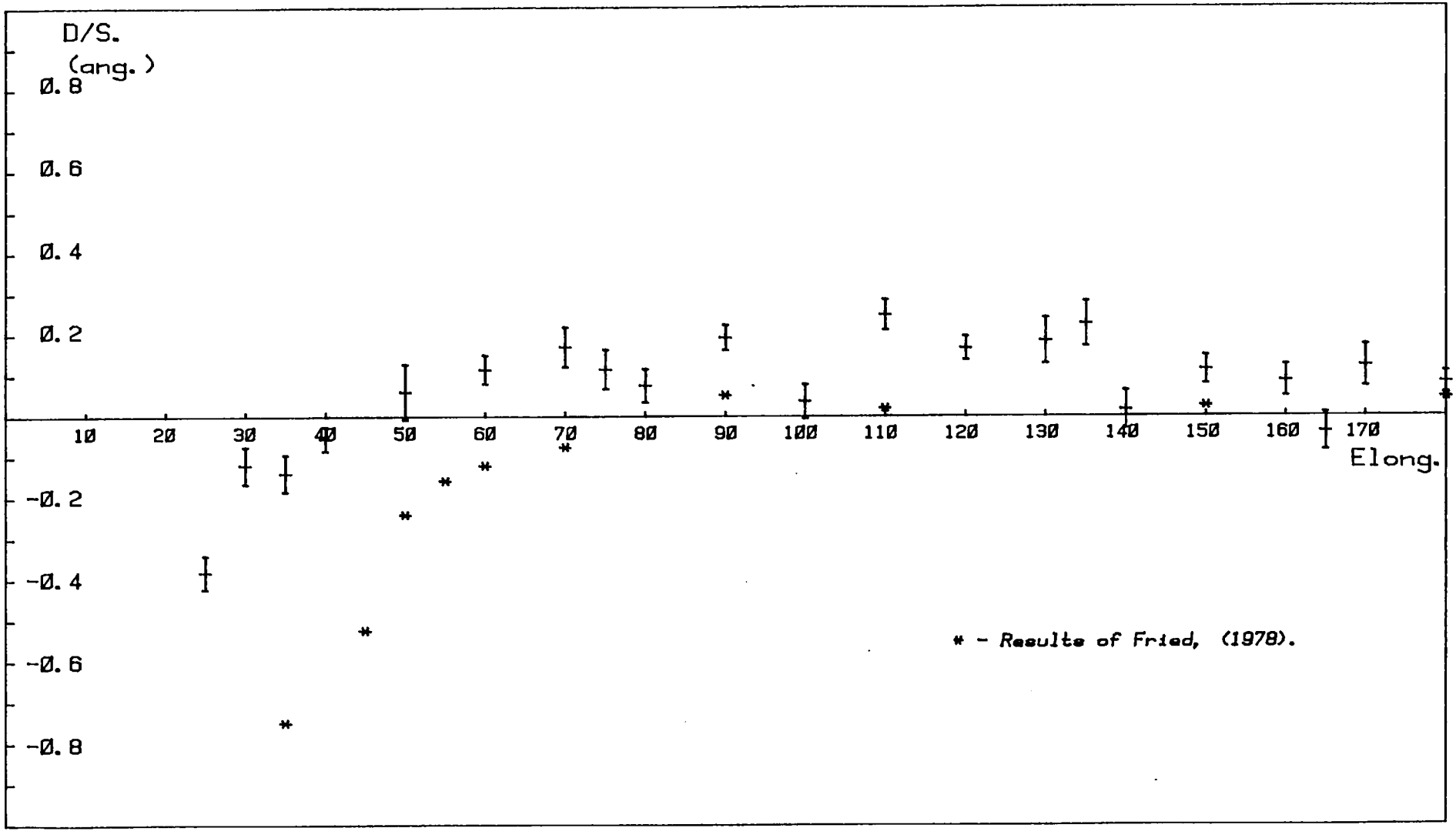

FIG. 3.13 Cross-Correlation Results for Whole Data Set Folded into 180 deg..

ELONGATION	D/S.	ERROR ESTIMATE
75.00000	2.6299970E-02	0.1373162
90.00000	2.6299970E-02	0.1296615
135.0000	0.3917000	0.1296615
165.0000	0.1046000	0.1157845
180.0000	0.1674272	6.3359521E-02
195.0000	9.8163240E-02	8.8517271E-02
270.0000	-0.1128372	8.6362943E-02
285.0000	1.9996241E-04	0.1157845
325.0000	0.2139098	5.4532003E-02
330.0000	0.4875903	9.5053189E-02

SEPT. 1981

ELONGATION	D/S.	ERROR ESTIMATE
40.00000	0.1670963	6.7102969E-02
70.00000	0.1829000	0.1296615
90.00000	0.1467915	0.1018097
110.0000	0.1492103	9.7869568E-02
150.0000	0.2351000	0.1296615
180.0000	-0.1303000	0.1296615
210.0000	-0.1303000	0.1664676
250.0000	-0.2939883	7.3106073E-02
270.0000	-0.2608000	0.1373162
300.0000	7.8499958E-02	0.1469033
320.0000	9.8466180E-02	5.6130014E-02
330.0000	0.3395000	0.1157845

JULY 1981

FIG.3.14 Cross-Correlation Results from July and Sept. 1981.

ELONGATION	D/S.	ERROR ESTIMATE
25.00000	-0.1584412	8.0797754E-02
30.00000	7.1974978E-02	5.7892248E-02
35.00000	2.4939133E-02	8.0797754E-02
40.00000	-0.1842157	8.2341336E-02
50.00000	6.0405776E-02	6.7743145E-02
60.00000	0.3205389	8.0817893E-02
70.00000	0.3409536	8.4341124E-02
80.00000	5.3836502E-02	6.2997706E-02
90.00000	0.3264500	8.1871994E-02
100.0000	-3.3741605E-02	5.8139224E-02
110.0000	0.2966593	7.7476099E-02
120.0000	0.1067625	6.0042255E-02
130.0000	0.3254294	8.0797754E-02
140.0000	-1.6439110E-02	7.5113349E-02
150.0000	0.1827115	8.6362943E-02
160.0000	0.2644870	6.1333362E-02
170.0000	0.1989459	6.4965867E-02
180.0000	6.0434200E-02	5.9675481E-02
190.0000	1.9996241E-04	8.1871994E-02
200.0000	-1.3989465E-02	7.6203011E-02
210.0000	-0.1303000	0.1128044
220.0000	2.6299970E-02	0.1270075

APRIL 1982

FIG.3.15 Cross-Correlation Results from April 1982.

ELONGATION	D/S.	ERROR ESTIMATE
40.00000	2.5213102E-02	7.4338712E-02
60.00000	0.2090000	5.9416488E-02
75.00000	0.1594830	5.8121543E-02
90.00000	0.4053668	6.9566764E-02
110.0000	0.2858234	7.8739807E-02
120.0000	0.4279792	7.4450411E-02
135.0000	0.2915510	8.8933751E-02
150.0000	0.1110834	6.8739019E-02
165.0000	1.8190615E-03	9.0731621E-02
180.0000	0.1218275	4.0593345E-02
195.0000	9.0529375E-02	8.0797754E-02
210.0000	-4.2793572E-02	7.5748160E-02
225.0000	-9.2353888E-02	8.5565135E-02
240.0000	-0.1122900	8.9727677E-02
270.0000	-5.7299938E-02	6.7102969E-02
300.0000	0.1307000	0.1128044
320.0000	0.1784918	6.4108782E-02

JULY 1982

FIG.3.16 Cross-Correlation Results from July 1982.

ELONGATION	D/S.	ERROR ESTIMATE
180.0000	-1.2153811E-02	5.9416488E-02
200.0000	6.9799960E-02	6.6848196E-02
210.0000	-7.4403107E-02	8.4721580E-02
220.0000	-5.2000005E-02	6.6848196E-02
230.0000	-4.9846523E-02	7.8421675E-02
240.0000	-0.1265784	3.9907973E-02
250.0000	-0.1303000	9.6713059E-02
260.0000	-0.1111871	5.9907194E-02
270.0000	-0.1042000	8.1871994E-02
280.0000	-9.0751968E-02	5.3698123E-02
290.0000	-5.4869819E-02	6.7743145E-02
300.0000	6.8136007E-03	6.3145176E-02
335.0000	0.4610532	4.8243936E-02

SEPT. 1982

FIG.3.17 Cross-Correlation Results from Sept. 1982.

ELONGATION	O/S	ERROR ESTIMATE
25.00000	-0.1584412	8.0797739E-02
30.00000	7.1974978E-02	5.7892248E-02
35.00000	2.4939133E-02	8.0797739E-02
40.00000	2.6341410E-02	4.2619649E-02
50.00000	6.0405780E-02	6.7743130E-02
60.00000	0.2481347	4.7871340E-02
70.00000	0.2939619	7.0700027E-02
75.00000	0.1392477	5.3524364E-02
80.00000	5.3836498E-02	6.2997699E-02
90.00000	0.2895600	4.4203870E-02
100.0000	-3.3741601E-02	5.8139224E-02
110.0000	0.2570062	4.8096467E-02
120.0000	0.2333495	4.6737183E-02
130.0000	0.3254294	8.0797739E-02
135.0000	0.3235922	7.3340155E-02
140.0000	-1.6439108E-02	7.5113334E-02
150.0000	0.1529896	4.9678560E-02
160.0000	0.2644870	6.1333347E-02
165.0000	4.0921800E-02	7.1416348E-02
170.0000	0.1989459	6.4965867E-02
180.0000	8.2064994E-02	2.5998045E-02
190.0000	1.9996241E-04	8.1871994E-02
195.0000	9.3998976E-02	5.9675466E-02
200.0000	3.3361316E-02	5.0252605E-02
210.0000	-7.6506488E-02	4.8321273E-02
220.0000	-3.5014346E-02	5.9154775E-02
225.0000	-9.2353888E-02	8.5565113E-02
230.0000	-4.9846519E-02	7.8421675E-02
240.0000	-0.1242187	3.6463983E-02
250.0000	-0.2344675	5.8319099E-02
260.0000	-0.1111871	5.9907179E-02
270.0000	-0.1024941	4.2319015E-02
280.0000	-9.0751961E-02	5.3698123E-02
285.0000	1.9996241E-04	0.1157845
290.0000	-5.4869819E-02	6.7743130E-02
300.0000	4.1567143E-02	5.1590286E-02
320.0000	0.1331919	4.2230766E-02
325.0000	0.2139098	5.4532003E-02
330.0000	0.4279671	7.3467344E-02
335.0000	0.4610532	4.8243936E-02

COMBINED RESULTS

FIG.3.18 Cross-Correlation Results Combined from Whole Data Set.

ELONGATION	D.S.	ERROR ESTIMATE
25.00000	-0.3815204	4.1421812E-02
30.00000	-0.1195405	4.5471203E-02
35.00000	-0.1391599	4.5200441E-02
40.00000	-5.4156400E-02	2.9998198E-02
50.00000	6.0405783E-02	6.7743123E-02
60.00000	0.1141008	3.5091307E-02
70.00000	0.1693116	4.8913553E-02
75.00000	0.1146948	4.8584320E-02
80.00000	7.5217485E-02	4.0866625E-02
90.00000	0.1919539	3.0568697E-02
100.0000	3.6552671E-02	4.1721661E-02
110.0000	0.2478822	3.7105560E-02
120.0000	0.1655116	2.8749254E-02
130.0000	0.1835263	5.6273747E-02
135.0000	0.2256581	5.5684436E-02
140.0000	1.5317975E-02	4.6473231E-02
150.0000	0.1136890	3.4638196E-02
160.0000	8.6274624E-02	3.8871370E-02
165.0000	-3.8526233E-02	4.5792878E-02
170.0000	0.1220016	5.0890636E-02
180.0000	8.2064994E-02	2.5998045E-02

COMBINED DATA SET FOLDED INTO 180deg.

FIG.5.19 Cross-Correlation Results Combined from Whole Data Set Folded into 180deg.

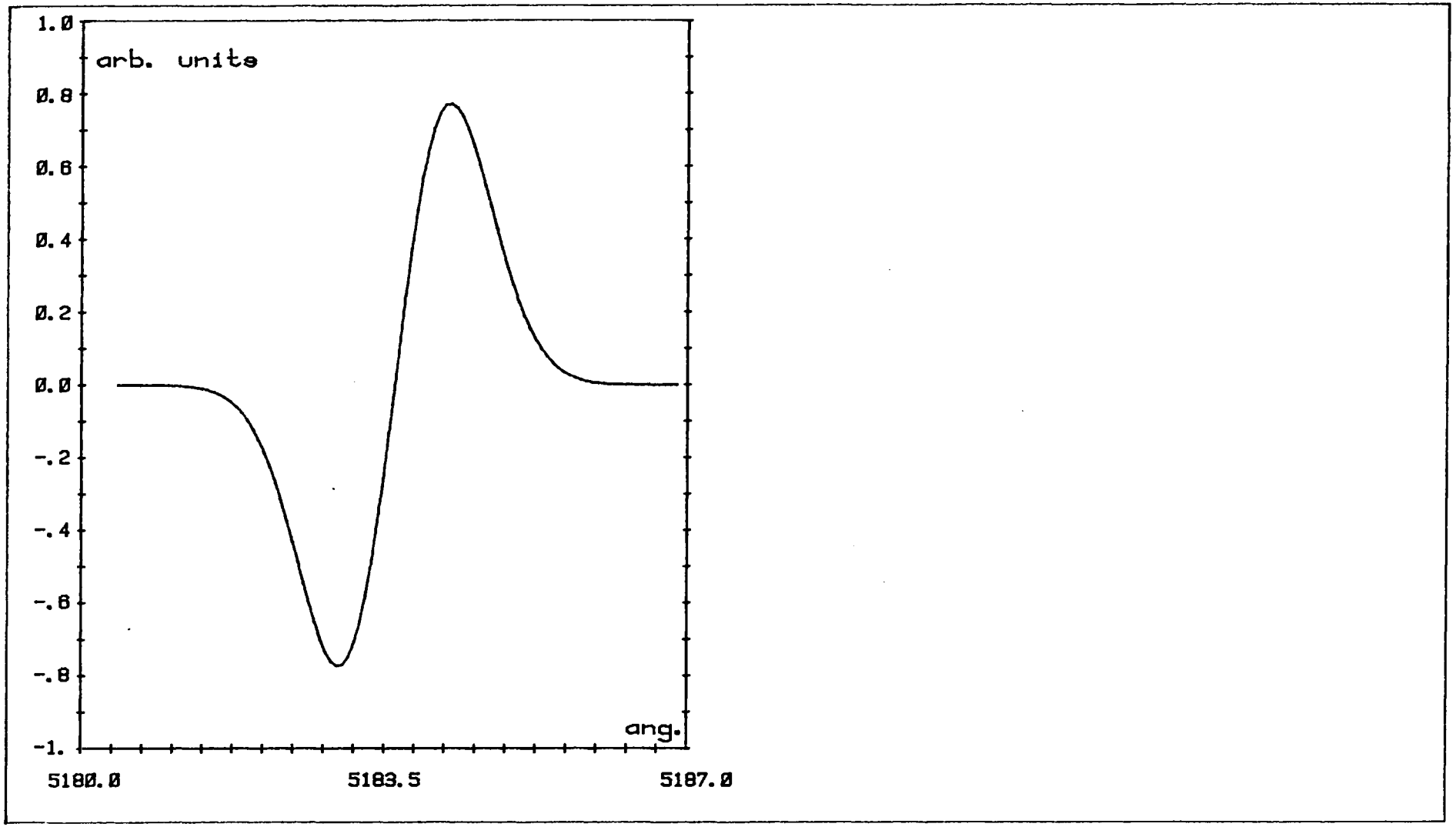

FIG. 3.20 Form of Cross-Correlation Function with Antisymmetric Ref. Function.

```
      program chred
c*********************************************************************
c**                                                                 *
c**               USES TABLE OF D/S.vs. RATIO TO INFER D/S.         *
c**               FROM A GIVEN RATIO AND FILTER POSN.               *
c**                                                                 *
c**                                                                 *
c*********************************************************************
      real f(280),xf(280),x(280),try(41),dop(41),s(280)
c**
c**READ IN FILTER PROFILE AND SIMULATED LINE PROFILE:
      call assign(2,'ifs.ire')
      call assign(3,'sim1.ire')
      do 5 i=1,280
      read(2,*)xf(i),f(i)
5     read(3,*)xd,s(i)
      type *,'D/S.        DIFF.'
c**
c**INQUIRE CHOP AMP.,RATIO AND FILTER POSN.:
      type *,'Enter chop amp.,difference,filter posn. and ratio error.'
      accept *,dl,rat,kfs,err
      n=int(dl/0.05)
c**
c**LOCATE POSN. OF SIMULATED LINE GIVING CORRECT RATIO:
c**SET UP TABLE APPROPRIATE TO THIS FILTER POSN.
      do 30 m=-20,20
      do 20 i=71,210
20          x(i)=s(i+m)/f(i-kfs)
      try(m+21)=(x(141-n)-x(141+n))/(x(141-n)+x(141+n))
      dop(m+21)=m*0.05
30          type *,dop(m+21),try(m+21)
      type *,
c**
c**LOOK UP VALUE:
      do 40 i=1,41
      if(try(i).ge.rat)kd=i
40          continue
      ds=dop(kd)
c**
c**ASSESS ERROR:
      ke=-1
50          if(try(kd+ke)-try(kd).ge.err)go to 60
      ke=ke-1
      if(kd+ke.gt.0)go to 50
60          err=dop(kd)-dop(kd+ke)
c**
c**OUTPUT:
      type *,'D/S.=',ds,'+/-',err
c**
      stop
      end
```

FIG.3.21 Program for Deriving a Doppler-Shift from a Chop Ratio.

```
      program db
c**********************************************************************
c**                                                                   *
c**       COMBINES RESULTS BY METHOD OF LEAST ERROR                   *
c**                (See e.g. BARFORD)                                 *
c**                                                                   *
c**********************************************************************
      real er(200),ds(200),e(200)
      type *,'Enter file for input'
      type *,
      call assign(3,'fname1.ire',-1)
      type *,'Enter file for output'
      type *,
      call assign(4,'fname2.ire',-1)
      type *,'no. of pts.?'
      accept *,npt
      do 10 i=1,npt
10          read(3,*)e(i),ds(i),er(i)
c**FIND NEXT ELONGATION:
      rmax=0.
      rmin=360.
15          rmin=360.
      do 20 i=1,npt
      if(e(i).gt.rmin)go to 20
      if(e(i).gt.rmax)rmin=e(i)
20          continue
      if(rmin.eq.360.)go to 60
      rmax=rmin
      ek=rmin
      type *,ek
c**
c**COMBINE RESULTS FROM ALL POINTS OF EQUAL ELONGATION:
      sum=0.
      dss=0.
      do 50 i=1,npt
      if(e(i).ne.ek)go to 50
      sum=sum+(1./(er(i)**2))
      dss=dss+(ds(i)/(er(i)**2))
50          continue
      dss=dss/sum
      err=1./(sum**0.5)
c**OUTPUT RESULTS:
      write(4,*)ek,dss,err
      j=j+1
      go to 15
60          stop
      end
```

FIG.3.22 Program for Combining Results from Different Frames.

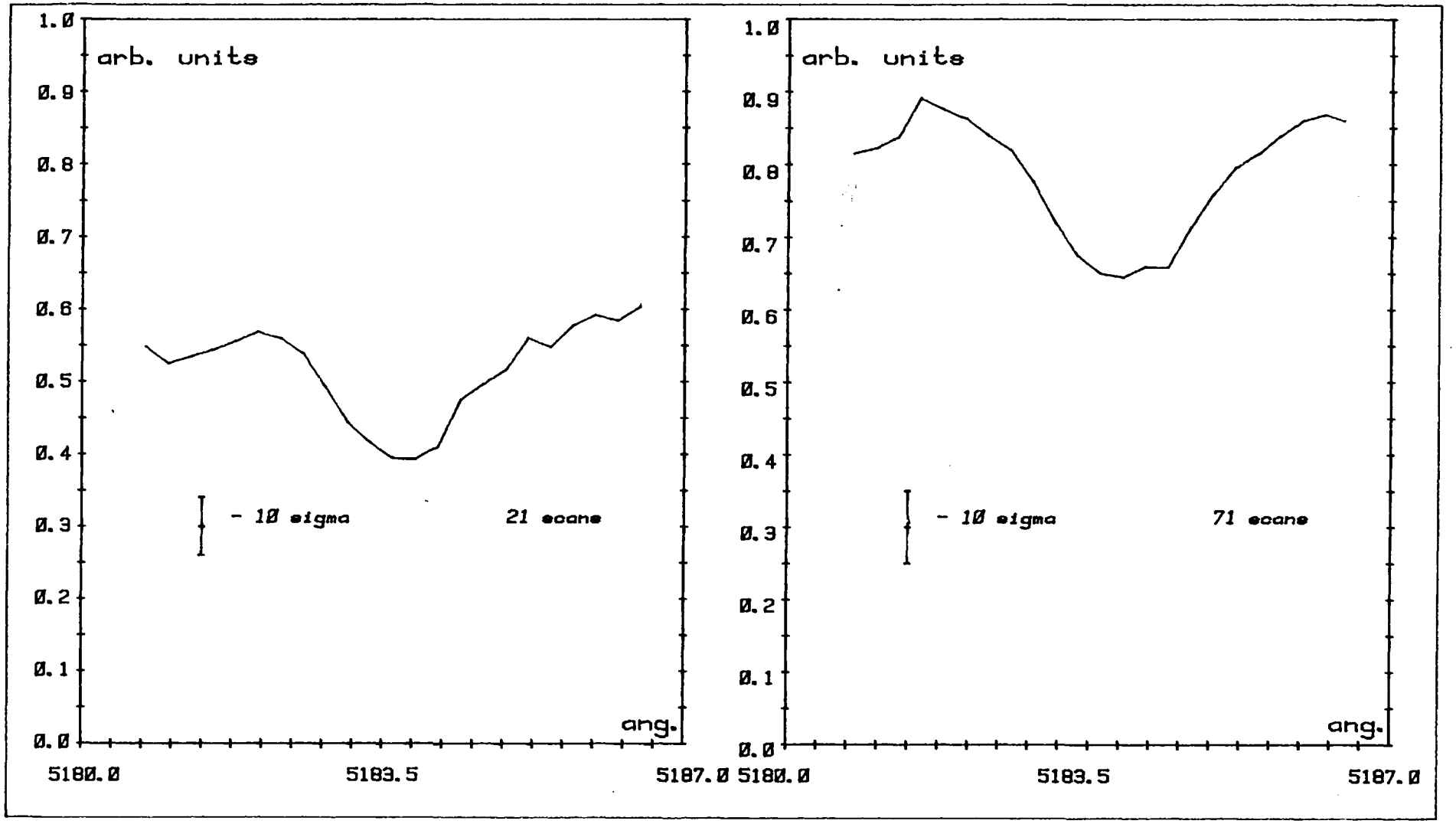

FIG. 3.23 Measured Profile from 3Ødeg. Elongation.

FIG. 3.24 Measured Profile from 11Ødeg. Elongation.

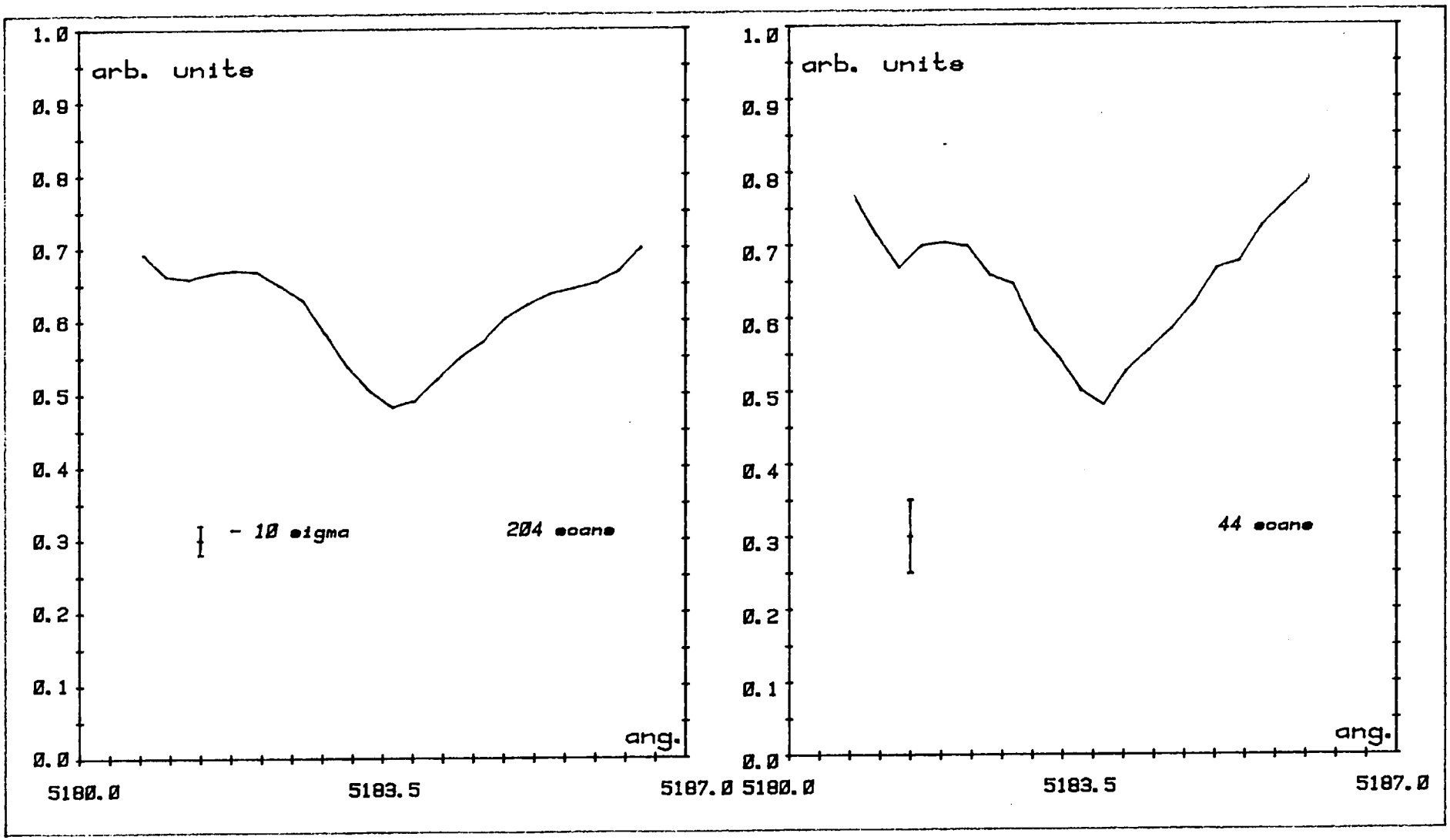

FIG. 3.25 Measured Profile from 180deg. Elongation.

FIG. 3.26 Measured Profile from 40deg. Elongation.

```
  program prof
c*********************************************************************
c**                                                                  *
c** LOCATES FRAMES OF A GIVEN ELONGATION,RESAMPLES AND SUMS.         *
c**                                                                  *
c** Uses resampling function from IBM J.Res.Dev.,20,no.1,1976        *
c**       I         I                                               *
c**       I         I                                               *
c**       I         I                        i=pt. on scan          *
c**       I<cal-13>I                         j=pt. on resampled      *
c**       I         I                         scan                  *
c**       I<--------------i------>^                                 *
c**       I         I                        cal=Cal. pt. on scan   *
c**       I<----------j----->^                                      *
c**       I         I                                               *
c**       I         I                                               *
c**^^^^^^^^^^^^^^^^^^^^^^^^^^^^^^^^^^^^^^^^^^^^^^^^^^^^^^^^^^^^^^^^^^*
c**                 1                    13                    25  *
c**                                      MsI                       *
c**                                                                *
c*********************************************************************
c**                                                                  *
c**       VALIDITY:Valid for MsI<+(13-Zmax)  > where Z=cal-13       *
c**                           <-(13-Zmin)  >                       *
c**                                                                  *
c*********************************************************************
  real x(25),x1(25),e(40),z(300)
  type *,'Data file name?'
  type *,
  call assign(4,'fname1.ire',-1)
  type *,'Output file name'
  type *,
  call assign(3,'fname2.ire',-1)
  type *,'How many frames in file,Elons.s to process?'
  accept *,m,n
  type *,'Enter them'
  do 10 i=1,n
10        accept *,e(i)
c**
c**OPEN ELONGATION LOOP:
  do 100 i=1,n
  call reset(x1,z,ns)
c**
c**OPEN FRAME LOOP:
  do 50 j=1,m
  call read(he,cal,x,hns)
  if(he.ne.e(i))go to 50
  call resamp(x,cal,z(j))
  call sum(x,x1,ns,hns)
50        continue
  call range(z,m,f,s)
100       call output(e(i),ns,x1,s,f)
  call reset(x1,z,ns)
```

FIG.3.27 Program for Recovery of Observed Line Profiles.

```
  type *,'Task complete!'
  stop
  end
c**
c**READ IN:
  subroutine read(he,hcal,x,hns)
  real x(25)
  read(4,*)hm,he,hd,hm,hns
  read(4,*)hdc,hcal,hpe,hce
  do 10 i=1,25
10        read(4,*)ns,x(i)
  return
  end
c**
c**SUMMATION:
  subroutine sum(x,x1,ns,hns)
  real x(25),x1(25)
  do 10 i=1,25
10        x1(i)=x1(i)+x(i)
  ns=ns+hns
  return
  end
c**
c**OUTPUT:
  subroutine output(e,ns,x1,s,f)
  real x1(25)
  write(3,*)e,ns,s,f
  do 10 i=1,25
  j=i
10        write(3,*)j,x1(i)
  type *,e,'finished.',ns,'scans.'
  type *,'VALID FOR',s,'to',f,'only.'
  type *,'*****************************************************'
  type *,
  return
  end
c**
c**RESAMPLE:
  subroutine resamp(x,cal,z)
  real x(25),x2(25)
  cal=(cal/10)+1
  z=cal-13
  do 10 J=1,25
  do 10 i=1,25
10        x2(J)=x2(J)+(x(i)*spibm(i-z-J))
  do 20 i=1,25
  x(i)=x2(i)
20        x2(i)=0
  return
  end
c**
c**RANGE:
  subroutine range(z,m,f,s)
```

(FIG.3.27 cont.)

```
      real z(300)
      th=0
      tl=0
      do 10 i=1,m
      if(z(i).gt.th)th=z(i)
10          if(z(i).lt.tl)tl=z(i)
      f=25-th
      s=1-tl
      return
      end
c**
c**RESET:
      subroutine reset(x1,z,ns)
      real z(300),x1(25)
      rewind 4
      ns=0
      do 10 i=1,200
10          z(i)=0
      do 20 i=1,25
20          x1(i)=0
      return
      end
```

(FIG.3.27 cont.)

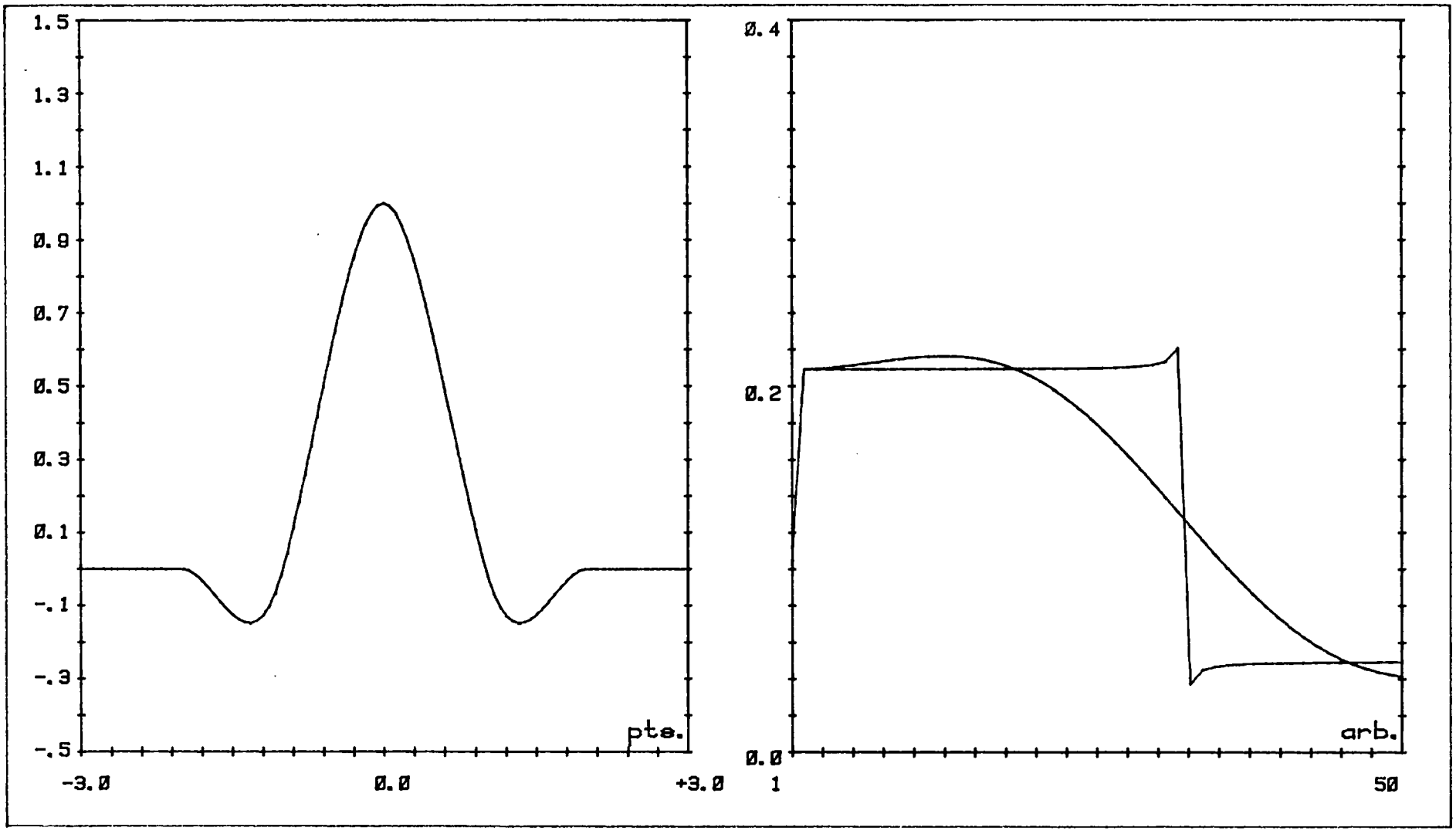

FIG. 3.28 Resampling Function Used.

FIG. 3.29 F.T. of Resampling Function Used Compared to that of a Sinc Function.

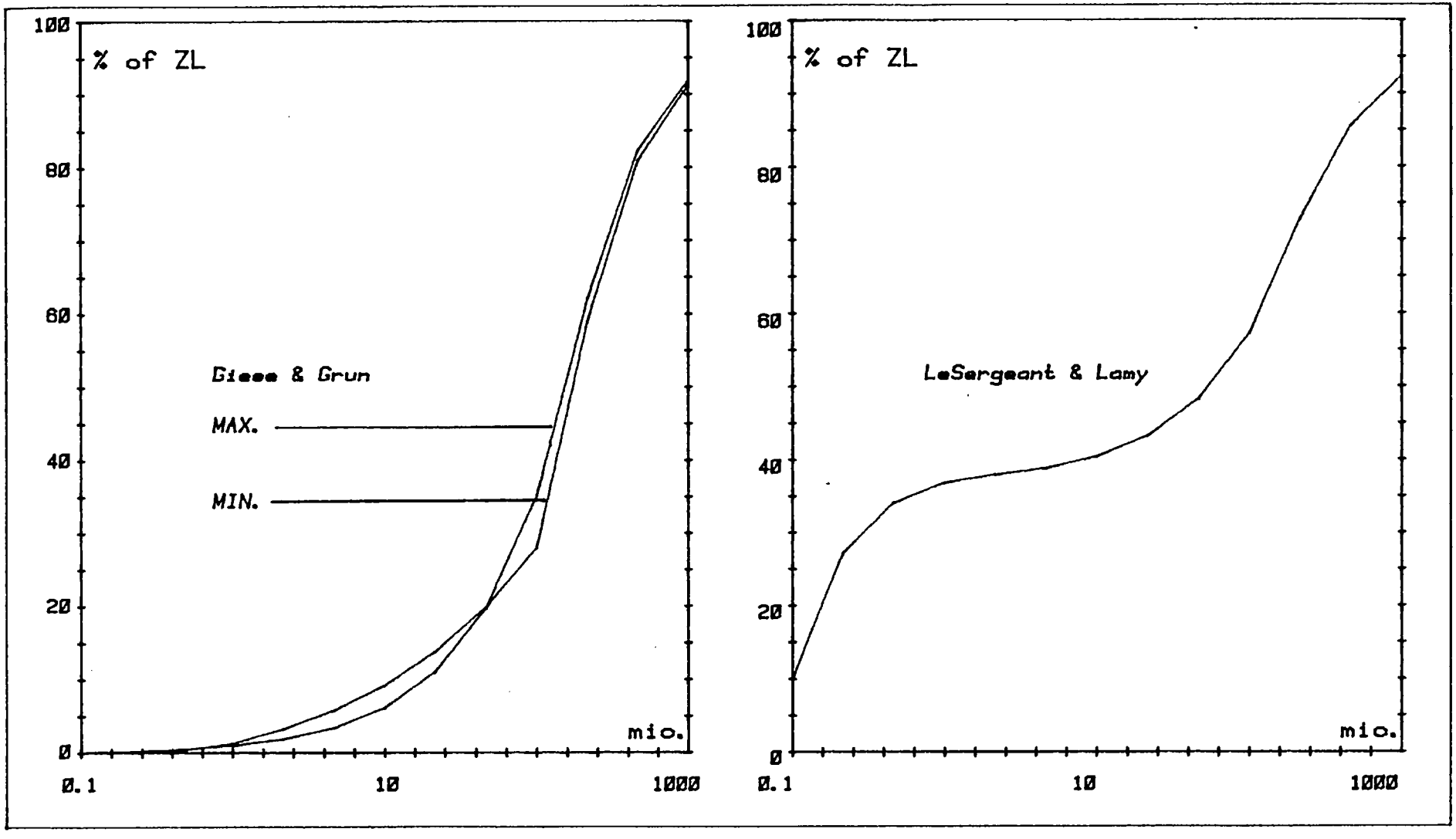

FIG. 4.1 Cumulative Brightness as a Function of Size for the Size Distributions of Giese & Grun, (1976), and LeSergeant & Lamy, (1978).

```
      program mod1
c*************************************************************************
c***MODEL/METHOD:see REAY;1969,Nature,224,54                              *
c***                                    ***                               *
c***                                                                      *
c***PARAMETERS:albedo(asumed const.),ptcle. size distbn. index,          *
c***           radial distbn. index,size limits,density                   *
c***                                                                      *
c***                                                                      *
c***ASSUMPTIONS:albedo;const. in radial distance                         *
c***            density;const.                                           *
c***            size distbn.;since rad. press. neglected not             *
c**                needed                                                *
c***                                                                     *
c***            rad. distbn.;  '      '    '                             *
c***            orbital distbn.;zero effect of eccentric and             *
c**                inclined orbits,i.e....circular orbits only.          *
c***               scattering fn.;selectable (accounts for               *
c***               size distbn. and albedo)                              *
c***            radiation pressure;neglected                             *
c***            secondary scattering;none                                *
c***                                                                     *
c***                                                                     *
c*************************************************************************
      real ss(201),ss1(201),s(19)
      type *,'ENTER SCATTERING FN. FILE'
      type *,
      call assign(8,'tt;namefl.ire',-1)
      type *,
      type *,'Beta?'
      accept *,bet
c***SET UP CONSTANTS.....................
      pi=3.14159265
      ve=2.977e06
      wl=5.183618e-05
      c=2.998e10
      c2=ve*wl/c
c***SET UP ARRAYS FOR INTEGRALS..........
      type *,
      type *,'    ELONG.    D/S.'
      type *,
c***READ IN SCATTERING FUNCTION.............;
      do 110 i=1,19
110         read(8,*)s(i)
c***LOOP IN ELONG.;2.5deg. INTERVALS.........
      de=pi*2.5/180
      el1=pi*20/180
      do 200 J=1,64
      el=el1+de*(J-1)
      sel=sin(el)
      dth=(pi-el)/200
c**
```

FIG.4.2 Program for deriving Doppler-shifts of particles in circular Keplarian orbits.

```
c**START THETA LOOP:
      do 150 i=1,201
      th=el+(dth*(i-1))
      sth=sin(th)
      if(th.lt.pi)go to 120
      ss1(i)=0.0
      ss(i)=0.0
      go to 150
120         pf=pfs(th,s)
      ss1(i)=pf*(sth**(bet))
      ss(i)=pf*(sth**(bet+1.5))
150         continue
c***INTEGRATIONS.............
      call asf(dth,ss,ss,201)
      call asf(dth,ss1,ss1,201)
c***COMPUTE D/S. AND OUTPUT.............
      aa=ss(201)/ss1(201)
      dop=c2*sel*(1.-(aa/(sel**1.5)))
      dop=dop*1.e08
      eld=el*180.0/pi
      write(4,300)eld,dop
200         type 300,eld,dop
300         format(3x,f5.1,6x,f6.3)
      stop
      end
c**
      function pfs(th,s)
      dimension s(19)
      pi=3.1415927
      dth=pi/18
      i=1
5   thd=(i-1)*dth
      if(thd.gt.th)go to 10
      if(i.eq.18)go to 10
      i=i+1
      go to 5
10  p=1+((th-((i-2)*dth))/dth)
      a=s(i-2)
      b=s(i-1)
      c=s(i)
      d=s(i+1)
      pfs=cubint(a,b,c,d,p)
      return
      end
c**
      function cubint(a,b,c,d,p)
      cubint=-(p-1.0)*(p-2.0)*(p-3.0)*a/6.0
        1      +p*(p-2.0)*(p-3.0)*b/2.0
        1      -p*(p-1.0)*(p-3.0)*c/2.0
        1      +p*(p-1.0)*(p-2.0)*d/6.0
      return
      end
```

(FIG.4.2. cont.)

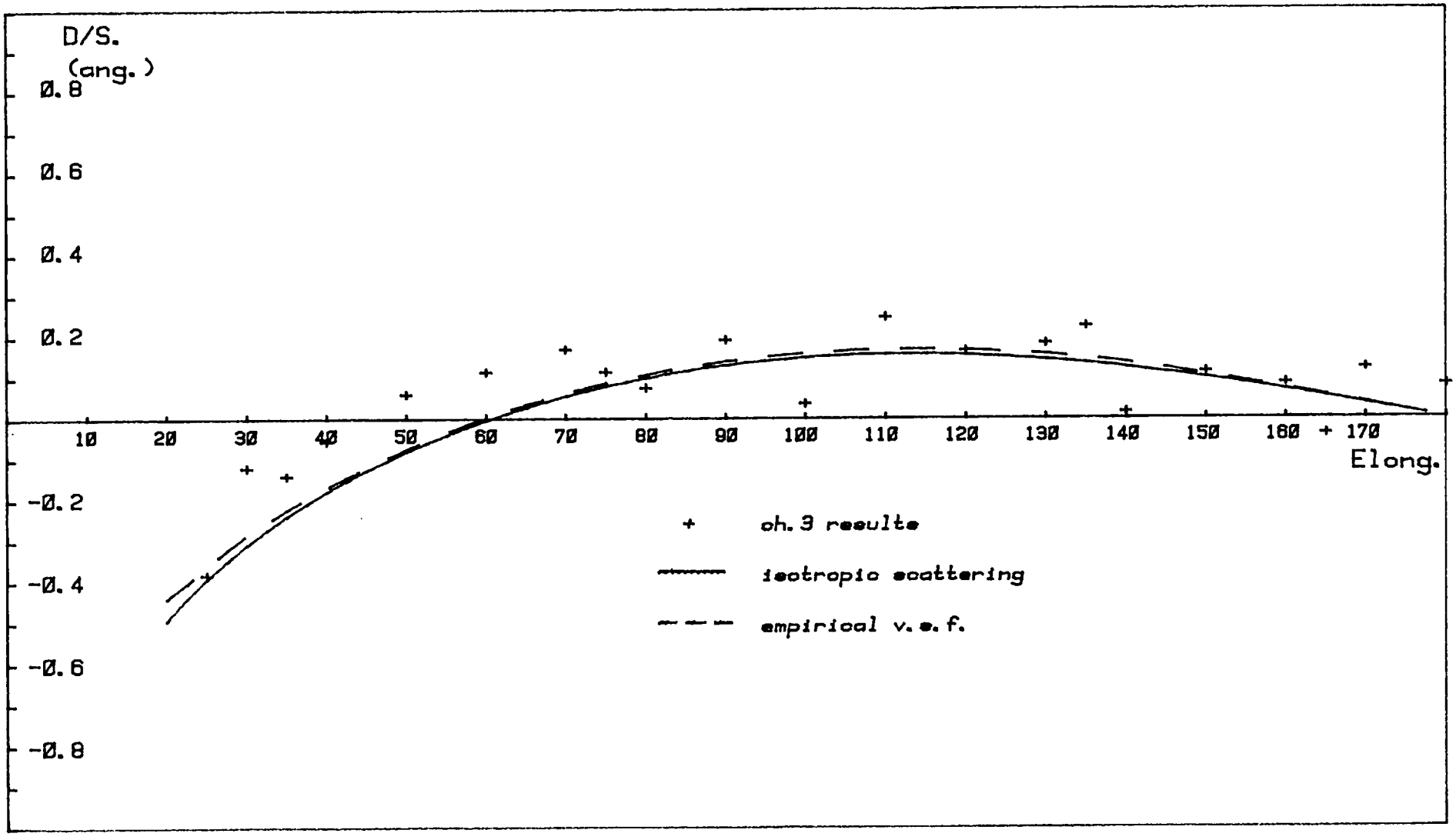

FIG. 4.3 Doppler-Shift vs. Elongation for Two Different Scattering Functions. (Circular Keplerian Orbits in the Ecliptic).

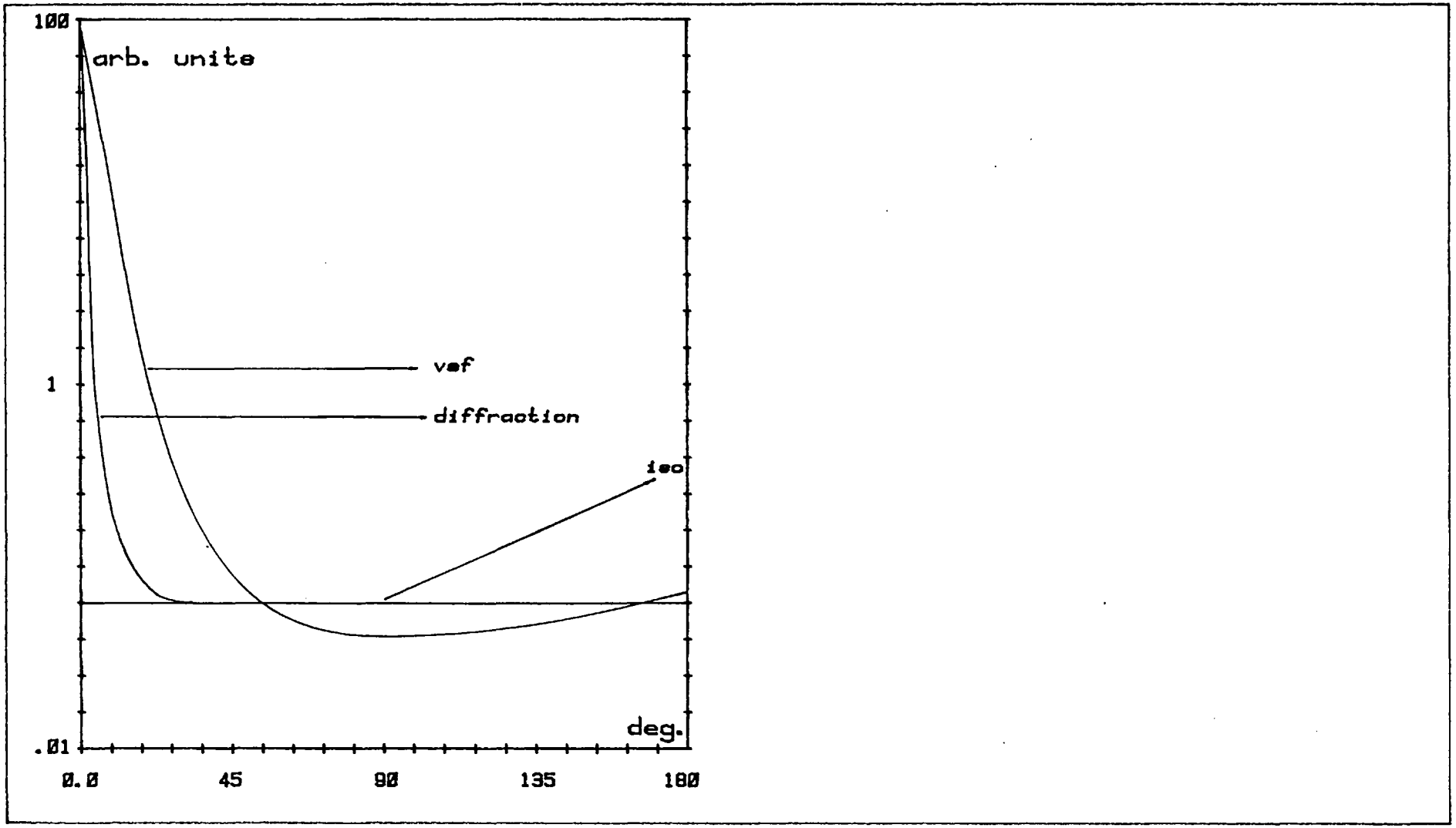

FIG. 4.4 The Two Scattering Functions Used in FIG. 4.3. Also Shown is the Contribution Diffraction Would Make.

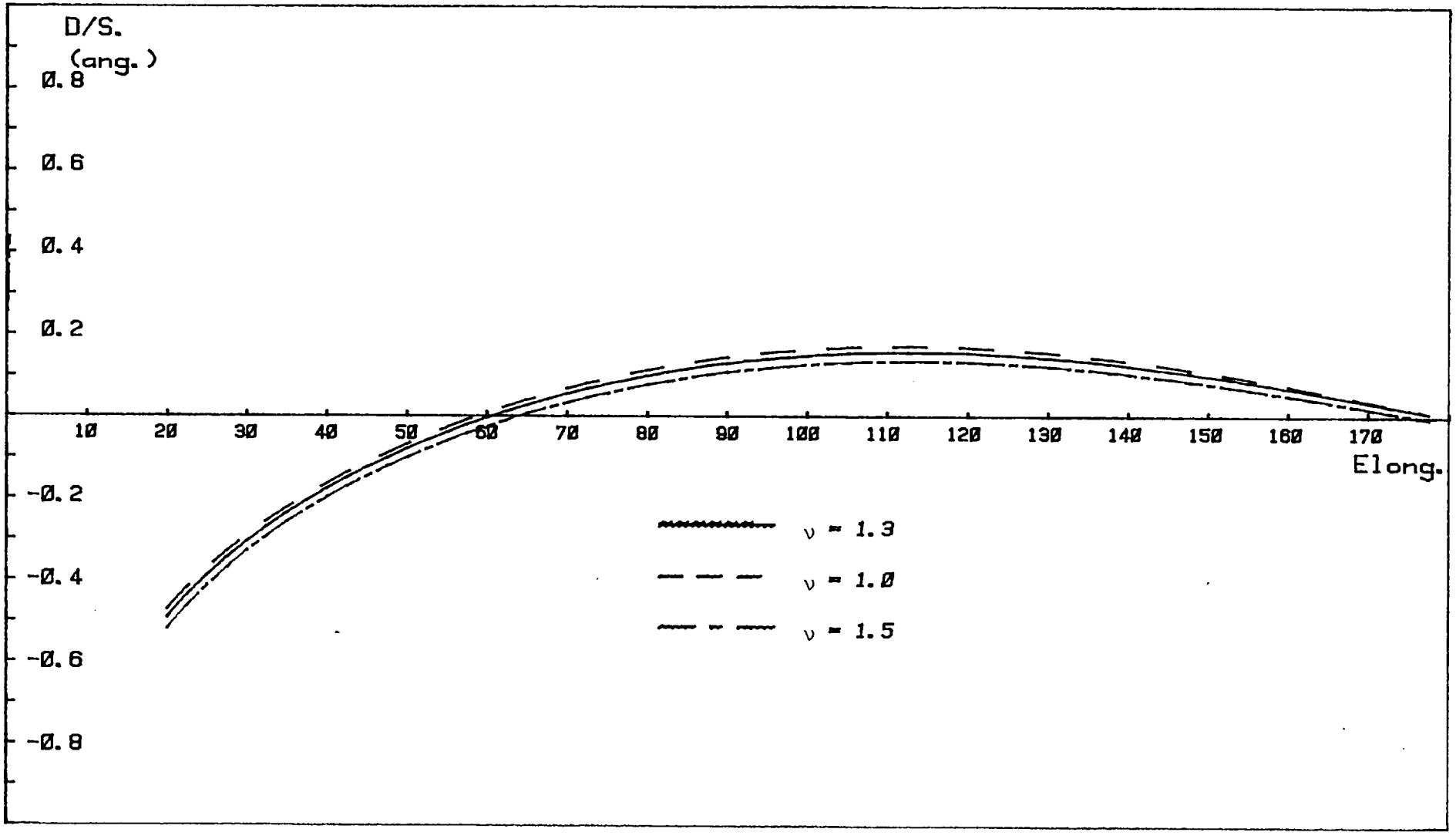

FIG. 4.5 Doppler-Shift vs. Elongation for 3 Different Radial Distribution Indeces. (Circular Orbits in the Ecliptic).

```
      program mod2
c*************************************************************
c**                                                         *
c**        FULL SCALE MODEL ,USES;                          *
c**                                                         *
c**        PARAMETERS;rad,distbn, index,Chi estimate,       *
c**                                                         *
c**        PARAMETER                                        *
c**         FUNCTIONS;scattering function,                  *
c**                                                         *
c**        ASSUMPTIONS;simple power laws for radial distbn,*
c**                                                         *
c**                    (as for chi,irp)                     *
c**                                                         *
c**                    constant value of chi                *
c**                                                         *
c**                    single scattering only               *
c**                    independant '      '                 *
c**                                                         *
c**                                                         *
c**                Uses external functions asf,pf,cubint    *
c*************************************************************
c**UNITS;c,s,s,,except solar distances(A,U,),
      real e(201),f(201),s(19)
c**SET-UP PRINTER HEADINGS;
      print *,'ELONGATION          D/S,'
      print *,
c**INPUT PARAMETERS;
      type *,'Value for chi,radial distbn, index,'
      accept *,chi,xnu
      type *,
      type *,'Enter filename for scattering function,'
      type *,
      call assign(2,'fname1,ire',-1)
      type *,
      type *,'Enter filename for results,'
      type *,
      call assign(4,'fname2,ire',-1)
      type *,
c**
c**
c**READ IN SCATTERING FUNCTION;
      do 10 i=1,19
10    read(2,*)s(i)
c**
c**SET UP CONSTANTS;
      pi=3,1415927
      ve=2,977e06
      wl=5,183618e-05
      cc=2,998e10
      c2=ve*wl/cc
c**
```

FIG,4,6, Program for derivins Doppler-shifts with sny constant value of χ .

```
c**.........DIFFERENTIALS.............dth;
c**        dth;variable.........
c**
c**OUTPUT SCREEN HEADINGS:
   type *,'   ELONG.        D/S.'
   type *,
c**
c**INITIATE ELONG. LOOP;
   do 600 ie=20,175,5
   el=pi*ie/180
   sel=sin(el)
   elon=ie
   dth=(pi-el)/200.
c**
c**INTEGRALS 4 AND 6;
   do 500 i=1,201
   th=el+(i-1)*dth
   snth=sin(th)
   if(i.eq.201)snth=0.
   pfs=pf(s,19,pi/18.,th)
   e(i)=(snth**(xnu+1.5))*pfs
500        f(i)=(snth**(xnu))*pfs
   call asf(dth,e,e,201)
   call asf(dth,f,f,201)
   xi4=e(201)
   xi6=f(201)
c**
c**
c**CALCULATE DELTA LAMBDA!;
   dl=c2*sel*(1.-(chi*xi4/((sel**1.5)*xi6)))
c**
c**OUTPUT (IN ANGSTROMS);
   dl=dl*1.e08
   type *,elon,dl
   write(4,*)elon,dl
600        print *,elon,dl
c**
c**THAT'S IT!!!!!!!!!!!!!!!!
   STOP
   end
```

(FIG.4.6 cont.)

```
  program chi
c*****************************************************************
c*                                                               *
c*  DERIVES VALUES FOR CHI OVER 0 TO 180 DEGREES ELONGATION:     *
c*                                                               *
c*        CHI=REDUCTION FACTOR FOR PARTICLE'S ORBITAL VELOCITY   *
c*        DUE TO;                                                *
c*                1.RADIATION PRESSURE                           *
c*                2.NON-ZERO ORBITAL ECCENTRICITY                *
c*                3. '    '     '    INCLINATION                *
c*                                                               *
c*        ----------**************************************-------  *
c*                                                               *
c*        ASSUMPTIONS:(As for MOD1)                              *
c*                                                               *
c*        PARAMETERS:Beta,no. of pts.                            *
c*                                                               *
c*****************************************************************
c**
c**
  real s(19),e(25),dl(25),er(25),a(101),b(101),cap(25),cer(25)
c**
c**INPUT BETA;
  type *,'Enter beta and no. of pts. in data set.'
  accept *,bet,npts
  ve=2.977e06
  wl=5.183618e03
  c=2.998e10
  c1=ve*wl/c
c**READ IN SCATTERING FUNCTION AND DATA SET;
  type *,'Enter scatterins funtion file'
  type *,
  call assign(8,'finame.ire',-1)
  type *,
  do 10 i=1,19
10        read(8,*)s(i)
  type *,'Enter data file'
  type *,
  call assign(9,'flname.ire',-1)
  type *,
  type *,'Filename for output?'
  type *,
  call assign(4,'fname3.ire',-1)
  type *,
  do 20 i=1,npts
20        read(9,*)e(i),dl(i),er(i)
c**
c**INITIATE ELONGATION LOOP;
  type *,
  type *,'ELONG.          CHI              ERROR'
  do 500 i=1,npts-1
  pi=3.14159265
  el=pi*e(i)/180
```

FIG.4.7 Program for Deriving the Particle Velocity Reduction Factor from Observed Doppler-Shifts.

```
  sel=sin(el)
  if(sel.lt.0)sel=0
  dth=(pi-el)/100
c**PERFORM I1 AND I2 INTEGRATIONS;
  do 30 j=1,101
  th=el+((j-1)*dth)
  sth=sin(th)
  if(sth.lt.0)sth=0
  pf=pfs(th,s)
  a(j)=pf*(sth**(bet+1.5))
30        b(j)=pf*(sth**(bet))
  call asf(dth,a,a,101)
  call asf(dth,b,b,101)
  xi1=a(101)
  xi2=b(101)
c**
c**CALCULATE CHI AND IT'S ERROR;
  cap(i)=((sel**1.5)-(d1(i)*sqrt(sel)/c1))*xi2/xi1
  er(i)=er(i)/d1(i)
  cer(i)=er(i)/((c1*sel/d1(i))-1)
  cer(i)=cer(i)*cap(i)
  write(4,*)e(i),cap(i),cer(i)
  write(7,*)e(i),cap(i),cer(i)
c**
500       continue
c**
c**CALCULATE MEAN AND MEAN ERROR OF CHI;
  sum1=0
  sum2=0
  do 600 i=1,npts-1
  sum1=sum1+(cap(i)/(cer(i)**2))
600       sum2=sum2+(1/(cer(i)**2))
  sum1=sum1/sum2
  sum2=1/sqrt(sum2)
  type *,'MEAN CHI=',sum1
  type *,'MEAN ERROR=',sum2
  stop
  end
c**
c**
  function pfs(th,s)
  real s(19)
  pi=3.1415927
  dth=pi/18
  i=1
5 thd=(i-1)*dth
  if(thd.gt.th)go to 10
  if(i.eq.18)go to 10
  i=i+1
  go to 5
10        p=1+((th-((i-2)*dth))/dth)
  a=s(i-2)
  b=s(i-1)
```

(FIG. 4.7 cont.)

```
      c=s(i)
      d=s(i+1)
      pfs=cubint(a,b,c,d,p)
      return
      end
c**
      function cubint(a,b,c,d,p)
      cubint=-(p-1.0)*(p-2.0)*(p-3.0)*a/6.0
     1     +p*(p-2.0)*(p-3.0)*b/2.0
     1     -p*(p-1.0)*(p-3.0)*c/2.0
     1     +p*(p-1.0)*(p-2.0)*d/6.0
      return
      end
```

(FIG. 4.7 cont.)

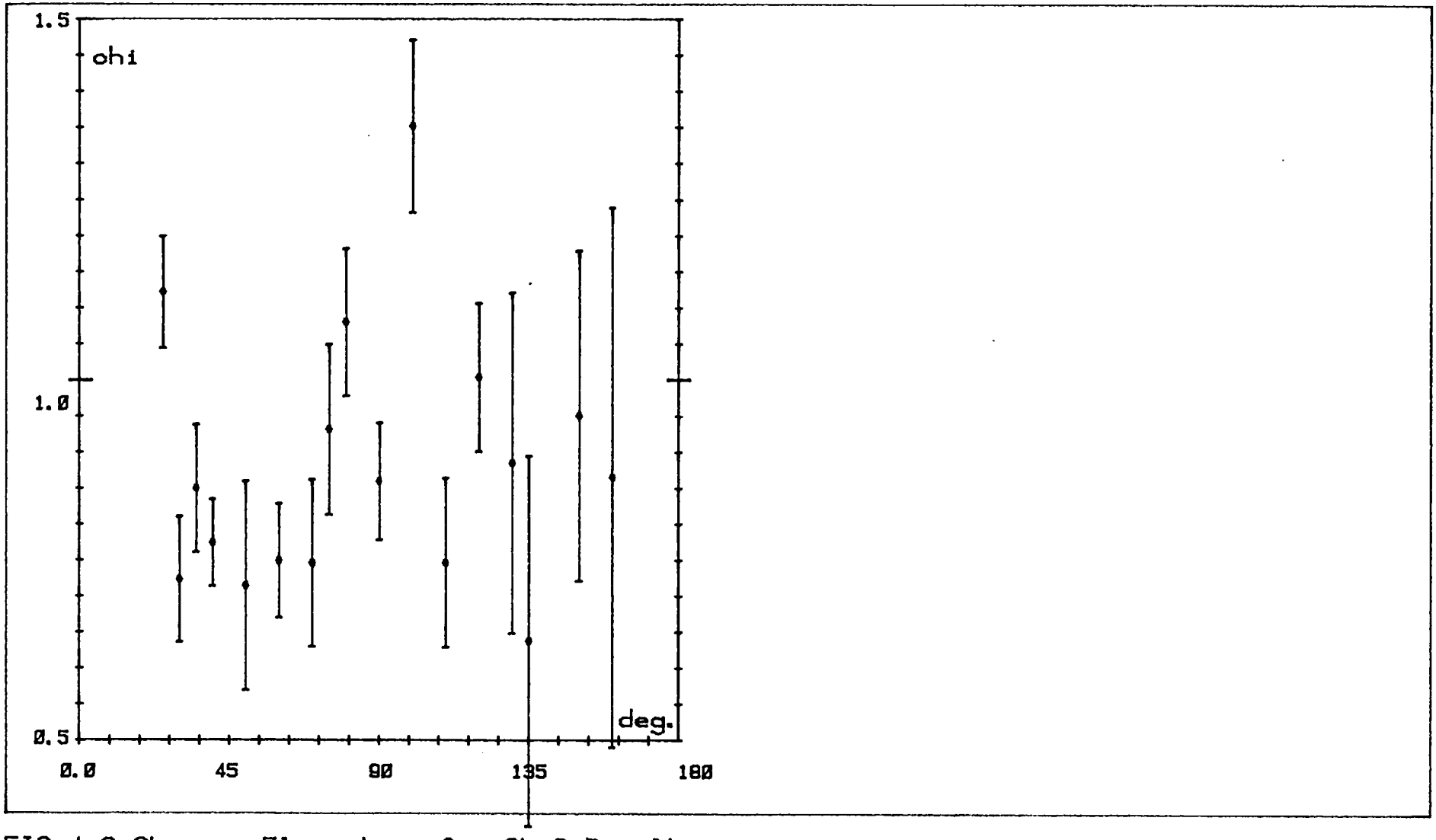

FIG. 4.8 Chi vs. Elongation for Ch. 3 Results.
(Radial Distbn. Index=1.3; Isotropic Scattering).

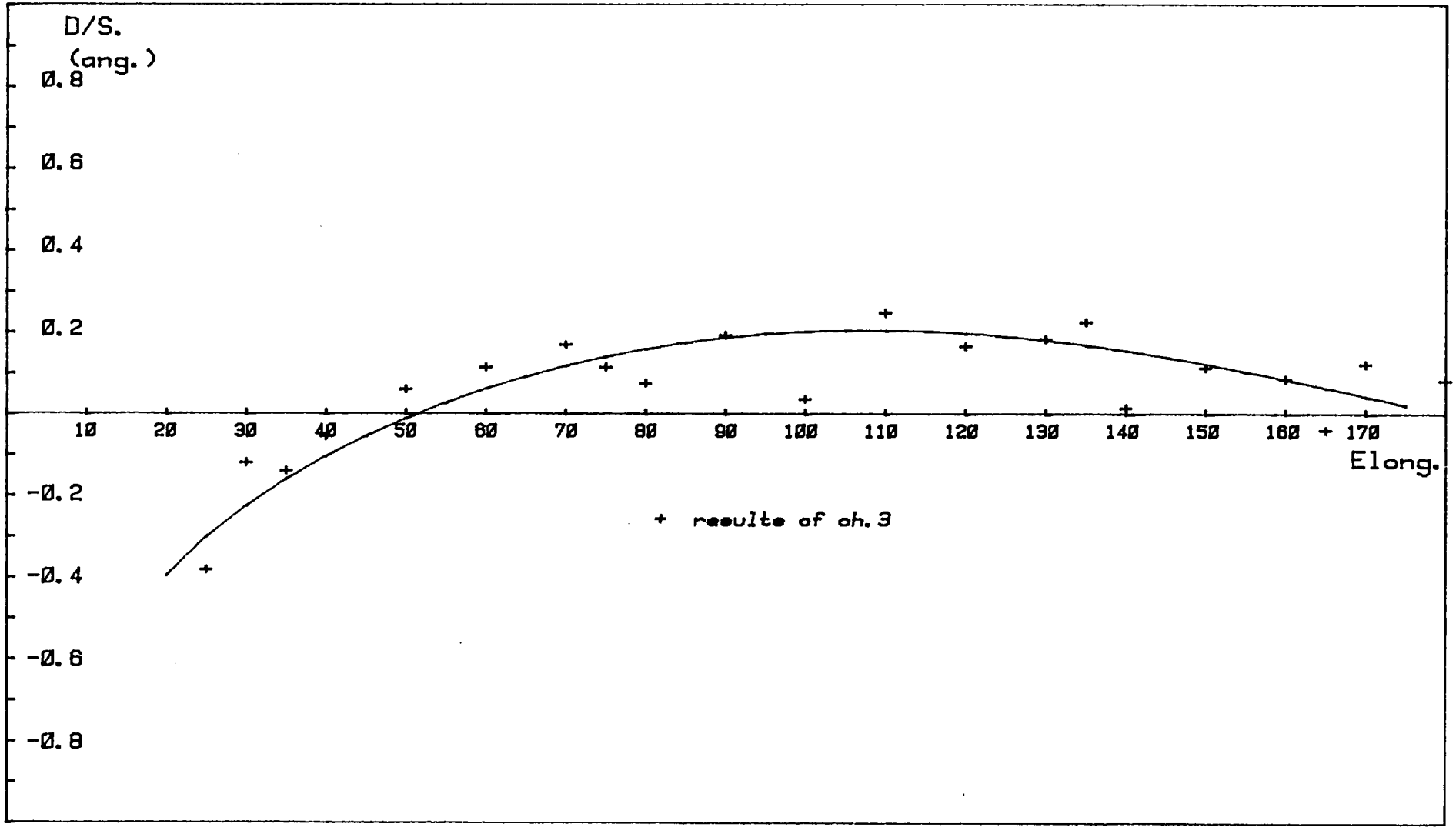

FIG. 4.9 Doppler-Shift vs. Elongation for Chi=0.854.
(Radial distbn. Index=1.3; Isotropic Scattering).

```
      program etaor
c*************************************************************
c**                                                         *
c**        CALCULATE THEORETICAL ETA(i),ETA(e);             *
c**        ~~~~~~~~~~~~~~~~~~~~~~~~~~~~~~~~~~               *
c**                                                         *
c**                                                         *
c**        PARAMETERS:i-distbn. parameter,mean ecc.         *
c**                                                         *
c**        PARAMETER                                        *
c**         FUNCTIONS:eccentricity distbn.,                 *
c**                   inclination distbn.                   *
c**                                                         *
c**        ASSUMPTIONS:i-distbn. + e distbn. independant of*
c**                    solar distance                       *
c**                    single scattering only               *
c**                    independant '     '                  *
c**                                                         *
c**                                                         *
c**                 Uses external functions pfe,pfi,gsf     *
c*************************************************************
c**UNITS:c,g,s.,except solar distances(A.U.),
      real a(1001),b(1001),c(179),d(179),g(181),h(181)
     1     ,g(91),pp(91)
c**INPUT PARAMETERS;
      type *,'Rad. distbn. index?'
      accept *,bet
      type *,'a,mean ecc.?'
      accept *,aa,ebar
      type *,'Enter empirical estimate of chi.'
      accept *,radbar
c**
c**SET UP CONSTANTS;
      pi=3.1415927
      ve=2.977e06
      wl=5.183618e-05
      cc=2.998e10
      c2=ve*wl/cc
c**
c**DIFFERENTIALS:
60 di=pi/180
      de=0.01
      dv=pi/180
c**
c**.....<COSi>.......
      do 200 i=1,179
      xi=i*di
      ppfi=pfi(xi,aa)
      c(i)=ppfi*cos(xi)/sin(xi)
200         d(i)=ppfi/sin(xi)
      call gsf(di,c,c,179)
      call gsf(di,d,d,179)
```

FIG.4.10 Program used to derive ETA(i),ETA(e) from mean values of i,e.

```
      xi3=c(179)
      xi3n=d(179)
      csibar=xi3/xi3n
      type *,'MEAN COSINE OF INCLIN.=',csibar
      type *,
c**
c**INTEGRALS 5 AND 7.(Eccentricity only integrated from 0 to 0.9);
      do 400 i=1,91
      xe=(i-1)*de
      e2=xe**2
      ac=pfe(xe,ebar)*((1-e2)**(bet-1.5))
      do 300 k=1,181
      v=(k-1)*dv
      ab=1+(xe*cos(v))
      g(k)=ab**(1.5-bet)
300         h(k)=ab**(1.-bet)
      call qsf(dv,g,g,181)
      call qsf(dv,h,h,181)
      pp(i)=g(181)*ac
400         q(i)=h(181)*ac
      call qsf(de,pp,pp,91)
      call qsf(de,q,q,91)
      xi5=pp(91)
      xi7=q(91)
c**
c**CALCULATE AND OUTPUT ECCENTRICITY FACTOR;
      ecf=xi5/xi7
      type *,'ECCENTRICITY FACTOR =',ecf
      type *,
c**
c**CALCULATE AND OUTPUT COSINE*ECCENTRICITY FACTORS;
      chicom=ecf*csibar
      radcom=radbar/chicom
      type *,
      type *,'COSINE FACTOR*ECC. FACTOR=',chicom
      type *,
      type *,'REQUIRED RADN. PRESS. COMP.=',radcom
      type *,
c**
      end
      function pfe(xe,ebar)
      pfe=exp(-((xe-ebar)**2)/0.014)
      return
      end
      function pfi(xi,q)
      pfi=sin(xi)*exp(-q*xi)
      return
      end
```

(FIG.4.10. cont.)

```
      program etarpl
c*****************************************************************
c**                                                              *
c**       CALCULATE THEORETICAL ETA(rp).                         *
c**       ******************************                         *
c**                                                              *
c**       PARAMETERS:Choice of size distbn. model                *
c**                  (assumed const. in space ),density,         *
c**                  efficiency factor (Qpr).                    *
c**                                                              *
c**       ASSUMPTIONS:Non-diffractive part of scattering function*
c**                   independant of size.                       *
c**                                                              *
c**                   Particles responsible for ZL are.large     *
c**                   compared to wavelength of obsevation.      *
c**                                                              *
c**                   Qpr,Qsca=const.(radius > zcrit microns )   *
c**                           =0     (radius <      "     "  )   *
c**                                                              *
c**                   'Max' or'Min'mass distbn. converted to sizes*
c**                   as per GiesetGrun 1976 Lect. Notes in Phys.*
c**                   ,48,135 .                                  *
c**                    **                                        *
c**                   const. density,albedo with solar distance  *
c**                   size distbn. independant of  "     "       *
c**                   single scattering only                     *
c**                   independant  "     "                       *
c**                                                              *
c**                                                              *
c*****************************************************************
c**UNITS:c,g.s.,except solar distances(A.U.).
      real p(3),p1(3),p2(3)
      common coeff(3),z(4),xlo,xup
c**INPUT PARAMETERS;
      type *,''Max.'(1) or 'Min'(0) model,'
      type *,'Qpr,density ?'
      accept *,model,qpr,rho
      type *,'Enter lower limit for x.'
      accept *,xcrit
c**
c**SET UP CONSTANTS;
      pi=3.1415927
      e1=3.0716
      gm=1.3276
      cc=2.998e10
      c1=3*e1/(4*cc*gm)
      c1=c1*1.e06
c**
c**SIZE INTEGRATION LIMITS:
      zcrit=0.5*xcrit/(2*pi)
      xlo=zcrit*1.e-04
      xup=1.e06
c**
      if(model.eq.0)go to 30
c**
c**PARAMETERS FOR MAX. MODEL:
      z(1)=0.008e-04
      z(2)=0.159e-04
      z(3)=28.8e-04
      z(4)=339.e-04
      p(1)=2.7
      p(2)=2.0
      p(3)=4.33
c**
c**CALCULATE COEFFICIENTS:
      coeff(1)=1.0
      coeff(2)=z(2)**(p(2)-p(1))
      coeff(3)=coeff(2)*(z(3)**(p(3)-p(2)))
      go to 40
c**
c**PARAMETERS FOR MINIMUM MODEL:
30          z(1)=0.008e-04
```

FIG.4.11 Program for Estimating ETA(r,p) from Q,density and size distribution.

```
      z(2)=0.398e-04
      z(3)=21.4e-04
      z(4)=339.e-04
      p(1)=2.7
      p(2)=2.5
      p(3)=4.33
      coeff(1)=1.27e-23
      coeff(2)=7.51e-22
      coeff(3)=5.03e-26
c**
c**ACCOUNT FOR DENSITY(Giese+Grun models are for 3.0g/cc):
40          corrf=(3.0/rho)**(1.0/3.0)
      xlo=xlo/corrf
c**
c**LOWER SIZE LIMIT FOR BOUND ORBITS:
      zlo1=c1*qpr/rho
      zlo=zlo1/corrf
c**
c**
c**.....<RADIATION PRESSURE>.....:
      p1(1)=1-p(1)
      p1(2)=1-p(2)
      p1(3)=1-p(3)
      p2(1)=2-p(1)
      p2(2)=2-p(2)
      p2(3)=2-p(3)
      xin=xint(p2)
      xib=xint(p1)
      rz1bar=xib/(xin*corrf)
      be=c1*qpr*rz1bar/rho
      if(be.le.1.0)go to 100
      type *,'<Beta> exceeds unity'
      go to 150
100         xmubar=sqrt(1-be)
c**
c**OUTPUT TO T/T :
      type *,
      type *,'<1/z>=',rz1bar,'per micron.'
      type *,
      type *,'MIN. z CORRESPONDING TO MIN. x OF',XCRIT,'=',zcrit,'mns.'
      type *,
      type *,'MIN. PTCLE. RADIUS FOR BOUND ORBIT=',zlo1*1.e04,'mns.'
      type *,'FOR GIVEN Qpr AND DENSITY OF',qpr,rho,'RESPECTIVELY.'
      type *,
      type *,'MEAN RADN. PRESS. PRESSURE FACTOR=',xmubar
      type *,'<BETA>=',be
      type *,
c**
c**OUTPUT TO PRINTER :
      print *,
      print *,'<1/z>=',rz1bar,'per micron.'
      print *,
      print *,'MIN. z CORRESPONDING TO MIN. x OF',xcrit,'=',zcrit,'mns.'
      print *,'FOR GIVEN Qpr AND DENSITY OF',qpr,rho,'RESP.'
      print *,
      print *,'MIN. PTCLE. RADIUS FOR BOUND ORBIT=',zlo1*1.e04,'mns.'
      print *,'FOR GIVEN Qpr AND DENSITY OF',qpr,rho,'RESPECTIVELY.'
      print *,
      print *,'MEAN RADN. PRESS. PRESSURE FACTOR=',xmubar
      print *,'<BETA>=',be
      print *,


150         end

      function xint(p)
      common coeff(3),z(4),xlo,xup
      real p(3)
      z(1)=xlo
      z(4)=xup
      xint=0.0
      i=1
```

(FIG. 4.11 cont.)

```
  if(xlo.gt.z(2))i=2
  if(xlo.gt.z(2))z(2)=xlo
10          po=p(i)                                                    258
  if(po.ne.-1)go to 15
  xi1=coeff(i)*(alog(z(i+1))-alog(z(i)))
  go to 17
15          xi1=coeff(i)*((z(i+1)**(po+1))-(z(i)**(po+1)))/(po+1)
17          xint=xint+xi1
  if(i.eq.3)go to 20
  i=i+1
  go to 10
20          return
  end
```

(FIG.4.1.1 cont.)

```
      program etaref
c**********************************************************************
c**                                                                   *
c**       CALCULATE THEORETICAL ETA(rp).                              *
c**       ~~~~~~~~~~~~~~~~~~~~~~~~~~~~~~                              *
c**                                                                   *
c**       PARAMETERS:Choice of size distbn. model                     *
c**                  (assumed const. in space ),density,              *
c**                                                                   *
c**       ASSUMPTIONS:Non-diffractive part of scattering function     *
c**                   independant of size.                            *
c**                                                                   *
c**                   'Max' or'Min'mass distbn. converted to sizes    *
c**                   as per Giese+Grun 1976 Lect. Notes in Phys.     *
c**                   ,48,135 .                                       *
c**                    ~~                                             *
c**                   const. density,albedo with solar distance       *
c**                   size distbn. independant of  '     '            *
c**                   single scattering only                          *
c**                   independant '      '                            *
c**                                                                   *
c**                   Uses pf,cubint,xn,asf                           *
c**********************************************************************
c**UNITS:c.g.s.,except solar distances(A.U.).
      real p(3),p1(3),asca(21),arp(21),xi1(1001),xin1(1000),bet(200)
      real p2(3)
      common coeff(3),z(4),xlo,xup
c**INPUT PARAMETERS;
      type *,''Max.'(1) or 'Min'(0) model,'
      type *,'density ?'
      accept *,model,rho
      type *,
      type *,'Enter filename for scattering efficiency.'
      type *,
      call assign(2,'fname1.ire',-1)
      type *,
      type *,'Enter filename for radn. press. efficiency.'
      type *,
      call assign(3,'fname2.ire',-1)
      type *,
      type *,'Enter filename for Beta(z).'
      type *,
      call assign(4,'fname3.ire',-1)
      type *,
c**
c**READ IN EFFICIENCIES:
      do 10 i=1,21
      read(2,*)asca(i)
10          read(3,*)arp(i)
c**
c**SET UP CONSTANTS;
      pi=3.1415927
      e1=3.0716
      gm=1.3276
      cc=2.998e10
      c1=3*e1/(4*cc*gm)
      c1=c1*1.e06
c**
      if(model.eq.0)go to 30
c**
c**PARAMETERS FOR MAX. MODEL:
      z(1)=0.008e-04
      z(2)=0.159e-04
      z(3)=28.8e-04
      z(4)=339.e-04
      p(1)=2.7
      p(2)=2.0
      p(3)=4.33
c**
c**CALCULATE COEFFICIENTS:
      coeff(1)=1.0
      coeff(2)=z(2)**(p(2)-p(1))
```

FIG.4.12 Program used to derive ETA(r,p,) from c,r,i, and density.

```
      coeff(3)=coeff(2)*(z(3)**(p(3)-p(2)))
      go to 40
c**
c**PARAMETERS FOR MINIMUM MODEL:
30          z(1)=0.008e-04
      z(2)=0.398e-04
      z(3)=21.4e-04
      z(4)=339.e-04
      p(1)=2.7
      p(2)=2.5
      p(3)=4.33
      coeff(1)=1.27e-23
      coeff(2)=7.51e-22
      coeff(3)=5.03e-26
c**
c**ACCOUNT FOR DENSITY(Giese+Grun models are for 3.0g/cc):
40          corrf=(3.0/rho)**(1.0/3.0)
c**
c**BETA (z):
      do 50 i=1,200
      zz=i*1.e-06
50          bet(i)=c1*pf(grp,21,4.e-06,zz)/(zz*rho)
c**
c**OUTPUT BETA(z):
      type *,'      z(mns.)    BETA'
      print *,'       z(mns.)    BETA',
      do 55 i=10,200,10
      print *,i*0.01,bet(i)
55          type *,i*0.01,bet(i)
      do 57 i=1,200
57          write(4,*)i*0.01,bet(i)
c**
c**
c**CALCULATE ETA(rp):
      p1(1)=1-p(1)
      p1(2)=1-p(2)
      p1(3)=1-p(3)
      p2(1)=2-p(1)
      p2(2)=2-p(2)
      p2(3)=2-p(3)
c**
c**1-10 MICRONS FIRST :
      dz=1.e-06
      do 60 i=1,1000
      zz=i*dz
      xnz=xn(zz/corrf,p)
      pfsca=(zz**2)*pf(gsca,21,4.e-06,zz)
      xi1(i)=pfsca*pf(grp,21,4.e-06,zz)*xnz/zz
60          xin1(i)=pfsca*xnz
      call gsf(dz,xi1,xi1,1000)
      call gsf(dz,xin1,xin1,1000)
      xi1a=xi1(1000)
      xin1a=xin1(1000)
c**
c**NOW FOR 10 MICRONS TO 'INFINITY' :
      xlo=1.e-03/corrf
      xup=1.0e06
      pfgsca=pf(gsca,21,4.e-06,2.e-03)
      xi1b=xint(p1)*pfgsca*pf(grp,21,4.e-06,2.e-03)
      xin1b=xint(p2)*pfgsca
      xi1b=xi1b/corrf
      xib=xi1a+xi1b
      xin=xin1a+xin1b
      goverz=xib/xin
      be=c1*goverz/rho
      if(be.le.1.0)go to 100
      type *,'<Beta> exceeds unity'
      go to 150
100         xmubar=sqrt(1-be)
c**
c**OUTPUT TO T/T :
      type *,
```

(FIG.4.12 cont.)

```
      type *,'<Q/z>=',qoverz,'per micron.'
      type *,
      type *,'MEAN RADN. PRESS. PRESSURE FACTOR=',xmubar
      type *,'<BETA>=',be
      type *,
c**
c**OUTPUT TO PRINTER :
      print *,
      print *,
      print *,'<Q/z>=',qoverz,'per micron.'
      print *,
      print *,'MEAN RADN. PRESS. PRESSURE FACTOR=',xmubar
      print *,'<BETA>=',be
      print *,
150         end

      function xint(p)
      common coeff(3),z(4),xlo,xup
      real p(3),zd(4)
      zd(1)=xlo
      zd(2)=z(2)
      zd(3)=z(3)
      zd(4)=xup
      xint=0.0
      i=1
      if(xlo.gt.z(2))i=2
      if(xlo.gt.z(2))zd(2)=xlo
10          po=p(i)
      if(po.ne.-1)go to 15
      xi2=coeff(i)*(alog(z(i+1))-alog(z(i)))
      go to 17
15          xi2=coeff(i)*((zd(i+1)**(po+1))-(zd(i)**(po+1)))/(po+1)
17          xint=xint+xi2
      if(i.eq.3)go to 20
      i=i+1
      go to 10
20          return
      end
```

(FIG.4.12 cont.)

Mean Inlination	η_i
5^o	0.997
10^o	0.991
15^o	0.980
20^o	0.965
25^o	0.946
30^o	0.922
35^o	0.890
40^o	0.853

Mean Eccentricity	ν	η_e
0.1	1.3	0.998
0.2	"	0.993
0.3	"	0.986
0.4	"	0.975
0.5	"	0.960
0.6	"	0.942
0.7	"	0.913
0.8	"	0.883
0.9	"	0.862
0.4	1.0	0.989

FIG.4.13 Table of η_i, η_e for Various Values of Mean Inclination and Eccentricity.

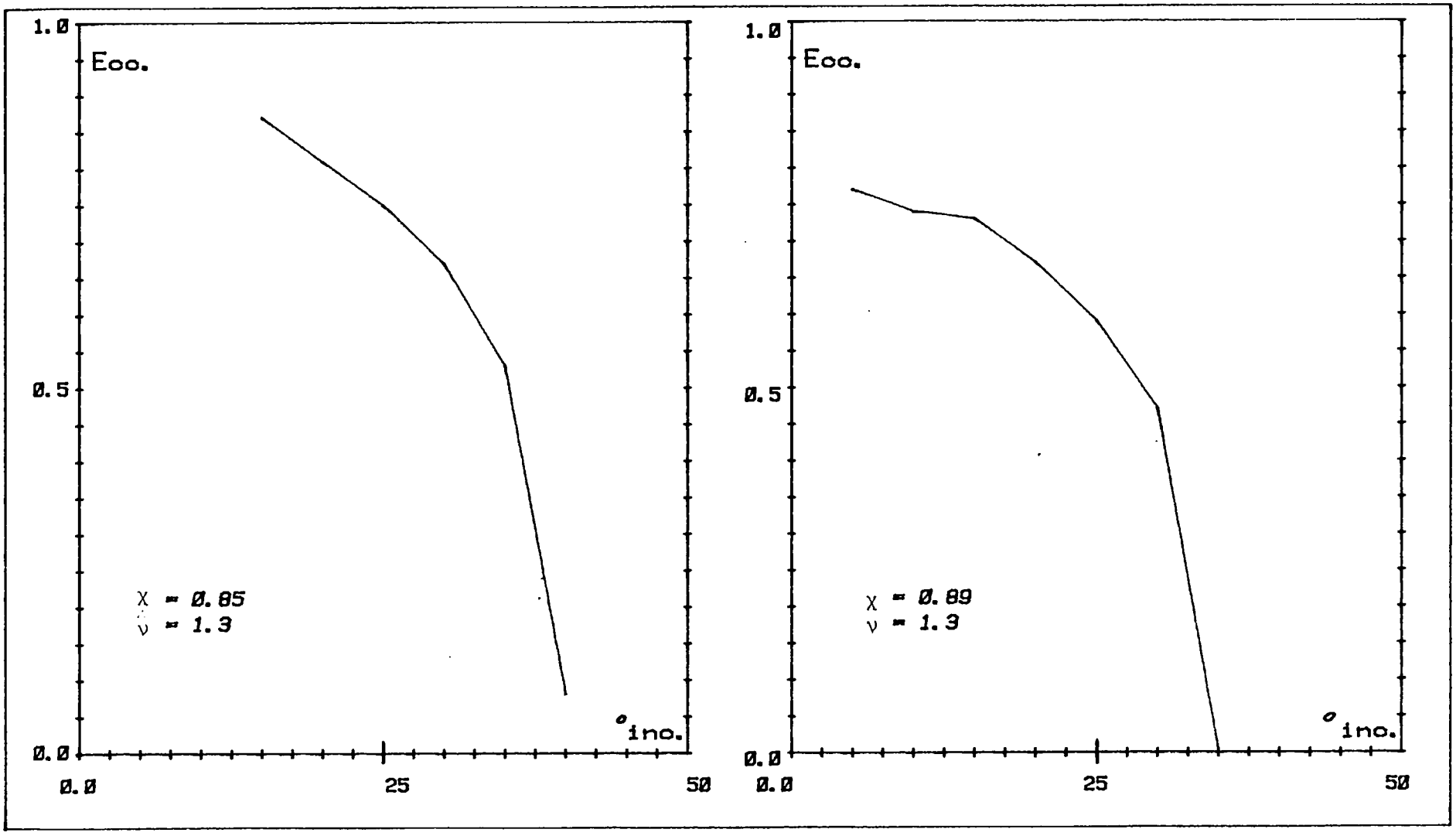

FIG. 4.14 Curves of Mean Eccentricity vs. Mean Inclination for η_e, η_i Alone to Produce Observed Value of χ.

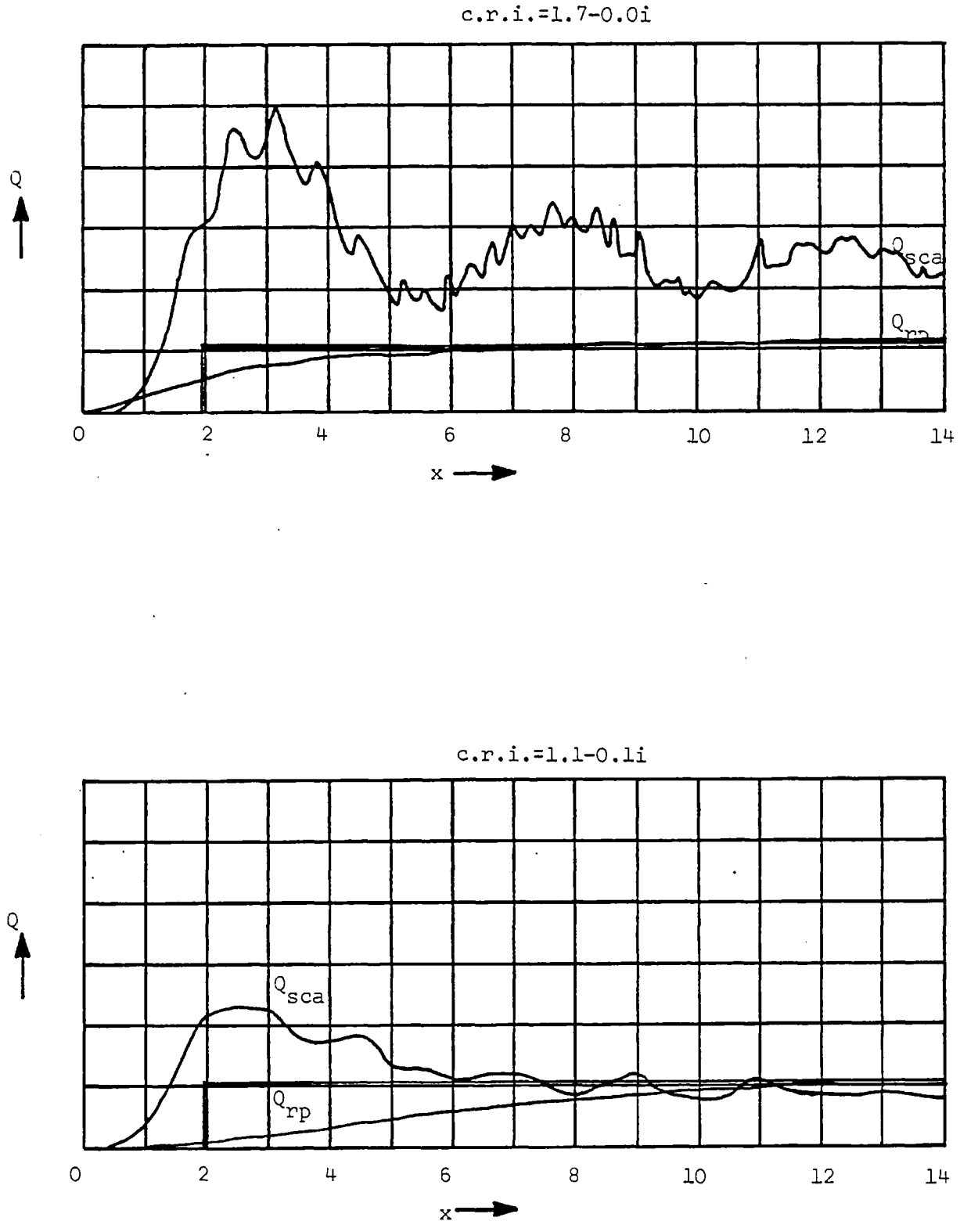

FIG.4.15 Examples of Q_{sca} and Q_{rp} taken from Wickramasinghe, (1973), Showing Approximation Used Here.

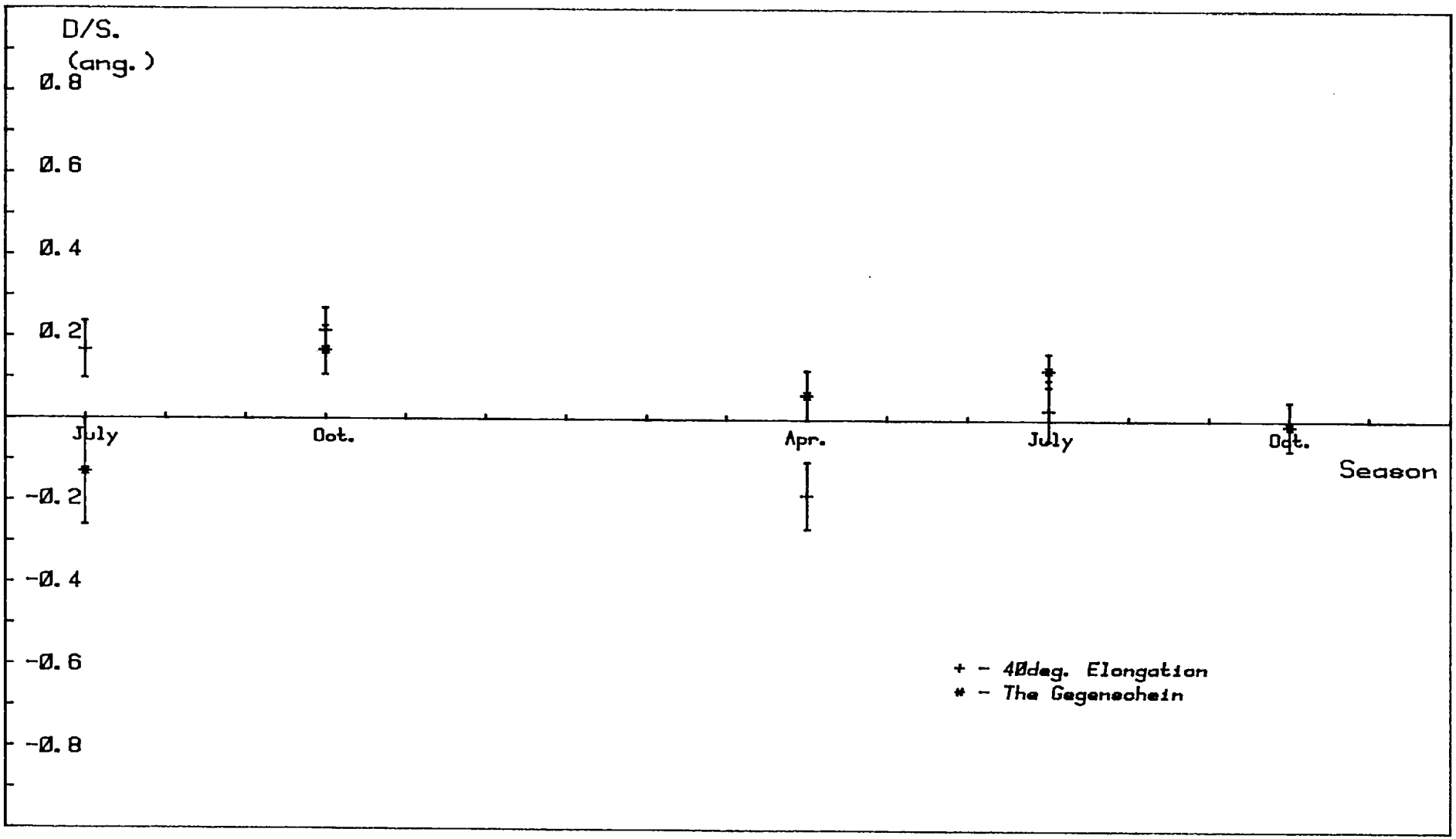

FIG. 4.16 Doppler-Shift vs. Season for Elongations 40 and 180deg..